CELL TYPE-SPECIFIC GLYCOME PROFILING ANALYSIS OF SECONDARY CELL-WALLS DURING XYLEM DIFFERENTIATION

by:

ANGELO G PERALTA

(Under the Direction of Michael G Hahn)

ABSTRACT

Plant cell-walls are important biostructures underpinning plant grow, are major reservoirs for photosynthetically accumulation, and have tremendous impact on the human use of plants. These walls consist mainly of cellulose, hemicelluloses, and lignin. The proportions of these polymers depend upon the specific functions of the cell and its stage of development. To investigate these properties, we develop an immunological approach using plant cell-wall directed monoclonal antibodies combined with laser capture microdissection. Our approach was directed at secondary cell wall master regulators involved in vessel secondary cell-wall deposition and programmed cell death. The results show that specific glycan epitopes are regulated in different cell types and at different plant developmental stages. Thus, we open up the possibility of the molecular understanding of cell-wall spatial heterogeneity of individual cell types. Lastly, the understanding of cell-wall glycan epitope composition at a cell type-specific context offers a powerful tool for understanding cell-wall biosynthetic gene function and the regulatory processes involved during such events.

INDEX WORDS: Plant Cell-Wall, Glycome Profiling, Laser Capture Microdissection, *Arabidopsis thaliana*, Monoclonal Antibodies, Glycans

CELL TYPE-SPECIFIC GLYCOME PROFILING ANALYSIS OF SECONDARY CELL-WALLS DURING XYLEM DIFFERENTIATION

by:

ANGELO G PERALTA

Under the Direction of Michael G Hahn

B.S. Ateneo de Manila University, Philippines, 2011

MPhil University of Manchester, U.K., 2013

A Dissertation Submitted to the Graduate Faculty of the University of Georgia in Partial Fulfilment of the Requirements for the Degree

DOCTOR OF PHILOSOPHY

ATHENS, GEORGIA

2019

© 2019

ANGELO G PERALTA

All Rights Reserved

CELL TYPE-SPECIFIC GLYCOME PROFILING ANALYSIS OF SECONDARY CELL-WALLS DURING XYLEM DIFFERENTIATION

by:

ANGELO G PERALTA

Major Professor: Michael G Hahn

Committee: Alan Darvill
Joseph Dahlen
Wolfgang Lukowitz
William York

Electronic Version Approved:
Suzanne Barbour
Dean of the Graduate School
The University of Georgia
August 2019

DEDICATION

Per condo ti Samantha, mia luce nelle tenebre.

Trust… but verify!

-Michael G Hahn

ACKNOWLEDGEMENTS

First and most importantly, I would like to express my gratitude and appreciation to my advisor, Dr. Michael G Hahn, for giving me the opportunity to study and work in his group with an extraordinary environment. I am really grateful for his constant guidance, support, and encouragement throughout all the years of my graduate study.

I would like to thank my committee, Dr. Alan Darvill, Dr. Joseph Dahlen, Dr. William York and Dr. Wolfgang Lukowitz for their invaluable time and expertise.

Many thanks go to the past and present members of the Complex Carbohydrate Research Center: Sivakumar Pattathil, Christina Hopper, Sivasankari Venketachalam, Sheilah Huckabee, and Jarrod Glatz. Best wishes in their future endeavors.

TABLE OF CONTENTS

Page

ACKNOWLEDGEMENTS……vii

LIST OF TABLES……ix

LIST OF FIGURES……x-xi

CHAPTER

1 INTRODUCTION AND LITERATURE REVIEW……1

2 XYLAN EPITOPE PROFLING: AN APPROACH TO STUDY ORGAN DEVELOPMENT CHANGES IN XYLAN PLANT CELL-WALL STRUCTURE, BIOSYNTHESIS, AND ITS DEPOSITION……48

3 GLYCOME PROFILING OF VASCULAR TISSUES IN WILD-TYPE AND MUTANT ARABIDOPSIS STEMS……86

4 CONCLUSIONS……177

LIST OF TABLES

Table 1.1: List of commonly used antibodies from different glycan groups……31

Table 2.1: Xylan epitope patterning in Arabidopsis…….……75

Table 3.1: Description of *VND6* and *VND7* genes in *A. thaliana*……98

Table 3.2: Glycosyl residue composition of apical and basal stems…….……108

Table 3.3: Selected list of glycan-directed mAbs for *in situ* visualisation……134-135

LIST OF FIGURES

Figure 1.1 Cross section of a Toluidine blue-stained wild-type Arabidopsis stem……2

Figure 1.2 Two different forms of xyloglucan structures……8

Figure 1.3: Structures of the main pectin cell-wall polysaccharides……9

Figure 1.4: Helical arrangement of cellulose microfibrils……12

Figure 1.5 Structure of β-1,4-glucan oligomer that forms cellulose……14

Figure 1.6: Xylan structure of dicots……17

Figure 1.7: Lignin Subunits……19

Figure 1.8: Resonance structures of lignin monolignols……23

Figure 1.9: Secondary cell-wall transcriptional pathway……24

Figure 2.1 *Arabidopsis thaliana* Col-0 background stems grown to ~24cm……60

Figure 2.2: Glycome profiling of cell walls extracted from inflorescence stems……61

Figure 2.3: Xylan profiling of Col-0 inflorescence stems……63

Figure 2.4: Immunolabelling of xylan epitopes of Col-0 stems at different development stages (D1-D4)……66

Figure 2.5: Heat map showing gene expression from publicly available microarray data……70

Figure 3.1 Schematic diagram *VND6* and VND7 genes……98

Figure 3.2: 8-week old *Arabidopsis thaliana* Col-0, *vnd6*, *vnd7*, and *vnd6 vnd7* double mutants……101

Figure 3.3: Glycome profile of Arabidopsis inflorescence stem apical and basal sections……104

Figure 3.4 Principal components analysis of whole stem glycome profiling……106

Figure 3.5: Monosaccharide composition analysis of Col-0 and *vnd* mutants……108

Figure 3.6: Principal components analysis of total monosaccharide composition using TMS methods……111

Figure 3.7: Vascular bundles and Intefascicular fibres subjected to laser capture microdissection……115

Figure 3.8: Method for cell type-specific glycome profiling……116

Figure 3.9: Glycome profile from laser capture microdissected cells……121,124

Figure 3.10: Principal components analysis of LCM-glycome profiling……125

Figure 3.11: Loading plots of oxalate and 4M KOH fractions of LCM-GP……126

Figure 3.12: Reproducibility of LCM harvested ELISAs……132

Figure 3.13: Robustness of LCM harvested ELISAs ……133

Figure 3.14: Immunofluorescent labelling of XG epitopes 1……137

Figure 3.15: Immunofluorescent labelling of XG epitopes 2……138

Figure 3.16: Immunofluorescent labelling of Xylan/XG epitopes ……139

Figure 3.17: Immunofluorescent labelling of Xylan epitopes 1……140

Figure 3.18: Immunofluorescent labelling of Xylan epitopes 2……141

Figure 3.19: Immunofluorescent labelling of Xylan epitopes 3……142

Figure 3.20: Immunofluorescent labelling of Xylan epitopes 4……143

Figure 3.21: Immunofluorescent labelling of Pectin epitopes……144

Figure 3.22: Arabidopsis stems grown to 13-15 cm for LCM tissue harvesting……154

Figure 3.23: Whole stem glycome profiling workflow……155

CHAPTER 1: INTRODUCTION AND LIT REVIEW

1.1Introduction

1.1.1 Plant Cell Walls

Terrestrial plants require specific structures that perform various functions allowing them to cope with their sessile nature. One such specific structure is the plant cell wall. Some noted functions of plant cell walls are: imparting mechanical strength, regulating turgor pressure, allowing transpiration and serving as a physical barrier (Lucas et al., 2013). Due to the numerous roles of plant cell walls, much of the assimilated carbon from photosynthesis is directed to forming cell wall polysaccharides (Loque et al., 2015). Plant cell walls are diverse in both appearance and composition. For example, cortical parenchyma is often thin and lack distinguishing features. On the other hand, xylem tracheary elements possess much thicker cell walls that may be deposited in distinctive patterns (Figure 1.1) (Zeiger and Taiz, 2010, Smith et al., 2017).

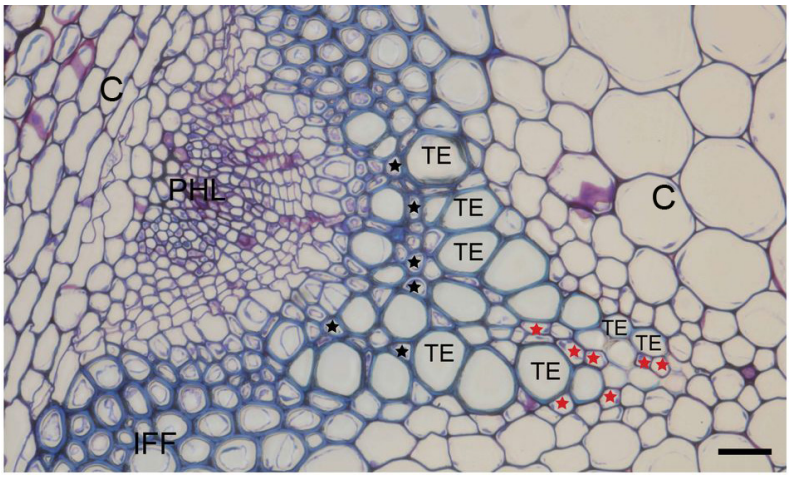

Figure 1.1: Bright-field cross-section of a Toluidine blue-stained wild-type Arabidopsis stem from the basal portion. The image displays both the vascular bundle, phloem (PHL), and xylem. The xylem tissue contains treachery elements (TEs), xylary parenchyma cells (red stars), xylary fibers (black stars), and, interfascicular fibers (IFF). Scale bar = 20 µm. Adapted from Smith et al. (2017)

1.1.2 Arabidopsis as a Model Plant

Arabidopsis thaliana, a small annual plant of the mustard family (Brassicaceae) is the model organism for modern plant biology. Initially promoted by Friedrich Laibach in 1943, it has become well-established for plant genetics, molecular biology, and development (Koornneef and Meinke, 2010). Arabidopsis contains many attributes suited for molecular studies. Firstly, Arabidopsis has a very small size. When grown at low density, its leaf rosette can reach a maximum diameter of four to six centimetres and its inflorescence stem height reaches 30 to 40 cm. The plant size of Arabidopsis allows for large numbers of plants to be grown in a small indoor growth chamber, thus negating the need for field plot studies. It also produces thousands of seeds that are small enough to grow on Petri dishes allowing evaluation of specific nutritional requirements or selection of transgenic lines via antibiotic resistance (Koornneef and Meinke, 2010).

Arabidopsis also has a short generation time, it will flower within a month and produce seeds in two months. Generation time can be shortened by two weeks if grown under continuous light conditions (Koornneef and Meinke, 2010). Self-fertility and large numbers of progeny allows the maintenance of genetic stocks and the analyses of genetic inheritance. The small genome (125 megabase pairs) and the number of chromosomes (n =5) of Arabidopsis decreases labour and effort in order to clone, perform forward and reverse genetic studies, and streamlines its genetic mapping. The complete sequencing of *Arabidopsis thaliana* completed in 2000 has ushered in the era of its genomics study and drives to determine the function of its 28,000 genes in its genome (The Arabidopsis Genome, 2000).

1.1.3 Arabidopsis as a Model for Cell Wall Deposition

Arabidopsis is also a model plant to use to discover genes and proteins that play roles in a wide range of plant traits. Of particular interest are wood formation-related traits, such as cellulose and hemicellulose biosynthesis, secondary growth regulation and secondary cell wall synthesis. The inflorescence stems of Arabidopsis mimics the tree-trunk by serving as a load-bearing organ, although it is limited by undergoing incomplete secondary growth. Nevertheless, Arabidopsis inflorescence stems have been utilised in identifying genes and networks involved secondary cell wall development (Strabala and Macmillan, 2013). More specifically, genes and processes

that are responsible for xylem and fibre identity, and how cell-wall carbohydrate contents are involved in this differentiation process (Liu et al., 2014, Oda and Fukuda, 2012, Kondo et al., 2015, Kondo et al., 2014, Zhong and Ye, 1999).

In terms of cell wall research, Arabidopsis allow the identification and functional characterisation of genes that play key roles in plant cell-wall biosynthesis. The plethora of data gathered from the genome sequence of Arabidopsis complemented with powerful analytical tools, i.e., forward and reverse genetics, and functional genomics have aided cell-wall researchers in identifying specific cell-wall encoding enzymes involved in cell-wall biosynthesis (Liepman et al., 2010, The Arabidopsis Genome, 2000). For example, gain-of-function studies have demonstrated the roles of cellulose synthase-like F (CSLF) and cellulose synthase-like H (CSLH) in mixed-linkage β-glucan biosynthesis (Burton et al., 2006, Doblin et al., 2009). Additionally, studies such as the characterisation of GAUT1, a galacturonan transferase involved in pectin biosynthesis and identification of xylan biosynthetic genes such has *irx7*, *irx8*, *irx9*, and *parvus* that play functions in xylan backbone biosynthesis were identified through the availability of Arabidopsis genome sequence and subsequent functional analysis (Atmodjo et al., 2011, Zhong et al., 2005, Kong et al., 2009). Arabidopsis has also played a crucial role in defining lignin biosynthesis genes and their function. For example, the *ref* phenotype exhibited by different mutant alleles such as *ref3-1*, *ref3- 2*, and *ref3-3* which is caused by chemically induced lesions in the *C4H* gene. These mutations in the alleles result in phenotypes such as dwarfism, decreased lignin deposition and vascular collapse.

Furthermore, these mutants accumulate cinnamoylmalate instead of sinapoylmalate, a change in phenylpropanoid content that results in red fluorescence of the plant during UV-light exposure instead of blue-green found in *REF3* plants. The discovery of the *ref* phenotype has made it possible to isolate plants deficient in monolignol synthesis that is required for lignin formation (Bonawitz and Chapple, 2010). Studying monolignol synthesis pathways in Arabidopsis has yielded the discovery of a new enzyme, Caffeoyl Shikimate Esterase (CSE), an enzyme central to lignin biosynthesis. Knock-out *cse* mutants resulted in less lignin deposited compared to wild-type Arabidopsis and resulted in the accumulation of *p*-hydroxyphenyl (H) units (Vanholme et al., 2013). In addition, a systems biology approach, i.e. combining metabolomics and transcriptomics, demonstrated that certain monolignol biosynthetic genes are responsible for supplying monolignols to the phenylpropanoid pathway. In contrast, other genes in the phenylpropanoid pathway were responsible for monolignol compositional shifts, i.e. *p*-hydroxyphenyl (H), guaicyl (G), syringyl (S) units and other derivatives. Lastly, the systems approach also discovered that lignin deficiency in Arabidopsis will not produce more cellulose to compensate for the loss in lignin content of Arabidopsis (Vanholme et al., 2012). All in all, Arabidopsis continues to play an integral role in identifying genes and functional analyses of proteins that are related to plant cell-wall biosynthesis. It is, for this reason, my main focus of the cell-wall literature is based on Arabidopsis and dicot studies. However, there will be certain exceptions, where cell-wall biosynthesis genes and their products allude to monocots instead.

1.2.1 Primary Cell Walls

Plant cell walls can contain primary and secondary cell walls. Primary cell walls are typically uniform in their architecture, thin, and occur during the establishment of the wall when plant cell division occurs. Primary walls are able to resist the tensile forces derived from osmotic pressure, but exhibit enough plasticity allowing for cell expansion, an essential part of plant growth. Lastly, primary cell walls have the ability to integrate new secondary cell-wall polymers into the wall in order to provide structural integrity to the plant as it grows and to resist the forces of turgor pressure during water transport and transpiration (Albersheim et al., 2010, Cosgrove, 2005, Hamant and Traas, 2010). In terms of composition, the proportion of polysaccharides that contribute to primary cell-wall composition varies. Primary cell-walls in dicots are usually composed of approximately 25% cellulose, 25% hemicellulose, 35% pectins and 1-8% structural proteins (Cosgrove, 1997). However, the composition is not definitive for all plant tissues: for example, in monocot grasses, coleoptiles contain 60-70% hemicellulose, 20-25% cellulose and 10% pectin, while cereal endosperm walls can contain up to 85% hemicellulose. Plant primary walls, therefore, display a lot of diversity amongst species and cell types (Zeiger and Taiz, 2010).

1.2.2 Xyloglucan biosynthesis and function

Xyloglucan (XG) is an abundant hemicellulosic polysaccharide in dicot and non-grass monocot primary cell-walls. For example, XG represents approximately 20% of leaf cell-walls in dicots (Zablackis et al., 1995). This polysaccharide consists of a β-1,4-linked glucan backbone that is highly branched, containing substitutions of α-1,6-linked

xylosyl residue or side chains that are composed of xylosyl, galactosyl and fucosyl residues (Figure 1.2) (Zabotina, 2012). A new discovery demonstrated that cell-walls in the root hairs of Arabidopsis contain a previously unidentified xyloglucan consisting of both neutral and galacturonic acid-containing side chains (Peña et al., 2012). Xyloglucan was believed to be the major tether between cellulose microfibrils. However, studies by Cavalier et al. (2008) demonstrated that the double knock-out of the xylosyltransferases *XXT1* and *XXT2* lacked detectable XG and only produced slightly shorter plants compared to Col-0. Additionally, reverse genetics studies of multiple *XXT* genes showed that *XXT1* and *XXT2* are xylosyl transferases and are the main contributor to xylosylation of the glucan backbone. On the other hand, *XXT5,* a xylosyltransferase in the GT43 family, is also involved in XG biosynthesis, although its activity has yet to be demonstrated *in vivo*. Interestingly combinations to produce different knock-outs for these three transferases demonstrated that XXT1 and XXT2 have additive effects in terms of xylosyltransferase activity; also, they are much more efficient when XXT1, XXT2, and XXT5 are present (Zabotina, 2012). Also, despite XXT5 displaying no xylosyltransferase activity *in vitro*, the absence of this protein has a severe impact on XG biosynthesis (Zabotina, 2012). Therefore, the lack of XG contradicts the conventional models of the type and abundance of glycans that contribute to the primary cell-wall. However, it was recently demonstrated using solid-state nuclear magnetic resonance (SSNMR) that rhamnogalacturonan-I (RG-I) and a portion of homogalacturonan (HG) display significant interactions with cellulose microfibrils in the native primary wall

(Wang et al., 2015). Xyloglucan's role in primary cell-walls have been revised to embed with cellulose solely via polymer entanglements (Cosgrove, 2005, Wang et al., 2015).

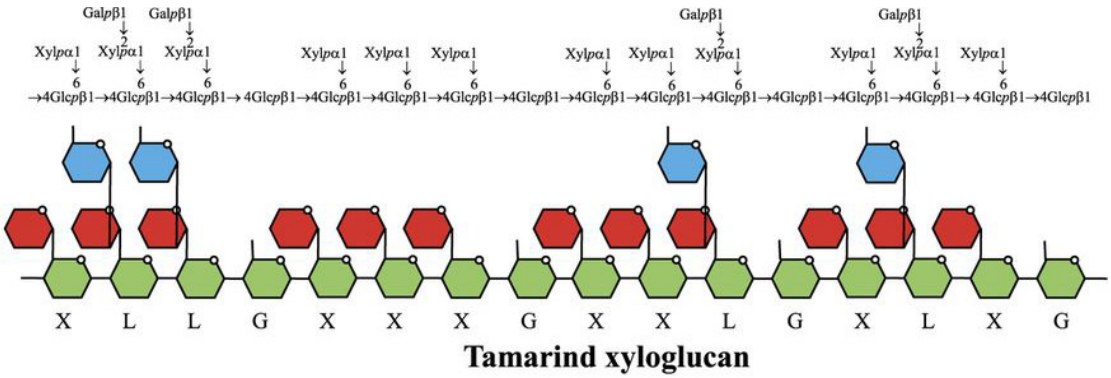

Figure 1.2: Two different depictions of xyloglucan structure extracted from tamarind (*T. indica*). Adapted from Ravachol et al. (2016)

1.2.3 Pectin biosynthesis and function

Pectin polysaccharide are abundant in the primary cell-walls of eudicot plant species and can even comprise up to one-third of the non-water mass of the primary cell wall (Somerville et al., 2004). However, their abundance is much lower in secondary walls in which other secondary cell wall polysaccharides and phenolics are deposited after plant cells cease growth (Vogel, 2008). Pectins were generally classified into so-called 'domains' including homogalacturonan (HG), xylogalacturonan, apiogalacturonan, rhamnogalacturonan-I (RG-I) and rhamnogalacturonan-II (RG-II) (Atmodjo et al., 2013).

HG is said to be the most abundant form of pectin found in the primary walls of eudicot plants, with 50–70% of recoverable pectins from the primary cell-walls of Arabidopsis (Figure 1.3) (Zablackis et al., 1995). This polysaccharide is composed of unbranched α-1,4-linked galacturonic acid (GalA) chains that can be substituted with xylose to form xylogalacturonan, apiose to form apiogalacturonan, and acetylated with

acetyl groups located at the O2 and O3 positions of GalA (Atmodjo et al., 2013). Additionally, the carboxyl groups of GalA residues in HG can be methyl-esterified. The methyl- and de-methyl-esterification status can significantly alter the chemistry rheology, charge, and pH of HG (Levesque-Tremblay et al., 2015). RG-I is the second-most abundant form of pectin that possesses a backbone of alternating rhamnose (Rha) and GalA subunits that are decorated with arabinogalactan, arabinan, and galactan side chains (Figure 1.3). Lastly, RG-II is the most structurally complex pectin domain and consists of an HG-like GalA backbone that is modified with four different side chains; these side chains can include 12 different monosaccharide constituents (Figure 1.3). Side chain A contains apiose residues capable of forming borate diester linkages to crosslink RG-II molecules that allows generating RG-II dimers (Funakawa and Miwa, 2015)

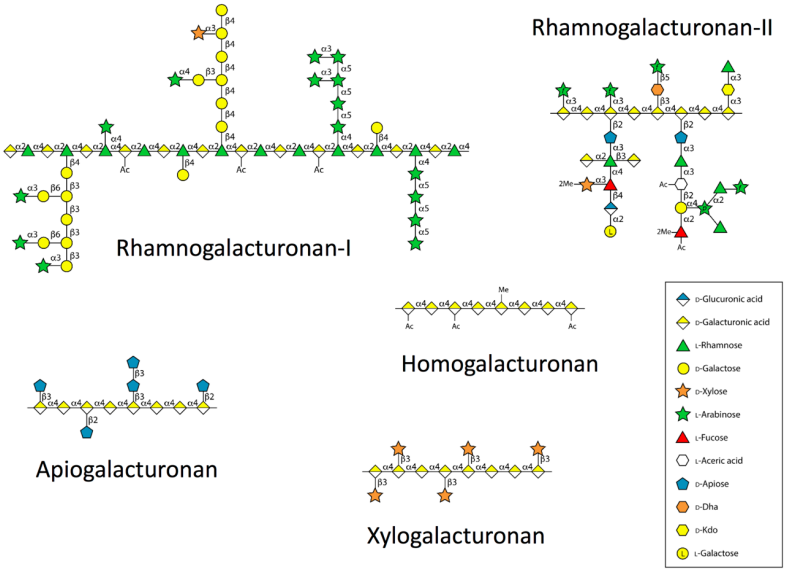

Figure 1.3: Structures of the main pectin cell-wall polysaccharides: homogalacturonan (HG) (top), rhamnogalacturonan-II (RG-II) (middle), and rhamnogalactan-I (RG-I) (bottom). A-D represents the four distincts side chains of RG-II. Taken from (Urbanowicz, 2019)

1.3.1 Secondary Cell Wall

In contrast to primary cell-walls, secondary cell-wall deposition occurs during the cessation of cell expansion that is associated with primary cell-walls. When the primary plant cell wall has reached cessation of expansion, the cell still retains the capacity to add layers of cell wall material at the plasma membrane. The secondary cell wall is made of three layers: S1, S2 (oriented parallel with the cell axis), and S3. This process is designated as the secondary cell wall formation (Albersheim et al., 2010). Cellulose microfibrils in secondary cell walls orient themselves in a helical formation along the cell axis that forms a microfibril angle relative to the cell axis (Figure 1.4) (Barnett and Bonham, 2004). It should be noted that microfibril angles are important delineating factors in determining plant cell wall structure. Low microfibril angles relative to the cells axis, i.e. where the angle θ is small, allow cellulose microfibrils to easily compact around the cell, resulting in an increase in stiffness that prevents trees from buckling under compressive forces. In contrast, high microfibril angles, i.e. where the angle θ is large, tend to elicit flexibility when plants encounter wind and snow (Mellerowicz and Sundberg, 2008). Additionally, plant secondary cell wall hemicelluloses and lignin also make up the major constituents of tracheary elements and fibres in wood. The formation of these tissues involves the differentiation of procambial or cambial stem cells into xylem fibres, interfascicular fibres, and tracheary elements, which include vessels and tracheids. This differentiation requires a shift in production from primary cell-wall (PCW) to secondary cell-wall (SCW) biosynthesis. This requires remodelling of the entire biosynthetic machinery by responding to transcriptomic cascades in these

tissues (Nakano et al., 2015, Taylor-Teeples et al., 2015). The completion of SCW biosynthesis also requires a shift in various cellular processes. Some these processes include reorganisation of microtubules and the shift from primary cellulose synthases (CESAs) to secondary CESAs (Watanabe et al., 2018). Further, Golgi production diverts from producing pectin and primary cell-wall hemicelluloses (e.g. xyloglucans and arabinans) to secondary cell-wall hemicellulose such as xylan and glucomannan. Finally, lignification occurs by transporting monolignols from the cytosol to the wall where they are polymerised by oxidative enzymes (Meents et al., 2018). This is results in the differentiation of xylem tracheary elements (vessels and tracheids) facilitating the transport of water and solutes between the organs of plants, while fibres provide structural support to the stem during plant growth. Vessels are then further distinguished into protoxylem and metaxylem structures. Protoxylem vessels are formed during primary stem growth and are characterised by the deposition of secondary cell walls in a helical or annular pattern. In contrast, metaxylem vessels are marked by pitted or reticulate patterns of secondary cell wall deposition. Both cells eventually undergo partial programmed cell death (PCD) by expressing xylanases and proteases, resulting in a system of hollow tubes that allow water and solute transport throughout the plant (Schuetz et al., 2013, Kubo et al., 2005). Xylary and interfascicular fibres, on the other hand, delay their PCD processes, resulting in thicker secondary cell wall formation compared to tracheary elements and extensive lignification occurs for providing structural support to the stem as it grows (Schuetz et al., 2013, Smith et al., 2013).

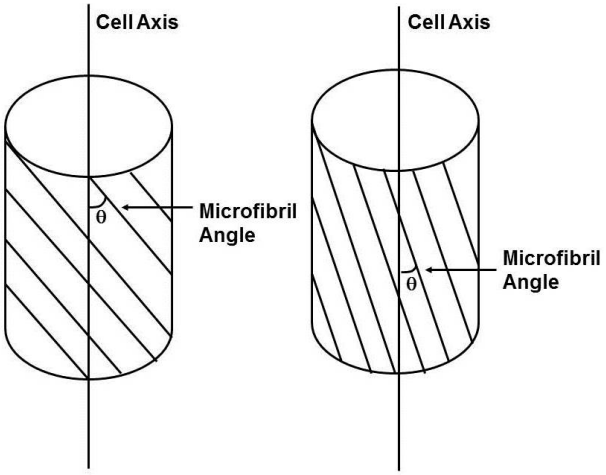

Figure 1.4: Helical arrangement of cellulose microfibrils. This pattern of cellulose microfibril deposition forms an angle relative to the cell axis. Large microfibril angles confer flexibility (left) while low microfibril angles (right) provide stiffness,

1.3.2 Structure and Composition of Secondary Cell Wall Components

The most abundant elements of secondary cell walls found in plants are cellulose, hemicellulose, and lignin, which form a composite material that bestows strength and maintains plant structure. These polymers occur in different proportions depending on the plant species and within tissues (Lee et al., 2011).

1.3.3 Cellulose Structure and Biosynthesis

Cellulose is a linear polysaccharide comprised of β-1, 4-linked D-glucopyranosyl (Glc*p*) residues and is the major load bearing component in secondary cell walls (Figure 1.5) (Zhong et al., 2019). These polymers are organised into microfibrils by intra and intermolecular forces, H-bonds, and Van der Waals forces (Van Acker et al., 2013). Cellulose is synthesised in the plasma membrane by large multimeric protein complexes resembling a hexameric rosette structure (Endler and Persson, 2011). This early model, as a result, proposed that each rosette or cellulose synthase complex (CSC), with its six

globular complexes and six subunits per complex forms 36 individual glucan chains in order to produce a cellulose microfibril (Cosgrove, 2005, Somerville, 2006, Newman et al., 2013, Fernandes et al., 2011). In *Arabidopsis thaliana*, cellulose synthase complexes are formed by specific CESA subunits. These CESA subunits are responsible for forming the rosette-like structures and are needed for catalytic synthesis of cellulose polymers. CESA4, CESA7, and CESA8 subunits are non-redundant glycosyltransferases 2 (GT2) that coalesce into rosettes that biosynthesise cellulose in secondary walls (Taylor et al., 2003, Taylor et al., 2000). Any mutations of these *CESA* genes produce a minimal effect towards the amount of secondary cell wall xylose and phenolics (Turner and Somerville, 1997, Zhong et al., 2003). Recently, however, the number of CSC subunits have been disputed to be trimeric instead of hexameric rosette structure as mentioned above by using computational analysis and experimental methods, producing an 18-glucan chain cellulose microfibril model (Nixon et al., 2016, Jarvis, 2018). Quantitative immunoblotting also demonstrated that the three Arabidopsis CESAs had equimolar stoichiometry further supporting the 18-glucan chain model (Hill et al., 2014, Nixon et al., 2016). It should also be noted that Kumar et al. (2018) demonstrated that there are different catalytic activities amongst CESA subunits resulting in different cellulose biosynthesis rates.

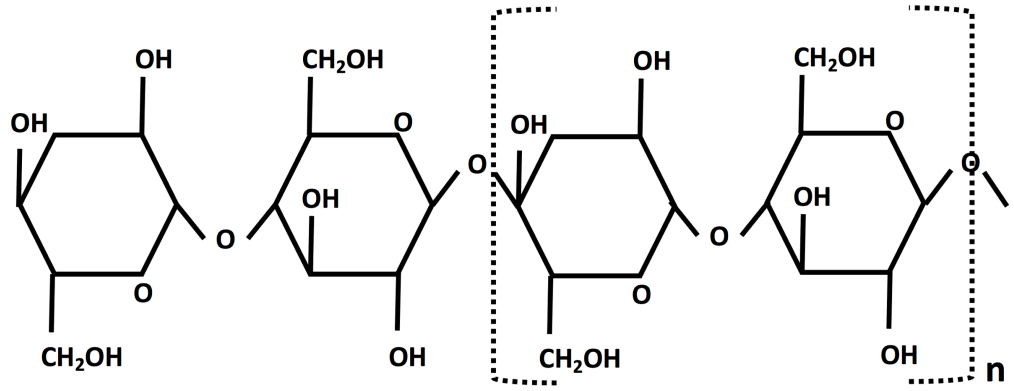

Figure 1.5 Structure of β-1,4-glucan oligomer that forms cellulose through repeating Glucose monomer units. Adapted from NCBI. PubChem Database (accessed on 30 July, 2019)

Asides from the CESA protein subunits, accessory proteins may be involved alongside the CSC for cellulose biosynthesis to occur. Examples of such accessory proteins include COBRA (COB), a glycosylphosphatidylinositol-anchored protein, and KORRIGAN (KOR1), an endo-β -1,4 glucanase. KOR1 may be involved in the release of the cellulose chain from a cellulose primer, the crystallization of the formed microfibrils, or lastly, the release of these microfibrils from the CSC attached to the plasma membrane and into the primary cell wall (Peng et al., 2002, Szyjanowicz et al., 2004, Takahashi et al., 2009). COB has been previously demonstrated to regulate cellulose biosynthesis and characterisation of the *cob-4* null allele displayed defects in anisotropic expansion in most developing organs. Additionally, this phenotype was accompanied by disorientated cellulose microfibrils as well as the subsequent reduction of crystallinity of cellulose microfibrils (Roudier et al., 2005). Other evidence points towards the COB proteins as part of defense responses to pathogenic attack through adjusting cell

growth. Using the T-DNA insertion mutants in *COB-5* followed by genomics and biochemical analysis, Ko et al. (2006) demonstrated induction of defense- and stress-related genes in a coordinated fashion occurred when *COB-5* was silenced. In *cob-5* mutants, this coordinated event was initialised and regulated by the plant stress signal jasmonic acid. In addition, mutations in *KOBITO* (*KOB*) and *CHITINASE-LIKE* (*CTL*) have been demonstrated to cause reductions in cellulose content and cellulose synthase complexes (CSC) (Pagant et al., 2002, Sanchez-Rodriguez et al., 2012, Vain et al., 2014). KOB is a single transmembrane domain protein that localises to at least three different cellular compartments: the endomembrane system, the apoplast and/or plasma membrane. Due to the conflicting localization reports, the exact function that KOB plays in cellulose biosynthesis is still unknown. Nevertheless, it was surmised that KOB may have glycosylation activities for other molecules due to distant relation to glycosyltransferases (Pagant et al., 2002).

Cellulose microfibrils made by CESA complexes are deposited around the plasma membrane of the cell and the movement of these complexes are driven by the energy produced during glucan chain polymerisation (Paredez et al., 2006). The discovery of the roles microtubules play in cellulose microfibril deposition was demonstrated by disrupting cortical microtubules using pharmacological inhibitors or genetic mutations. These resulted in altered patterning of secondary cell wall thickening and abnormal cellulose microfibril deposition (Burk and Ye, 2002, Oda et al., 2005, Wightman and Turner, 2008).

1.4.1 Xylan Structure and Biosynthesis

Hemicelluloses in secondary cell walls in angiosperms are comprised of xylans and glucomannans formed in the Golgi apparatus that are transported via vesicles to the cell walls (Lampugnani et al., 2018). They either function as cross-linkers of cellulose microfibrils in secondary cell walls or also provide the framework for other secondary cell wall components to adhere to (Smith et al., 2017). Different species of plants contain varying ratios of the hemicellulose polysaccharide. In angiosperms, they are predominantly composed of xylan, as seen in Poplar with a 24% xylan and 3% glucomannan, while gymnosperm hemicellulose is primarily composed of glucomannan [particularly galactoglucomannan] *with Pinus* wood containing 18% galactoglucomannan and 9% xylan (Zhong and Ye, 2009).

The major hemicellulose component in the secondary cell walls of angiosperms is xylan, a linear cell wall polymer that consists of a backbone made of β-(1,4)-linked xylose residues (Figure 1.6) that are typically substituted with arabinose, glucuronic acid (GlcA), and 4-*O*-methylglucoronic acid residues at varying degrees depending on the plant species (Rennie and Scheller, 2014). Xylans can also be acetylated at the C-2 and C-3 position (Busse-Wicher et al., 2014). In addition to the xylosyl backbone, some xylans contain a unique glycosyl sequence composed of 4-β-d-Xyl*p*-(1→4)-β-d-Xyl*p*-(1→3)-α-l-Rha*p*-(1→2)-α-d-Gal*p*A-(1→4)-d-Xyl*p* at their reducing end that is evolutionary conserved in herbaceous and woody plants (Pena et al., 2007). Along with cellulose and lignin, xylan is one of the main structural components in xylem vessels, facilitating the rapid movement of water while additionally maintaining its structural

integrity despite the negative pressure that occurs. On the other hand, xylans found in interfascicular fibres contribute to the thickness of the fibre cell walls allowing them to maintain mechanical support of the stem (Zhong et al., 2005, Persson et al., 2007). The importance of xylans as a major constituent of the secondary cell wall is well-emphasised by xylan deficient mutants exhibiting weakened stems (Mortimer et al., 2010).

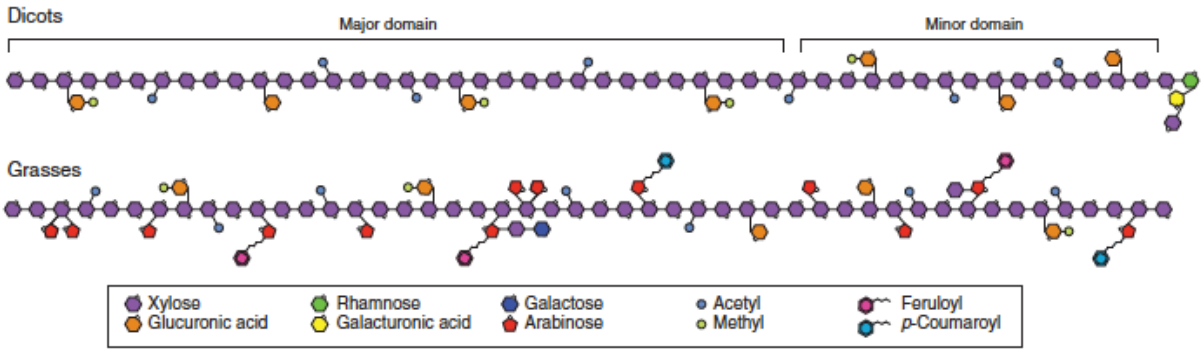

Figure 1.6: Xylan structure of dicots, with its domains, and of grasses. Adapted from Rennie and Scheller (2010).

Xylan backbone synthesis as well as attachment of its side groups occurs in the Golgi apparatus and the completed polymer is secreted using vesicles. The vesicle types employed for polysaccharide transport are dependent on the plant species, tissue type, and cell differentiation pattern (Wang et al., 2017, Wilkop et al., 2019, Okekeogbu et al., 2019, Sinclair et al., 2018). Genetic and biochemical analyses demonstrated that GT47 (IRX10/IRX10L), and non-redundant GT43 (IRX9/IRX9L and IRX14/IRX14L) proteins are responsible for xylan backbone synthesis. Arabidopsis mutants in these genes exhibited various phenotypes such as reductions in xylan content, chain length, xylotransferase activity, and reduced secondary cell wall thickening (Brown et al., 2007, Brown et al.,

2009, Pena et al., 2007). Recombinant expression of Arabidopsis IRX10 and IRX10L proteins using human embryonic kidney (HEK) 293 cells yielded xylosyltransferase activity, the transfer of Xyl-monomers from UDP-Xyl onto xylan oligomers. On the other hand, IRX9/IRX9L and IRX10/IRX10L expressed in HEK 293 cells displayed no xylosyl-transferase activity. Therefore, it has been proposed that IRX9/IRX9L and IRX14/IRX14L serve as structural proteins along with IRX10/IRX10L as the catalytic subunit in a xylan synthase complex (Urbanowicz et al., 2014, Zeng et al., 2016).

Xylan backbones in dicots are often substituted with GlcA or 4-*O*-MeGlcA residues or acetylated. Recent studies using Arabidopsis as a model have demonstrated that xylan substitution and acetylation occurs in an even spacing motif along the xylan backbone. Molecular dynamics simulations have suggested that the glycosyl substitution and acetylation occurring in the backbones of gymnosperm and angiosperm xylans play a role in stabilising its conformational transition from a threefold screw in solution to a two-fold helical structure when attached to cellulose microfibrils (Martinez-Abad et al., 2017, Simmons et al., 2016). Furthermore, it was recently demonstrated using sold-state NMR that lignin polymers preferentially bind to xylans in either a 3-fold or distorted 2-fold helical screw conformations and have particularly tight contacts with S-lignin. This implies that lignin does not serve as the “glue” holding cellulose and xylans together under the conventional views of lignocellulose complexes. Rather, lignin binds with well-hydrated xylans with uneven polymer conformations via electrostatic forces between lignin methyl esters and sugar polar groups. Unlike previous models where lignin-cellulose interactions are thought to occur frequently,

ssNMR data only detected minor lignin-cellulose interactions. Therefore a proposed updated model is that lignin-cellulose interactions are mediated through contacts with xylans (Kang et al., 2019).

1.5.1 Lignin Biosynthesis and Structure

Lignin is an aromatic polymer composed of 4-hydroxyphenylpropanoids imparting rigidity to secondary cell walls and is also part of the response to biotic and abiotic stresses, i.e. wounding, pathogen attack and cell wall perturbations (Bonawitz and Chapple, 2010, Gallego-Giraldo et al., 2018). Coniferyl, sinapyl and *p*-coumaryl alcohol are monolignols that are the building blocks of lignin and once incorporated into the growing polymer, are termed guaiacyl (G), syringyl (S) and *p*-hydroxyphenyl (H) units respectively (Figure 1.7). These units are synthesised in the cytosol from phenylalanine that originates from the shikimate pathway and then undergo further modification to produce 4-hydroxyphenylpropanoids (Boerjan et al., 2003, Liu, 2012, Vanholme et al., 2010). Once these phenylpropanoids are synthesised, they are deposited into the layers of the secondary cell wall subsequent to carbohydrate deposition.

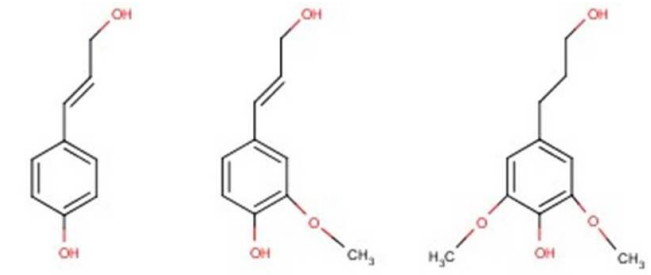

Figure 1.7: Lignin Subunits. Adapted from Vanholme et al. (2010).

The transport of lignin monomers is achieved by passive diffusion and/or through active transport by ATP-binding cassette (ABC) transporters localised in the plasma membrane (Kaneda et al., 2008). Experiments have shown in Arabidopsis that the ABC transporter AtABCG29 exhibits transport of *p*-coumaryl alcohol in yeast cells *in vitro* (Miao and Liu, 2010, Alejandro et al., 2012). However, it is interesting that wild-type Arabidopsis do not normally transport *p*-coumarylated monolignols, yet possess the aforementioned transporter. Moreover, *p*-coumaryl alcohol transporters from grasses that were heterologously expressed in Arabidopsis allow these monomers to be incorporated into its cell wall (Sibout et al., 2016). Thus, it is still unclear how monolignols are transported across the plasma membrane of the cell. Once monolignols are deposited in the cell-walls, these monomers can either be oxidised by laccases or peroxidases to form monolignol radicals (Berthet et al., 2011). Subsequently, these monolignol radicals are then polymerised through non-enzymatic radical coupling (Bonawitz and Chapple, 2010). Monolignol polymerisation involves the action of peroxidases and or laccases, enzymes that belong to large gene families with overlapping activities (McCaig et al., 2005). Laccases and peroxidases, however, differ in substrate specificity during their redox activities using hydrogen peroxide and oxygen respectively (Wang et al., 2013). These enzymes differ in activation during plant development as well: laccases are said to polymerise monolignols into oligolignols during early stages of lignification; on the other hand, cell wall peroxidases are generated during late-stage xylem formation or during abiotic stresses (Sterjiades et al., 1993)

Lignin accumulation primarily occurs at the corners of the middle lamella and at the primary cell wall during the formation of the S1 layer (secondary cell-wall layer that forms on top of the primary cell-wall). Lignification at the S2 layer (middle layer) occurs once the polysaccharide matrix has been formed. Finally, after the majority of the cellulose and hemicellulose polysaccharides are deposited into the inner (S3) (towards the lumen) layer, lignin polymers concentrate in this layer by attaching to hemicellulose. Subunits of lignin are also incorporated in a coordinated manner (Boerjan et al., 2003). Typically, *p*-hydroxyphenyl (H) units are initially deposited, and then subsequently followed by guaiacyl (G) units and syringyl (S) units (Rencoret et al., 2011). The proportion of individual lignin subunits that make up the wall localised polymer vary amongst different plant species. Secondary cell-walls in angiosperms contain lignin predominantly comprised of G and S lignin units, while the lignin produced by gymnosperms is composed of primarily G lignin. Moreover, lignin differs in cell types of a plant species as well; in *Arabidopsis*, secondary wall vessels are predominantly lignified with G units whereas its fibres are composed of G and S units (Vanholme et al., 2010).

Studies have revealed that lignification proceeds in a combinatorial manner and varies depending on the plant tissue where the lignin is deposited. As mentioned, once transport and deposition in the cell wall occur, monolignols undergo dehydrogenation to produce radicals that are stabilised via resonance structures (Figure 1.8) (Liu, 2012). Subsequently, the radicalised phenols then couple to form a dimer with a covalent bond between the monomers (Vanholme et al., 2010). This coupling happens in a

combinatorial fashion and depends mostly on the chemical nature of each of the monomers and on apoplastic conditions (Ralph, 2010). Dehydrogenation polymers (DHP) to produce synthetic lignin have been employed to support the combinatorial mechanism of lignification. The Zulauf (bulk method) and Zutropf (dropwise method) of adding monolignols have different effects on bonding propensity, the latter produced near *in vivo* bonding patterns as compared to the former (Hatfield and Vermerris, 2001). These studies provided clear evidence that it is only the rate of transfer of monolignols that is needed to mimic monolignol polymerisation and lignin deposition *in vivo*, whilst at the start of polymerisation, dimerisation needs to occur. The stereospecific formation of a pinoresinol dimer from β-β bonding of monolignols may cause the random coupling mechanism to come into question and resulted in the alternative proposal that lignin polymerisation is template driven (Davin and Lewis, 2000, Ralph, 2010). However as noted by the review of Ralph (2010), even though such dimerization cannot occur in a random fashion, what causes dimerization are: relative energies of the transition states and pH, solvent polarity, temperature, etc.; and any change in these states will cause alterations in dimerisation. Therefore, lignin polymerisation occurs in a "combinatorial" fashion instead of at random. Recent studies have also supported lignification in a combinatorial manner. A systems approach by Vanholme et al. (2012) showed that despite a majority of lignin gene mutants displaying no visible phenotypes, their metabolomics analyses revealed that mutants producing less lignin upregulated specific shikimate, methyl-donor, and phenylpropanoid pathways. By contrast, lignin compositional mutants induced down-regulation in the same phenylpropanoid

pathways. More importantly, any flux in the lignin levels induced various classes of 4-*O*- and 9-*O*-hexosylated phenylpropanoids. This system-wide approach further supports a model involving a combinatorial method of synthesis and supports the plasticity by which the plant cell wall is lignified (Vanholme et al., 2012).

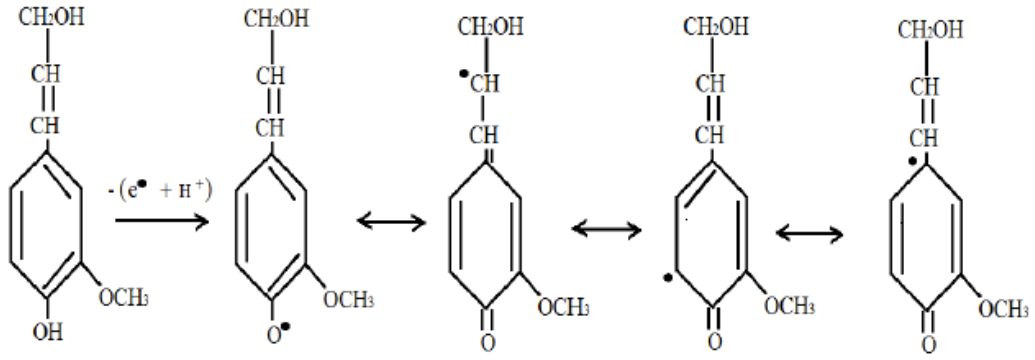

Figure 1.8: Resonance structures of lignin monolignols that produce radicals (dots) for stabilisation. Adapted from Nasir et al. (2015)

1.6.1 Arabidopsis Secondary Cell Wall Transcription Network

Secondary cell wall biosynthesis is highly regulated by a large array of transcription factors (TFs) using hierarchical and non-hierarchical regulatory networks (Figure 1.8) (Hussey et al., 2011). These networks are divided into three tiers. Tier 3 contains transcription factors with *NAC (NO APICAL MERISTEM, ATAF1/2, and CUP-SHAPED COTYLEDON*) domains. Tier 2 are MYB domain regulators and Tier 1 are TFs directly involved in SCW biosynthesis (Hussey et al., 2013).

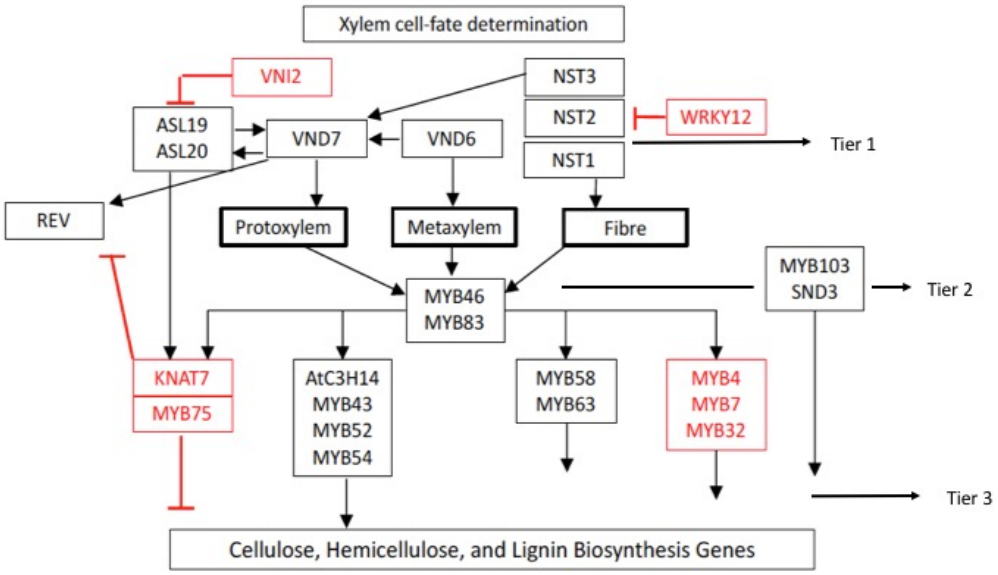

Figure 1.9: Secondary cell-wall transcriptional pathway showing complexity and spatiotemporal specificity. Black arrows and red lines depict positive and negative regulation respectively. Adapated from Ko et al., 2014

1.6.2 Arabidopsis Xylary Fibre-Specific Cell-Wall Transcription Factors

Formation of the secondary cell-wall of xylary fibre cells, which develop thick evenly deposited secondary cell-wall, is a result of delayed PCD in order to allow for more extensive thickening and lignification of the secondary cell wall. The main NAC domain TFs/master regulators that control cellulose, hemicellulose, and lignin biosynthesis in xylary fibre cells are encoded by the following genes: *NAC SECONDARY WALL THICKENING PROMOTING FACTOR 1* (*NST1*), *NST2*, and *NST3/SECONDARY WALL-ASSOCIATED NAC DOMAIN PROTEIN 1* (*SND1*) (Zhong et al., 2006, Mitsuda et al., 2007). Arabidopsis knockout lines in these TFs displayed almost no secondary cell wall deposition in fibre cells (Mitsuda et al., 2007, Zhong et al., 2005). In contrast, their overexpression led to ectopic deposition of secondary cell wall biopolymers in a variety

of tissues. It is also worth noting that *REV/IFL1*, a member of class III homeodomain-leucine zipper (HD-ZIP III) TFs is known to initiate interfascicular fibre SCW depostion in Arabidopsis inflorescence stems (Zhong and Ye, 1999, Liu et al., 2014, Lev-Yadun et al., 2004). Similarly, functional characterisation of *rev* t-DNA insertional mutants demonstrated that *rev* loss-of-function mutants had reduced secondary cell wall deposition in interfascicular fibres and a reduced number of xylary fibre cells per vascular bundle (Liu et al., 2014).

1.6.3 Arabidopsis Vessel-Specific Cell Wall Transcription Factors

Formation of the secondary cell walls of xylem vessels, which are vascular tissues that appear at plant maturity and when primary growth ceases. Vessels, consisting of metaxylem TEs, possess SCW patterning in a pitted manner that prohibits continued cell elongation. In contrast, protoxylem TEs possess a helical SCW arrangement, allowing for a limited degree of continued cell elongation (Schuetz et al., 2013). Vessel cell-wall formation as compared to fibre cell-wall formation, is controlled by *VASCULAR-RELATED NAC DOMAIN* TFs, by regulating both SCW biosynthesis and PCD. In Arabidopsis roots, specifically, ectopic expression of *VND6* and *VND7* triggers metaxylem and protoxylem formation respectively (Kubo et al., 2005, Yamaguchi et al., 2010). This was achieved by upregulating secondary cell-wall biosynthesis or PCD genes containing the tracheary-element-regulating *cis*-element (TERE) sequences in their promoter sequence. For instance, plants overexpressing *VND6* displayed phenotypic characteristics resembling metaxylem-like patterning in roots and hypocotyls (Kubo et al., 2005). Numerous secondary cell wall biosynthesis genes have been reported to be induced by *VND6*. For

instance, Arabidopsis *VND6-YFP* suspension cells demonstrated the upregulation of secondary cell-wall cellulose biosynthetic genes *IRX5*, *IRX3*, and *IRX1* (Ohashi-Ito et al., 2010). On the contrary, Yamaguchi et al. (2010) demonstrated an increase in xylose content with no significant changes in other cell wall monosaccharides using a dexamethasone (DEX) inducible *VND6-VP16-GR* and *VND7-VP16-GR* system in transgenic Arabidopsis seedlings. Furthermore, aside from demonstrating an increase in xylan content, these transgenic lines display an upregulation of *IRX10* expression upon DEX application. These results suggest that *VND6* and *VND7* are able to induce expression of genes involved in secondary cell-wall biosynthesis including those specific for xylan and cellulose deposition to the wall. Further, *VND6* and *VND7* also activate a broad range of PCD genes, for example, xylem-specific papain-like cysteine peptidase (*XCP1)* (Yamaguchi et al., 2011). Despite advances towards the functional characterisations of these vessel specific transcription factors, there is still little known about identifying regulators upstream of *VND6* and *VND7* (Hussey et al., 2013). However, recent progress has been made towards identifying upstream regulators of *VND6* and *VND7*. By using a yeast-one hybrid approach, Taylor-Teeples et al. (2015) discovered that At*E2Fc* is a transcription factor upstream of *VND6* and *VND7*. At*E2Fc* normally functions as a negative regulator during endoreduplication, however in the context of regulating *VND6* and *VND7* activity, it acts as either a transcriptional activator or repressor for *VND6* and *VND7* in a dosage-dependent manner.

Tier 2 regulators of SCW biosynthesis act downstream of the NAC domain tier 3 regulators. In Arabidopsis, these are MYB TFs such as *MYB46* and *MYB83* (Zhong et al., 2007, Zhong and Ye, 2012). Studies have demonstrated that *SND1*, a tier 1 regulator binds to *MYB46* downstream thereby activating its expression (Zhong et al., 2007). *VND6* and *VND7* have also been shown to directly target these MYBs, demonstrating their role in SCW formation in both xylary vessels and fibres (Ohashi-Ito et al., 2010, Yamaguchi et al., 2011). Other MYB and NAC domain TFs act downstream of tier 1 and tier 2 regulators and are known as tier 3 TFs. Tier 3 TFs include the following genes: *SND2, SND3,* and *MYB103* that are able to directly induce cellulosic biosynthesis genes in fibres (Zhong et al., 2008, Hussey et al., 2011), In contrast, *MYB52* and *MYB54* possess the ability to induce the expression of genes that are responsible for cellulose, hemicellulose, and lignin biosynthesis (Zhong et al., 2008, Zhou et al., 2009). Finally, these tier 3 TFs were demonstrated to be under the control of both upstream tier 1 master regulators and tier 2 regulators (Zhong et al., 2008, Zhong and Ye, 2014).

1.7.1 Cell Type-specific Cell Wall Deposition in Arabidopsis

Because transcriptional control of secondary cell wall (SCW) biosynthesis is a highly coordinated process, it is expected that particular cell wall-related events are based on controlling the activities of specific sets of cell wall-related genes in a tissue- or temporal-dependent manner. In turn, this may account for observing the differences in polysaccharide composition occurring during SCW deposition throughout plant development and in the different cell types. For instance, studies in Arabidopsis

demonstrated that the neutral sugar compositions of cell walls vary across different tissues such as stems, leaves, and roots (Sarkar et al., 2009, Rancour et al., 2012). Immunolabelling with plant cell wall glycan-directed monoclonal antibodies (mAbs), also provided examples of the spatial and temporal distribution of cell wall polysaccharides. Studies employing the mAb LM16 was used to examine arabinan heterogeneity within stem tissues of Arabidopsis (Burton et al., 2010, Verhertbruggen et al., 2009). Likewise, studies using the mAb CCRC-M1 demonstrated that additional fucosyl substituents to xyloglucan occurs in a cell-type and developmental stage-dependent in Arabidopsis (Freshour et al., 2003). Finally, the use of LM15 and LM21 mAbs revealed the heterogeneity of xyloglucan distribution in tomato fruit parenchyma and mannan epitope patterning in parenchyma cells of tobacco stem pith respectively (Lee et al., 2011, Burton et al., 2010, Marcus et al., 2010, Ordaz-Ortiz et al., 2009).

Other approaches have also provided further evidence of compositional heterogeneity existing within the cell wall structure. High-Performance Liquid Chromatography (HPLC) and Nuclear Magnetic Resonance (NMR) spectrometry showed that the cell wall composition, particularly the content of arabinoxylan and ferulic acid, varies during wheat seedling development (Obel et al., 2002). Oligosaccharide Mass Profiling (OLIMP) demonstrated that the outer layer and inner layer of epidermal tissues of Arabidopsis leaves possess distinct levels of xyloglucan galactosylation and xyloglucan fucosylation, respectively. More specifically, opposing sides of the epidermal cells in Arabidopsis leaves possess distinct xyloglucan substitution (Obel et al., 2009). *gxmt1-1* mutants and WT influorescence stems of Arabidopsis showed distinct patterns 4-*O*-

MeGlcA substituted glucuronoxylan (GX) distribution in the vascular bundles based on promoter studies and labelling with carbohydrate binding modules (Urbanowicz et al., 2012). Lastly, glycome profiling has proven invaluable in determining the alterations of cell-wall epitope composition and organisation during plant growth in switchgrass (*Miscanthus x giganteus*) (Crowe et al., 2017).

1.8.1 Using Plant Glycan-directed Monoclonal Antibodies as Tools for High-resolution Analysis of Cell Wall Polysaccharides

As previously mentioned, the analysis of the Arabidopsis genome suggested that around 15% of the genes are estimated to be devoted to plant cell-wall biosynthesis and modification (Carpita et al., 2001). Furthermore, it was previously mentioned that the cell-wall structural complexity combined with the heterogeneity in polysaccharide composition between cells of different tissues make plant cell-wall characterisation and analysis challenging, especially using high-throughput methodologies. Further, most experimental approaches relevant to plant cell-wall analysis are time-consuming, require specialised training and equipment, and still result in low-throughput outcomes.

Despite the availability of analytical methods for determining plant cell-wall composition, we still lack a comprehensive high-resolution cell-wall atlas of different cell types, particularly with regard to the vascular cells in Arabidopsis. Particularly, the compositional differences between differentiated cells from the vascular bundle and interfascicular region and the corresponding changes in wall composition throughout a developmental gradient have not been thoroughly investigated. Previous research has indicated differences in xylan and lignin composition (Corea et al., 2012, Urbanowicz et

al., 2012) between these two tissues, but a comprehensive inventory of the changes in non-cellulosic matrix cell wall glycans derived from different tissues throughout development in Arabidopsis is yet to be available. To develop an atlas based on the known structural and compositional heterogeneity existing in the plant cell-walls of Arabidopsis, immunological approaches like plant cell-wall directed monoclonal antibodies (mAbs) are appropriate and powerful methods in order to determine the structure and composition of non-cellulosic matrix polysaccharides, largely due to their monospecificity and high affinity (K_d ~ 10^{-6} M) in recognising specific plant glycan epitopes. In relation to the monospecific epitope recognition nature of mAbs, recent advances in deciphering the specific plant glycan epitope structures recognised by plant glycan-directed mAbs particularly for xylan and arabinogalactan structures, providing an even more invaluable resource of relevance for plant cell-wall studies (Table 1.1) (Ruprecht et al., 2017, Schmidt et al., 2015, Pattathil et al., 2010).

Table 1.1: Selection of commonly used antibodies from different glycan groups (homogalacturonan [HG], rhamnogalacturonan [RG-I], xyloglucan [XG], and xylan) and their corresponding recognised epitope structure.

	mAb	Epitope	Source	Reference
Homogalactouronan	JIM5		Rat	Knox et al., 1990; Willats et al., 2000; Clausen et al., 2003
	JIM7	HG with high DE	Rat	Knox et al., 1990; Willats et al., 2000; Clausen et al., 2003
	CCRC-M134		Mouse	Pattathil et al., 2010
	CCRC-M130 CCRC-M38	Unesterified HG DP > 5	Mouse	Pattathil et al., 2010
RG-I	CCRC-M60	Rhamnogalactouronan I and AGP	Mouse	Pattathil et al., 2010
	CCRC-M14 CCRC-M35 CCRC-M36 CCRC-M69	Rhamnogalactouronan I backbone		Ruprecht et al., 2017
	CCRC-M2	Rhamnogalactouronan Ia	Mouse	Pattathil et al., 2010
	CCRC-M7	6-linked β-D-galactan with at least three Gal units at the non-reducing end	Mouse	Pattathil et al., 2010
	CCRC-M11 CCRC-M12 CCRC-M15	Arabinogalactan epitope on RG-I and AGP	Mouse	Pattathil et al., 2010
Xyloglucan	CCRC-M86 CCRC-M100 CCRC-M103	Xyloglucan chain, with non-Glc residue near reducing end	Mouse	Ruprecht et al., 2017
	CCRC-M93 CCRC-M95 CCRC-M96 CCRC-M101 CCRC-M104	Xyloglucan with Gal substitution	Mouse	Dallabernadina et al., 2017
	CCRC-M1	Xyloglucan with terminal α-(1,3)-Fuc		
Xylans	LM10	(1-4)-β-D-xylan	Rat	Ruprecht et al., 2017
	LM11	(1-4)-β-D-xylan/arabinoxylan with high tolerance of backbone substitutions	Mouse	Ruprecht et al., 2017
	CCRC-M147 CCRC-M149 CCRC-M140 CCRC-M160 CCRC-M137 CCRC-M139 CCRC-M152	(1-4)-β-D-xylan with low tolerance for backbone substitutions	Mouse	Ruprecht et al., 2017
	CCRC-M150	(1-4)-β-D-xylan with GlcA substitution	Mouse	Ruprecht et al., 2017
	CCRC-M144 CCRC-M145 CCRC-M146 CCRC-M155	(1-4)-β-D-xylan with 4-O-MeGlcA substitution	Mouse	Ruprecht et al., 2017

An example of using an immunological approach to survey plant cell wall glycan composition, structure, dynamics, and function at a high-throughput scale is glycome profiling. Glycome profiling involves the sequential extraction of plant cell wall material followed by screening of the extracts with plant glycan-directed mAbs. Screening procedures can be performed using either enzyme-linked immunosorbent assay (ELISA) methods, (Pattathil et al., 2012) or through a dot-blot assay system termed comprehensive microarray polymer profiling (CoMPP) (Moller et al., 2007). Because of the current worldwide collection of over 200 mAbs that are available (Pattathil et al., 2010), these immunological-based techniques are useful in numerous experimental approaches by providing detailed information on the epitope composition and overall structure of cell walls based on the characterised glycan epitope structures recognised by specific mAbs (see Table 1.1 and Ruprecht et al., 2017). Furthermore, glycome profiling approaches can reveal the degree of integration of the various polysaccharide structures that are embedded into the cell wall.

While glycome profiling provides a moderate to a high-throughput comprehensive picture of the glycan epitope composition of the cell-wall, it has limitations that need to be addressed. Glycome profiling relies on wall fractionation using increasingly harsh reagents to be performed prior to the ELISA- or dot-blot-based analysis. This results in sequential fractionation, with specific wall-bound glycans being released depending on the type of glycan and the level of harshness of the extractive reagent. For example, ammonium oxalate and carbonate are mild reagents that typically release pectin epitopes bound to the wall. Conversely, 4M KOH is a harsh

reagent that is able to release tightly-bound xylan epitopes (Pattathil et al., 2012). The sequential extractions mentioned, however, are not epitope exclusive reagents, resulting in each extract containing diverse subclasses of glycans depending on the degree to which they are cross-linked to the cell-wall (Pattathil et al., 2015, Peralta et al., 2017). Additionally, this extraction process results in the loss of information regarding the distribution and cellular localisation of glycan epitopes. Glycan epitopes may be lost or are modified by the harsh chemicals during the fractionation process (Pattathil et al., 2012). In relation to this, it is important to note that positive binding observed does not unambiguously infer the presences of the specific glycan polymer. Glycans are repetitive in nature and are located in multiple macromolecular contexts, (e.g. arabinogalactan epitopes present in glycoproteins and rhamnogalacturonan I [RG-I]). Thus, interpreting positive mAb signals can result in ambiguity. Additionally, cross-reactivity may result in false positives to ELISA OD readings (e.g. CCRC-M1 binds strongly to a terminally α-(1,2)-linked fucose residue and moderately to RG-I epitopes; CCRC-M114 binds to epitopes found in the Xylan-4 clade and to galactose epitopes) (Puhlmann et al., 1994, Ruprecht et al., 2017). On the contrary, an absence of binding with a particular mAb glycan probe cannot conclusively determine that its corresponding epitope is not present. This is because the epitope may either be absent or chemically modified (either acetylated or methylated) resulting in the failure of the mAb to bind despite its corresponding glycan epitope being present (Pattathil et al., 2012, Pattathil et al., 2015). Finally, absolute quantification of cell-wall epitope composition using this approach has proven limited. There are several reasons for this

limitation. First, complete extractions rarely occur, which results in unknown amounts of glycans remaining within the solid residue left behind after sequential extractions. Second, since we cannot perform complete extractions, serial dilutions of the extracts cannot be accomplished. Thirdly, this in turn means that a sigmoidal curve of OD vs fluorescence cannot be graphed, resulting in the inability to derive glycan epitope quantities from the linear region of the sigmoidal curve and determining its EC_{50}. Thus, when employing a glycome profiling-based approach for cell-wall analysis comparative studies (mutant vs. wild-type or pretreated vs. untreated) are required because they provide important information regarding the changes in cell-wall epitope composition from a specific experimental manipulation (Pattathil et al., 2012, Pattathil et al., 2015).

Because of the aforementioned limitations, it is important that glycome profiling be complemented using immunohistochemistry to ascertain the localisations of epitopes *in situ*. This technique involves fixing and embedding biomass (either in plastic resins or paraffin wax), applying primary probes on semithin sections and subsequently probing with a fluorescently tagged secondary antibody in order to visualise glycan epitope localisation/distribution *in situ* under a fluorescent microscope (Avci et al., 2012, Pattathil et al., 2015). Aside from the visualisation of the *in situ* distribution glycan epitopes, immunolocalisation techniques are highly compatible for monitoring the structure and epitope composition along developmental gradients that exist in plant tissues. Immunolocalisation is also advantageous by minimising modifications of plant glycan epitopes, resulting in a fairly complete snapshot of the epitope distribution across cell types and tissues *in vivo*.

As with glycome profiling, limitations exist when performing immunohistochemical techniques. *In situ* visualisation is often laborious, requiring the need to narrow down the selection of mAbs used. Secondly, due to the *in situ* nature of the method, other wall components may limit the antibody's access to its epitope, producing a false negative result (Avci et al., 2012). Comparative studies on the different plant sample preparations methods and cell-wall immunolocalisation techniques were performed by Verhertbruggen et al. (2017) and determined that embedding plant tissue or organ samples in wax followed by sectioning them using a microtome were the best options to visualise glycan epitope distribution *in situ*. However, the study failed to account that the required de-waxing step prior to immunolocalisation exposes an additional axis plane (z-axis) which further complicates the analyses as compared to London Resin (LR) white resin sections that only expose epitopes at the surface (x and y-axis) (Michael Hahn, personal communication).

1.9.1 Summary of the Studies Described in This Thesis

The work performed during my tenure as a graduate student involved the development of methodologies to survey the differences in secondary cell-wall glycan epitope at a developmental and at a cell type/population-specific resolution. My primary hypothesis is that plant cells serve different functions and at differentiation events, it is therefore likely that glycan composition is heterogeneous based on its location and developmental stage. Therefore, monitoring the changes in glycan epitopes occurring at different cell types and differentiation stages would prove to be an invaluable tool that is potentially transformational in terms of the way we view the

cell biology of wall metabolism in plants. Recent epitope characterisation of xylan-directed mAbs using automated glycan synthesis provides a library of glycan epitope structures specifically recognised by their corresponding mAbs.

In our first study, studies incorporating GP techniques, *in situ* visualization, and integrating the resulting data with xylan biosynthesis gene expression information demonstrated this to be a powerful approach to study the patterning of xylan deposition in different stages of stem development. The information from our first study led us to investigate the possibility of developing a method of glycome profiling at a cell-type specific resolution. Our aims were to develop a reproducible and reliable method to survey plant cell wall glycans from different cell types/populations. If so, we would further our results by investigating any glycan epitope changes at distinct differentiation events of vascular and fibre cells. The probing of glycan epitope changes from different cell types and differentiation offers a powerful tool for understanding gene function and associated regulatory processes. Through the use of Arabidopsis and t-DNA mutations on vessel-specific master regulators, we hoped to understand the dynamics of glycan epitopes as certain cell types diffentiate. In relation we would like to examine whether or not changes in glycan epitope patterns in specific cell types affect its shape and structure.

1.10.1 References

ALBERSHEIM, P., DARVILL, A., ROBERTS, K., SEDEROFF, R. & STAEHELIN, A. 2010. *Plant Cell Wall,* New York City, Garland Science.

ALEJANDRO, S., LEE, Y., TOHGE, T., SUDRE, D., OSORIO, S., PARK, J., BOVET, L., LEE, Y., GELDNER, N., FERNIE, A. R. & MARTINOIA, E. 2012. AtABCG29 is a monolignol transporter involved in lignin biosynthesis. *Curr Biol,* 22**,** 1207-12.

ATMODJO, M. A., HAO, Z. & MOHNEN, D. 2013. Evolving views of pectin biosynthesis. *Annu Rev Plant Biol,* 64**,** 747-79.

ATMODJO, M. A., SAKURAGI, Y., ZHU, X., BURRELL, A. J., MOHANTY, S. S., ATWOOD, J. A., 3RD, ORLANDO, R., SCHELLER, H. V. & MOHNEN, D. 2011. Galacturonosyltransferase (GAUT)1 and GAUT7 are the core of a plant cell wall pectin biosynthetic homogalacturonan:galacturonosyltransferase complex. *Proc Natl Acad Sci U S A,* 108**,** 20225-30.

AVCI, U., PATTATHIL, S. & HAHN, M. G. 2012. Immunological approaches to plant cell wall and biomass characterization: immunolocalization of glycan epitopes. *Methods Mol Biol,* 908**,** 73-82.

BARNETT, J. R. & BONHAM, V. A. 2004. Cellulose microfibril angle in the cell wall of wood fibres. *Biol Rev Camb Philos Soc,* 79**,** 461-72.

BERTHET, S., DEMONT-CAULET, N., POLLET, B., BIDZINSKI, P., CEZARD, L., LE BRIS, P., BORREGA, N., HERVE, J., BLONDET, E., BALZERGUE, S., LAPIERRE, C. & JOUANIN, L. 2011. Disruption of LACCASE4 and 17 Results in Tissue-Specific Alterations to Lignification of Arabidopsis thaliana Stems. *Plant Cell,* 23**,** 1124-1137.

BOERJAN, W., RALPH, J. & BAUCHER, M. 2003. Lignin biosynthesis. *Annu Rev Plant Biol,* 54**,** 519-46.

BONAWITZ, N. D. & CHAPPLE, C. 2010. The genetics of lignin biosynthesis: connecting genotype to phenotype. *Annu Rev Genet,* 44**,** 337-63.

BROWN, D. M., GOUBET, F., VICKY, W. W. A., GOODACRE, R., STEPHENS, E., DUPREE, P. & TURNER, S. R. 2007. Comparison of five xylan synthesis mutants reveals new insight into the mechanisms of xylan synthesis. *Plant Journal,* 52**,** 1154-1168.

BROWN, D. M., ZHANG, Z. N., STEPHENS, E., DUPREE, P. & TURNER, S. R. 2009. Characterization of IRX10 and IRX10-like reveals an essential role in glucuronoxylan biosynthesis in Arabidopsis. *Plant Journal,* 57**,** 732-746.

BURK, D. H. & YE, Z. H. 2002. Alteration of oriented deposition of cellulose microfibrils by mutation of a katanin-like microtubule-severing protein. *Plant Cell,* 14**,** 2145-2160.

BURTON, R. A., GIDLEY, M. J. & FINCHER, G. B. 2010. Heterogeneity in the chemistry, structure and function of plant cell walls. *Nat Chem Biol,* 6**,** 724-32.

BURTON, R. A., WILSON, S. M., HRMOVA, M., HARVEY, A. J., SHIRLEY, N. J., MEDHURST, A., STONE, B. A., NEWBIGIN, E. J., BACIC, A. & FINCHER, G. B. 2006. Cellulose synthase-like CslF genes mediate the synthesis of cell wall (1,3;1,4)-beta-D-glucans. *Science,* 311**,** 1940-2.

BUSSE-WICHER, M., GOMES, T. C., TRYFONA, T., NIKOLOVSKI, N., STOTT, K., GRANTHAM, N. J., BOLAM, D. N., SKAF, M. S. & DUPREE, P. 2014. The pattern of xylan

acetylation suggests xylan may interact with cellulose microfibrils as a twofold helical screw in the secondary plant cell wall of Arabidopsis thaliana. *Plant J,* 79**,** 492-506.

CARPITA, N., TIERNEY, M. & CAMPBELL, M. 2001. Molecular biology of the plant cell wall: searching for the genes that define structure, architecture and dynamics. *Plant Mol Biol,* 47**,** 1-5.

CAVALIER, D. M., LEROUXEL, O., NEUMETZLER, L., YAMAUCHI, K., REINECKE, A., FRESHOUR, G., ZABOTINA, O. A., HAHN, M. G., BURGERT, I., PAULY, M., RAIKHEL, N. V. & KEEGSTRA, K. 2008. Disrupting two Arabidopsis thaliana xylosyltransferase genes results in plants deficient in xyloglucan, a major primary cell wall component. *Plant Cell,* 20**,** 1519-37.

COREA, O. R., KI, C., CARDENAS, C. L., DAVIN, L. B. & LEWIS, N. G. 2012. Laser microdissection and genetic manipulation technologies to probe lignin heterogeneity and configuration in plant cell walls. *Methods Mol Biol,* 908**,** 229-50.

COSGROVE, D. J. 1997. Assembly and enlargement of the primary cell wall in plants. *Annu Rev Cell Dev Biol,* 13**,** 171-201.

COSGROVE, D. J. 2005. Growth of the plant cell wall. *Nat Rev Mol Cell Biol,* 6**,** 850-61.

COSTA, G. & PLAZANET, I. 2016. *Plant Cell Wall, a Challenge for Its Characterisation*.

CROWE, J. D., FERINGA, N., PATTATHIL, S., MERRITT, B., FOSTER, C., DINES, D., ONG, R. G. & HODGE, D. B. 2017. Identification of developmental stage and anatomical fraction contributions to cell wall recalcitrance in switchgrass. *Biotechnol Biofuels,* 10**,** 184.

DAVIN, L. B. & LEWIS, N. G. 2000. Dirigent proteins and dirigent sites explain the mystery of specificity of radical precursor coupling in lignan and lignin biosynthesis. *Plant Physiol,* 123**,** 453-62.

DOBLIN, M. S., PETTOLINO, F. A., WILSON, S. M., CAMPBELL, R., BURTON, R. A., FINCHER, G. B., NEWBIGIN, E. & BACIC, A. 2009. A barley cellulose synthase-like CSLH gene mediates (1,3;1,4)-beta-D-glucan synthesis in transgenic Arabidopsis. *Proc Natl Acad Sci U S A,* 106**,** 5996-6001.

ENDLER, A. & PERSSON, S. 2011. Cellulose synthases and synthesis in Arabidopsis. *Mol Plant,* 4**,** 199-211.

FERNANDES, A. N., THOMAS, L. H., ALTANER, C. M., CALLOW, P., FORSYTH, V. T., APPERLEY, D. C., KENNEDY, C. J. & JARVIS, M. C. 2011. Nanostructure of cellulose microfibrils in spruce wood. *Proceedings of the National Academy of Sciences of the United States of America,* 108**,** E1195-E1203.

FRESHOUR, G., BONIN, C. P., REITER, W. D., ALBERSHEIM, P., DARVILL, A. G. & HAHN, M. G. 2003. Distribution of fucose-containing xyloglucans in cell walls of the mur1 mutant of Arabidopsis. *Plant Physiol,* 131**,** 1602-12.

FUNAKAWA, H. & MIWA, K. 2015. Synthesis of borate cross-linked rhamnogalacturonan II. *Front Plant Sci,* 6**,** 223.

GALLEGO-GIRALDO, L., POSE, S., PATTATHIL, S., PERALTA, A. G., HAHN, M. G., AYRE, B. G., SUNUWAR, J., HERNANDEZ, J., PATEL, M., SHAH, J., RAO, X., KNOX, J. P. &

DIXON, R. A. 2018. Elicitors and defense gene induction in plants with altered lignin compositions. *New Phytol,* 219**,** 1235-1251.
HAMANT, O. & TRAAS, J. 2010. The mechanics behind plant development. *New Phytol,* 185**,** 369-85.
HILL, J. L., JR., HAMMUDI, M. B. & TIEN, M. 2014. The Arabidopsis cellulose synthase complex: a proposed hexamer of CESA trimers in an equimolar stoichiometry. *Plant Cell,* 26**,** 4834-42.
HUSSEY, S. G., MIZRACHI, E., CREUX, N. M. & MYBURG, A. A. 2013. Navigating the transcriptional roadmap regulating plant secondary cell wall deposition. *Front Plant Sci,* 4**,** 325.
HUSSEY, S. G., MIZRACHI, E., SPOKEVICIUS, A. V., BOSSINGER, G., BERGER, D. K. & MYBURG, A. A. 2011. SND2, a NAC transcription factor gene, regulates genes involved in secondary cell wall development in Arabidopsis fibres and increases fibre cell area in Eucalyptus. *BMC Plant Biol,* 11**,** 173.
JARVIS, M. C. 2018. Structure of native cellulose microfibrils, the starting point for nanocellulose manufacture. *Philosophical Transactions of the Royal Society a-Mathematical Physical and Engineering Sciences,* 376.
KANEDA, M., RENSING, K. H., WONG, J. C., BANNO, B., MANSFIELD, S. D. & SAMUELS, A. L. 2008. Tracking monolignols during wood development in lodgepole pine. *Plant Physiol,* 147**,** 1750-60.
KANG, X., KIRUI, A., WIDANAGE, M. C. D., MENTINK-VIGIER, F., COSGROVE, D. J. & WANG, T. 2019. Lignin-polysaccharide interactions in plant secondary cell walls revealed by solid-state NMR. *Nature Communications,* 10.
KO, J. H., KIM, J. H., JAYANTY, S. S., HOWE, G. A. & HAN, K. H. 2006. Loss of function of COBRA, a determinant of oriented cell expansion, invokes cellular defence responses in Arabidopsis thaliana. *J Exp Bot,* 57**,** 2923-36.
KONDO, Y., FUJITA, T., SUGIYAMA, M. & FUKUDA, H. 2015. A novel system for xylem cell differentiation in Arabidopsis thaliana. *Mol Plant,* 8**,** 612-21.
KONDO, Y., TAMAKI, T. & FUKUDA, H. 2014. Regulation of xylem cell fate. *Front Plant Sci,* 5**,** 315.
KONG, Y., ZHOU, G., AVCI, U., GU, X., JONES, C., YIN, Y., XU, Y. & HAHN, M. G. 2009. Two poplar glycosyltransferase genes, PdGATL1.1 and PdGATL1.2, are functional orthologs to PARVUS/AtGATL1 in Arabidopsis. *Mol Plant,* 2**,** 1040-50.
KOORNNEEF, M. & MEINKE, D. 2010. The development of Arabidopsis as a model plant. *Plant J,* 61**,** 909-21.
KUBO, M., UDAGAWA, M., NISHIKUBO, N., HORIGUCHI, G., YAMAGUCHI, M., ITO, J., MIMURA, T., FUKUDA, H. & DEMURA, T. 2005. Transcription switches for protoxylem and metaxylem vessel formation. *Genes Dev,* 19**,** 1855-60.
KUMAR, M., MISHRA, L., CARR, P., PILLING, M., GARDNER, P., MANSFIELD, S. D. & TURNER, S. 2018. Exploiting CELLULOSE SYNTHASE (CESA) Class Specificity to Probe Cellulose Microfibril Biosynthesis. *Plant Physiology,* 177**,** 151-167.
LAMPUGNANI, E. R., KHAN, G. A., SOMSSICH, M. & PERSSON, S. 2018. Building a plant cell wall at a glance. *J Cell Sci,* 131.

LEE, K. J., MARCUS, S. E. & KNOX, J. P. 2011. Cell wall biology: perspectives from cell wall imaging. *Mol Plant,* 4**,** 212-9.

LEV-YADUN, S., WYATT, S. E. & FLAISHMAN, M. A. 2004. The inflorescence stem fibers of Arabidopsis thaliana revoluta (ifl1) mutant. *Journal of Plant Growth Regulation,* 23**,** 301-306.

LEVESQUE-TREMBLAY, G., PELLOUX, J., BRAYBROOK, S. A. & MULLER, K. 2015. Tuning of pectin methylesterification: consequences for cell wall biomechanics and development. *Planta,* 242**,** 791-811.

LIEPMAN, A. H., WIGHTMAN, R., GESHI, N., TURNER, S. R. & SCHELLER, H. V. 2010. Arabidopsis - a powerful model system for plant cell wall research. *Plant J,* 61**,** 1107-21.

LIU, C. J. 2012. Deciphering the enigma of lignification: precursor transport, oxidation, and the topochemistry of lignin assembly. *Mol Plant,* 5**,** 304-17.

LIU, Y. Y., YOU, S. J., TAYLOR-TEEPLES, M., LI, W. L., SCHUETZ, M., BRADY, S. M. & DOUGLAS, C. J. 2014. BEL1-LIKE HOMEODOMAIN6 and KNOTTED ARABIDOPSIS THALIANA7 Interact and Regulate Secondary Cell Wall Formation via Repression of REVOLUTA. *Plant Cell,* 26**,** 4843-4861.

LOQUE, D., SCHELLER, H. V. & PAULY, M. 2015. Engineering of plant cell walls for enhanced biofuel production. *Curr Opin Plant Biol,* 25**,** 151-61.

LUCAS, W. J., GROOVER, A., LICHTENBERGER, R., FURUTA, K., YADAV, S. R., HELARIUTTA, Y., HE, X. Q., FUKUDA, H., KANG, J., BRADY, S. M., PATRICK, J. W., SPERRY, J., YOSHIDA, A., LOPEZ-MILLAN, A. F., GRUSAK, M. A. & KACHROO, P. 2013. The plant vascular system: evolution, development and functions. *J Integr Plant Biol,* 55**,** 294-388.

MARCUS, S. E., BLAKE, A. W., BENIANS, T. A., LEE, K. J., POYSER, C., DONALDSON, L., LEROUX, O., ROGOWSKI, A., PETERSEN, H. L., BORASTON, A., GILBERT, H. J., WILLATS, W. G. & KNOX, J. P. 2010. Restricted access of proteins to mannan polysaccharides in intact plant cell walls. *Plant J,* 64**,** 191-203.

MARTINEZ-ABAD, A., BERGLUND, J., TORIZ, G., GATENHOLM, P., HENRIKSSON, G., LINDSTROM, M., WOHLERT, J. & VILAPLANA, F. 2017. Regular Motifs in Xylan Modulate Molecular Flexibility and Interactions with Cellulose Surfaces. *Plant Physiology,* 175**,** 1579-1592.

MCCAIG, B. C., MEAGHER, R. B. & DEAN, J. F. D. 2005. Gene structure and molecular analysis of the laccase-like multicopper oxidase (LMCO) gene family in Arabidopsis thaliana. *Planta,* 221**,** 619-636.

MEENTS, M. J., WATANABE, Y. & SAMUELS, A. L. 2018. The cell biology of secondary cell wall biosynthesis. *Annals of Botany,* 121**,** 1107-1125.

MELLEROWICZ, E. J. & SUNDBERG, B. 2008. Wood cell walls: biosynthesis, developmental dynamics and their implications for wood properties. *Curr Opin Plant Biol,* 11**,** 293-300.

MIAO, Y. C. & LIU, C. J. 2010. ATP-binding cassette-like transporters are involved in the transport of lignin precursors across plasma and vacuolar membranes. *Proc Natl Acad Sci U S A,* 107**,** 22728-33.

MITSUDA, N., IWASE, A., YAMAMOTO, H., YOSHIDA, M., SEKI, M., SHINOZAKI, K. & OHME-TAKAGI, M. 2007. NAC transcription factors, NST1 and NST3, are key regulators of the formation of secondary walls in woody tissues of Arabidopsis. *Plant Cell,* 19**,** 270-80.

MOLLER, I., SORENSEN, I., BERNAL, A. J., BLAUKOPF, C., LEE, K., OBRO, J., PETTOLINO, F., ROBERTS, A., MIKKELSEN, J. D., KNOX, J. P., BACIC, A. & WILLATS, W. G. 2007. High-throughput mapping of cell-wall polymers within and between plants using novel microarrays. *Plant J,* 50**,** 1118-28.

MORTIMER, J. C., MILES, G. P., BROWN, D. M., ZHANG, Z., SEGURA, M. P., WEIMAR, T., YU, X., SEFFEN, K. A., STEPHENS, E., TURNER, S. R. & DUPREE, P. 2010. Absence of branches from xylan in Arabidopsis gux mutants reveals potential for simplification of lignocellulosic biomass. *Proc Natl Acad Sci U S A,* 107**,** 17409-14.

NAKANO, Y., YAMAGUCHIZ, M., ENDO, H., REJAB, N. A. & OHTANI, M. 2015. NAC-MYB-based transcriptional regulation of secondary cell wall biosynthesis in land plants. *Frontiers in Plant Science,* 6.

NASIR, M., HASHIM, R., SULAIMAN, O., NOOR, A. N., LAMAMING, J. & ASIM, M. 2015. Laccase for Green Composites. *BioResources,* 10**,** 22.

NEWMAN, R. H., HILL, S. J. & HARRIS, P. J. 2013. Wide-Angle X-Ray Scattering and Solid-State Nuclear Magnetic Resonance Data Combined to Test Models for Cellulose Microfibrils in Mung Bean Cell Walls. *Plant Physiology,* 163**,** 1558-1567.

NIXON, B. T., MANSOURI, K., SINGH, A., DU, J., DAVIS, J. K., LEE, J. G., SLABAUGH, E., VANDAVASI, V. G., O'NEILL, H., ROBERTS, E. M., ROBERTS, A. W., YINGLING, Y. G. & HAIGLER, C. H. 2016. Comparative Structural and Computational Analysis Supports Eighteen Cellulose Synthases in the Plant Cellulose Synthesis Complex. *Sci Rep,* 6**,** 28696.

OBEL, N., ERBEN, V., SCHWARZ, T., KUHNEL, S., FODOR, A. & PAULY, M. 2009. Microanalysis of plant cell wall polysaccharides. *Mol Plant,* 2**,** 922-32.

OBEL, N., PORCHIA, A. C. & SCHELLER, H. V. 2002. Dynamic changes in cell wall polysaccharides during wheat seedling development. *Phytochemistry,* 60**,** 603-610.

ODA, Y. & FUKUDA, H. 2012. Secondary cell wall patterning during xylem differentiation. *Curr Opin Plant Biol,* 15**,** 38-44.

ODA, Y., MIMURA, T. & HASEZAWA, S. 2005. Regulation of secondary cell wall development by cortical microtubules during tracheary element differentiation in Arabidopsis cell suspensions. *Plant Physiology,* 137**,** 1027-1036.

OHASHI-ITO, K., ODA, Y. & FUKUDA, H. 2010. Arabidopsis VASCULAR-RELATED NAC-DOMAIN6 directly regulates the genes that govern programmed cell death and secondary wall formation during xylem differentiation. *Plant Cell,* 22**,** 3461-73.

OKEKEOGBU, I. O., PATTATHIL, S., GONZALEZ FERNANDEZ-NINO, S. M., ARYAL, U. K., PENNING, B. W., LAO, J., HEAZLEWOOD, J. L., HAHN, M. G., MCCANN, M. C. & CARPITA, N. C. 2019. Glycome and proteome components of Golgi membranes are common between two angiosperms with distinct cell wall structures. *Plant Cell*.

ORDAZ-ORTIZ, J. J., MARCUS, S. E. & KNOX, J. P. 2009. Cell wall microstructure analysis implicates hemicellulose polysaccharides in cell adhesion in tomato fruit pericarp parenchyma. *Mol Plant,* 2**,** 910-21.

PAGANT, S., BICHET, A., SUGIMOTO, K., LEROUXEL, O., DESPREZ, T., MCCANN, M., LEROUGE, P., VERNHETTES, S. & HOFTE, H. 2002. KOBITO1 encodes a novel plasma membrane protein necessary for normal synthesis of cellulose during cell expansion in Arabidopsis. *Plant Cell,* 14**,** 2001-2013.

PAREDEZ, A. R., SOMERVILLE, C. R. & EHRHARDT, D. W. 2006. Visualization of cellulose synthase demonstrates functional association with microtubules. *Science,* 312**,** 1491-1495.

PATTATHIL, S., AVCI, U., BALDWIN, D., SWENNES, A. G., MCGILL, J. A., POPPER, Z., BOOTTEN, T., ALBERT, A., DAVIS, R. H., CHENNAREDDY, C., DONG, R., O'SHEA, B., ROSSI, R., LEOFF, C., FRESHOUR, G., NARRA, R., O'NEIL, M., YORK, W. S. & HAHN, M. G. 2010. A comprehensive toolkit of plant cell wall glycan-directed monoclonal antibodies. *Plant Physiol,* 153**,** 514-25.

PATTATHIL, S., AVCI, U., MILLER, J. S. & HAHN, M. G. 2012. Immunological approaches to plant cell wall and biomass characterization: Glycome Profiling. *Methods Mol Biol,* 908**,** 61-72.

PATTATHIL, S., AVCI, U., ZHANG, T., CARDENAS, C. L. & HAHN, M. G. 2015. Immunological Approaches to Biomass Characterization and Utilization. *Front Bioeng Biotechnol,* 3**,** 173.

PENA, M. J., ZHONG, R., ZHOU, G. K., RICHARDSON, E. A., O'NEILL, M. A., DARVILL, A. G., YORK, W. S. & YE, Z. H. 2007. Arabidopsis irregular xylem8 and irregular xylem9: implications for the complexity of glucuronoxylan biosynthesis. *Plant Cell,* 19**,** 549-63.

PENG, L., KAWAGOE, Y., HOGAN, P. & DELMER, D. 2002. Sitosterol-beta-glucoside as primer for cellulose synthesis in plants. *Science,* 295**,** 147-50.

PERALTA, A. G., VENKATACHALAM, S., STONE, S. C. & PATTATHIL, S. 2017. Xylan epitope profiling: an enhanced approach to study organ development-dependent changes in xylan structure, biosynthesis, and deposition in plant cell walls. *Biotechnol Biofuels,* 10**,** 245.

PERSSON, S., CAFFALL, K. H., FRESHOUR, G., HILLEY, M. T., BAUER, S., POINDEXTER, P., HAHN, M. G., MOHNEN, D. & SOMERVILLE, C. 2007. The Arabidopsis irregular xylem8 mutant is deficient in glucuronoxylan and homogalacturonan, which are essential for secondary cell wall integrity. *Plant Cell,* 19**,** 237-55.

PUHLMANN, J., BUCHELI, E., SWAIN, M. J., DUNNING, N., ALBERSHEIM, P., DARVILL, A. G. & HAHN, M. G. 1994. Generation of monoclonal antibodies against plant cell-wall polysaccharides. I. Characterization of a monoclonal antibody to a terminal alpha-(1-->2)-linked fucosyl-containing epitope. *Plant Physiol,* 104**,** 699-710.

RALPH, J. 2010. Hydroxycinnamates in lignification. *Phytochemistry Reviews,* 9**,** 65-83.

RANCOUR, D. M., MARITA, J. M. & HATFIELD, R. D. 2012. Cell wall composition throughout development for the model grass Brachypodium distachyon. *Front Plant Sci,* 3**,** 266.

RAVACHOL, J., DE PHILIP, P., BORNE, R., MANSUELLE, P., MATE, M. J., PERRET, S. & FIEROBE, H. P. 2016. Mechanisms involved in xyloglucan catabolism by the cellulosome-producing bacterium Ruminiclostridium cellulolyticum. *Sci Rep,* 6**,** 22770.

RENCORET, J., GUTIERREZ, A., NIETO, L., JIMENEZ-BARBERO, J., FAULDS, C. B., KIM, H., RALPH, J., MARTINEZ, A. T. & DEL RIO, J. C. 2011. Lignin composition and structure in young versus adult Eucalyptus globulus plants. *Plant Physiol,* 155**,** 667-82.

RENNIE, E. A. & SCHELLER, H. V. 2014. Xylan biosynthesis. *Curr Opin Biotechnol,* 26**,** 100-7.

ROUDIER, F., FERNANDEZ, A. G., FUJITA, M., HIMMELSPACH, R., BORNER, G. H., SCHINDELMAN, G., SONG, S., BASKIN, T. I., DUPREE, P., WASTENEYS, G. O. & BENFEY, P. N. 2005. COBRA, an Arabidopsis extracellular glycosyl-phosphatidyl inositol-anchored protein, specifically controls highly anisotropic expansion through its involvement in cellulose microfibril orientation. *Plant Cell,* 17**,** 1749-63.

RUPRECHT, C., BARTETZKO, M. P., SENF, D., DALLABERNADINA, P., BOOS, I., ANDERSEN, M. C. F., KOTAKE, T., KNOX, J. P., HAHN, M. G., CLAUSEN, M. H. & PFRENGLE, F. 2017. A Synthetic Glycan Microarray Enables Epitope Mapping of Plant Cell Wall Glycan-Directed Antibodies. *Plant Physiology,* 175**,** 1094-1104.

SANCHEZ-RODRIGUEZ, C., BAUER, S., HEMATY, K., SAXE, F., IBANEZ, A. B., VODERMAIER, V., KONLECHNER, C., SAMPATHKUMAR, A., RUGGEBERG, M., AICHINGER, E., NEUMETZLER, L., BURGERT, I., SOMERVILLE, C., HAUSER, M. T. & PERSSON, S. 2012. CHITINASE-LIKE1/POM-POM1 and Its Homolog CTL2 Are Glucan-Interacting Proteins Important for Cellulose Biosynthesis in Arabidopsis. *Plant Cell,* 24**,** 589-607.

SARKAR, P., BOSNEAGA, E. & AUER, M. 2009. Plant cell walls throughout evolution: towards a molecular understanding of their design principles. *J Exp Bot,* 60**,** 3615-35.

SCHMIDT, D., SCHUHMACHER, F., GEISSNER, A., SEEBERGER, P. H. & PFRENGLE, F. 2015. Automated synthesis of arabinoxylan-oligosaccharides enables characterization of antibodies that recognize plant cell wall glycans. *Chemistry,* 21**,** 5709-13.

SCHUETZ, M., SMITH, R. & ELLIS, B. 2013. Xylem tissue specification, patterning, and differentiation mechanisms. *J Exp Bot,* 64**,** 11-31.

SIBOUT, R., LE BRIS, P., LEGEE, F., CEZARD, L., RENAULT, H. & LAPIERRE, C. 2016. Structural Redesigning Arabidopsis Lignins into Alkali-Soluble Lignins through the Expression of p-Coumaroyl-CoA: Monolignol Transferase PMT. *Plant Physiology,* 170**,** 1358-1366.

SIMMONS, T. J., MORTIMER, J. C., BERNARDINELLI, O. D., POPPLER, A. C., BROWN, S. P., DEAZEVEDO, E. R., DUPREE, R. & DUPREE, P. 2016. Folding of xylan onto cellulose fibrils in plant cell walls revealed by solid-state NMR. *Nature Communications,* 7.

SINCLAIR, R., ROSQUETE, M. R. & DRAKAKAKI, G. 2018. Post-Golgi Trafficking and Transport of Cell Wall Components. *Front Plant Sci,* 9**,** 1784.

SMITH, R. A., SCHUETZ, M., KARLEN, S. D., BIRD, D., TOKUNAGA, N., SATO, Y., MANSFIELD, S. D., RALPH, J. & SAMUELS, A. L. 2017. Defining the Diverse Cell Populations Contributing to Lignification in Arabidopsis Stems. *Plant Physiology,* 174**,** 1028-1036.

SMITH, R. A., SCHUETZ, M., ROACH, M., MANSFIELD, S. D., ELLIS, B. & SAMUELS, L. 2013. Neighboring parenchyma cells contribute to Arabidopsis xylem lignification, while lignification of interfascicular fibers is cell autonomous. *Plant Cell,* 25**,** 3988-99.

SOMERVILLE, C. 2006. Cellulose synthesis in higher plants. *Annu Rev Cell Dev Biol,* 22**,** 53-78.

SOMERVILLE, C., BAUER, S., BRININSTOOL, G., FACETTE, M., HAMANN, T., MILNE, J., OSBORNE, E., PAREDEZ, A., PERSSON, S., RAAB, T., VORWERK, S. & YOUNGS, H. 2004. Toward a systems approach to understanding plant cell walls. *Science,* 306**,** 2206-11.

STERJIADES, R., DEAN, J. F. D., GAMBLE, G., HIMMELSBACH, D. S. & ERIKSSON, K. E. L. 1993. Extracellular Laccases and Peroxidases from Sycamore Maple (Acer-Pseudoplatanus) Cell-Suspension Cultures - Reactions with Monolignols and Lignin Model Compounds. *Planta,* 190**,** 75-87.

STRABALA, T. J. & MACMILLAN, C. P. 2013. The Arabidopsis wood model-the case for the inflorescence stem. *Plant Sci,* 210**,** 193-205.

SZYJANOWICZ, P. M., MCKINNON, I., TAYLOR, N. G., GARDINER, J., JARVIS, M. C. & TURNER, S. R. 2004. The irregular xylem 2 mutant is an allele of korrigan that affects the secondary cell wall of Arabidopsis thaliana. *Plant J,* 37**,** 730-40.

TAKAHASHI, J., RUDSANDER, U. J., HEDENSTROM, M., BANASIAK, A., HARHOLT, J., AMELOT, N., IMMERZEEL, P., RYDEN, P., ENDO, S., IBATULLIN, F. M., BRUMER, H., DEL CAMPILLO, E., MASTER, E. R., SCHELLER, H. V., SUNDBERG, B., TEERI, T. T. & MELLEROWICZ, E. J. 2009. KORRIGAN1 and its aspen homolog PttCel9A1 decrease cellulose crystallinity in Arabidopsis stems. *Plant Cell Physiol,* 50**,** 1099-115.

TAYLOR-TEEPLES, M., LIN, L., DE LUCAS, M., TURCO, G., TOAL, T. W., GAUDINIER, A., YOUNG, N. F., TRABUCCO, G. M., VELING, M. T., LAMOTHE, R., HANDAKUMBURA, P. P., XIONG, G., WANG, C., CORWIN, J., TSOUKALAS, A., ZHANG, L., WARE, D., PAULY, M., KLIEBENSTEIN, D. J., DEHESH, K., TAGKOPOULOS, I., BRETON, G., PRUNEDA-PAZ, J. L., AHNERT, S. E., KAY, S. A., HAZEN, S. P. & BRADY, S. M. 2015. An Arabidopsis gene regulatory network for secondary cell wall synthesis. *Nature,* 517**,** 571-5.

TAYLOR, N. G., HOWELLS, R. M., HUTTLY, A. K., VICKERS, K. & TURNER, S. R. 2003. Interactions among three distinct CesA proteins essential for cellulose synthesis. *Proceedings of the National Academy of Sciences of the United States of America,* 100**,** 1450-1455.

TAYLOR, N. G., LAURIE, S. & TURNER, S. R. 2000. Multiple cellulose synthase catalytic subunits are required for cellulose synthesis in Arabidopsis. *Plant Cell,* 12**,** 2529-2539.

THE ARABIDOPSIS GENOME, I. 2000. Analysis of the genome sequence of the flowering plant Arabidopsis thaliana. *Nature,* 408**,** 796.

TURNER, S. R. & SOMERVILLE, C. R. 1997. Collapsed xylem phenotype of Arabidopsis identifies mutants deficient in cellulose deposition in the secondary cell wall. *Plant Cell,* 9**,** 689-701.

URBANOWICZ, B. R., PENA, M. J., MONIZ, H. A., MOREMEN, K. W. & YORK, W. S. 2014. Two Arabidopsis proteins synthesize acetylated xylan in vitro. *Plant Journal,* 80**,** 197-206.

URBANOWICZ, B. R., PENA, M. J., RATNAPARKHE, S., AVCI, U., BACKE, J., STEET, H. F., FOSTON, M., LI, H., O'NEILL, M. A., RAGAUSKAS, A. J., DARVILL, A. G., WYMAN, C., GILBERT, H. J. & YORK, W. S. 2012. 4-O-methylation of glucuronic acid in Arabidopsis glucuronoxylan is catalyzed by a domain of unknown function family 579 protein. *Proc Natl Acad Sci U S A,* 109**,** 14253-8.

VAIN, T., CROWELL, E. F., TIMPANO, H., BIOT, E., DESPREZ, T., MANSOORI, N., TRINDADE, L. M., PAGANT, S., ROBERT, S., HOFTE, H., GONNEAU, M. & VERNHETTES, S. 2014. The Cellulase KORRIGAN Is Part of the Cellulose Synthase Complex. *Plant Physiology,* 165**,** 1521-1532.

VAN ACKER, R., VANHOLME, R., STORME, V., MORTIMER, J. C., DUPREE, P. & BOERJAN, W. 2013. Lignin biosynthesis perturbations affect secondary cell wall composition and saccharification yield in Arabidopsis thaliana. *Biotechnology for Biofuels,* 6**,** 46.

VANHOLME, R., CESARINO, I., RATAJ, K., XIAO, Y. G., SUNDIN, L., GOEMINNE, G., KIM, H., CROSS, J., MORREEL, K., ARAUJO, P., WELSH, L., HAUSTRAETE, J., MCCLELLAN, C., VANHOLME, B., RALPH, J., SIMPSON, G. G., HALPIN, C. & BOERJAN, W. 2013. Caffeoyl Shikimate Esterase (CSE) Is an Enzyme in the Lignin Biosynthetic Pathway in Arabidopsis. *Science,* 341**,** 1103-1106.

VANHOLME, R., DEMEDTS, B., MORREEL, K., RALPH, J. & BOERJAN, W. 2010. Lignin biosynthesis and structure. *Plant Physiol,* 153**,** 895-905.

VANHOLME, R., STORME, V., VANHOLME, B., SUNDIN, L., CHRISTENSEN, J. H., GOEMINNE, G., HALPIN, C., ROHDE, A., MORREEL, K. & BOERJAN, W. 2012. A Systems Biology View of Responses to Lignin Biosynthesis Perturbations in Arabidopsis. *Plant Cell,* 24**,** 3506-3529.

VERHERTBRUGGEN, Y., MARCUS, S. E., HAEGER, A., VERHOEF, R., SCHOLS, H. A., MCCLEARY, B. V., MCKEE, L., GILBERT, H. J. & KNOX, J. P. 2009. Developmental complexity of arabinan polysaccharides and their processing in plant cell walls. *Plant J,* 59**,** 413-25.

VERHERTBRUGGEN, Y., WALKER, J. L., GUILLON, F. & SCHELLER, H. V. 2017. A Comparative Study of Sample Preparation for Staining and Immunodetection of Plant Cell Walls by Light Microscopy. *Front Plant Sci,* 8**,** 1505.

VOGEL, J. 2008. Unique aspects of the grass cell wall. *Curr Opin Plant Biol,* 11**,** 301-7.

WANG, P. F., CHEN, X. S., GOLDBECK, C., CHUNG, E. & KANG, B. H. 2017. A distinct class of vesicles derived from the trans-Golgi mediates secretion of xylogalacturonan in the root border cell. *Plant Journal,* 92**,** 596-610.

WANG, T., PARK, Y. B., COSGROVE, D. J. & HONG, M. 2015. Cellulose-Pectin Spatial Contacts Are Inherent to Never-Dried Arabidopsis Primary Cell Walls: Evidence from Solid-State Nuclear Magnetic Resonance. *Plant Physiol,* 168**,** 871-84.

WANG, Y., CHANTREAU, M., SIBOUT, R. & HAWKINS, S. 2013. Plant cell wall lignification and monolignol metabolism. *Frontiers in Plant Science,* 4.

WATANABE, Y., SCHNEIDER, R., BARKWILL, S., GONZALES-VIGIL, E., HILL, J. L., SAMUELS, A. L., PERSSON, S. & MANSFIELD, S. D. 2018. Cellulose synthase complexes display distinct dynamic behaviors during xylem transdifferentiation. *Proceedings of the National Academy of Sciences of the United States of America,* 115**,** E6366-E6374.

WIGHTMAN, R. & TURNER, S. R. 2008. The roles of the cytoskeleton during cellulose deposition at the secondary cell wall. *Plant Journal,* 54**,** 794-805.

WILKOP, T., PATTATHIL, S., REN, G., DAVIS, D. J., BAO, W., DUAN, D., PERALTA, A. G., DOMOZYCH, D., HAHN, M. G. & DRAKAKAKI, G. 2019. A hybrid approach enabling large scale glycome analysis of post-Golgi vesicles reveals a transport route for polysaccharides. *Plant Cell*.

YAMAGUCHI, M., GOUE, N., IGARASHI, H., OHTANI, M., NAKANO, Y., MORTIMER, J. C., NISHIKUBO, N., KUBO, M., KATAYAMA, Y., KAKEGAWA, K., DUPREE, P. & DEMURA, T. 2010. VASCULAR-RELATED NAC-DOMAIN6 and VASCULAR-RELATED NAC-DOMAIN7 effectively induce transdifferentiation into xylem vessel elements under control of an induction system. *Plant Physiol,* 153**,** 906-14.

YAMAGUCHI, M., MITSUDA, N., OHTANI, M., OHME-TAKAGI, M., KATO, K. & DEMURA, T. 2011. VASCULAR-RELATED NAC-DOMAIN7 directly regulates the expression of a broad range of genes for xylem vessel formation. *Plant J,* 66**,** 579-90.

ZABLACKIS, E., HUANG, J., MULLER, B., DARVILL, A. G. & ALBERSHEIM, P. 1995. Characterization of the cell-wall polysaccharides of Arabidopsis thaliana leaves. *Plant Physiol,* 107**,** 1129-38.

ZABOTINA, O. A. 2012. Xyloglucan and its biosynthesis. *Front Plant Sci,* 3**,** 134.

ZEIGER, E. & TAIZ, L. 2010. *Plant Physiology*, Oxford University Press.

ZENG, W., LAMPUGNANI, E. R., PICARD, K. L., SONG, L. L., WU, A. M., FARION, I. M., ZHAO, J., FORD, K., DOBLIN, M. S. & BACIC, A. 2016. Asparagus IRX9, IRX10, and IRX14A Are Components of an Active Xylan Backbone Synthase Complex that Forms in the Golgi Apparatus. *Plant Physiology,* 171**,** 93-109.

ZHONG, R., DEMURA, T. & YE, Z. H. 2006. SND1, a NAC domain transcription factor, is a key regulator of secondary wall synthesis in fibers of Arabidopsis. *Plant Cell,* 18**,** 3158-70.

ZHONG, R., LEE, C., ZHOU, J., MCCARTHY, R. L. & YE, Z. H. 2008. A battery of transcription factors involved in the regulation of secondary cell wall biosynthesis in Arabidopsis. *Plant Cell,* 20**,** 2763-82.

ZHONG, R., PENA, M. J., ZHOU, G. K., NAIRN, C. J., WOOD-JONES, A., RICHARDSON, E. A., MORRISON, W. H., 3RD, DARVILL, A. G., YORK, W. S. & YE, Z. H. 2005. Arabidopsis fragile fiber8, which encodes a putative glucuronyltransferase, is essential for normal secondary wall synthesis. *Plant Cell,* 17**,** 3390-408.

ZHONG, R., RICHARDSON, E. A. & YE, Z. H. 2007. The MYB46 transcription factor is a direct target of SND1 and regulates secondary wall biosynthesis in Arabidopsis. *Plant Cell,* 19**,** 2776-92.

ZHONG, R. & YE, Z. H. 1999. IFL1, a gene regulating interfascicular fiber differentiation in Arabidopsis, encodes a homeodomain-leucine zipper protein. *Plant Cell,* 11**,** 2139-52.

ZHONG, R. & YE, Z. H. 2009. Transcriptional regulation of lignin biosynthesis. *Plant Signal Behav,* 4**,** 1028-34.

ZHONG, R. & YE, Z. H. 2012. MYB46 and MYB83 bind to the SMRE sites and directly activate a suite of transcription factors and secondary wall biosynthetic genes. *Plant Cell Physiol,* 53**,** 368-80.

ZHONG, R. & YE, Z. H. 2014. Complexity of the transcriptional network controlling secondary wall biosynthesis. *Plant Sci,* 229**,** 193-207.

ZHONG, R. Q., CUI, D. T. & YE, Z. H. 2019. Secondary cell wall biosynthesis. *New Phytologist,* 221**,** 1703-1723.

ZHONG, R. Q., MORRISON, W. H., FRESHOUR, G. D., HAHN, M. G. & YE, Z. H. 2003. Expression of a mutant form of cellulose synthase AtCesA7 causes dominant negative effect on cellulose biosynthesis. *Plant Physiology,* 132**,** 786-795.

ZHOU, J., LEE, C., ZHONG, R. & YE, Z. H. 2009. MYB58 and MYB63 are transcriptional activators of the lignin biosynthetic pathway during secondary cell wall formation in Arabidopsis. *Plant Cell,* 21**,** 248-66.

CHAPTER 2: XYLAN-EPITOPE PROFILING: AN APPROACH TO STUDY ORGAN DEVELOPMENT-DEPENDENT CHANGES IN XYLAN STRUCTURE, BIOSYNTHESIS, AND DEPOSITION IN PLANT CELL WALLS[1]

[1] Angelo G Peralta, Sivasankari Venkatachalam, Sydney C Stone & Sivakumar Pattathil. 2017. *Biotechnology for Biofuels*. **10**. 245.
Reprinted here with permission of the publisher: http://creativecommons.org/licenses/by/4.0/

2.1 Abstract

We describe here an approach to enable the monitoring of xylan epitope structures in cell walls during stem maturation in Arabidopsis. The technique integrates glycome profiling, an *in vitro* immunoanalytical platform, and *in situ* immunolocalization to provide comprehensive details on the presence, relative abundances, and dynamics with which diverse xylan epitope structures are integrated into cell walls throughout the course of the stem maturation process. Our experimental results and the supporting *in silico* analysis demonstrate that xylan deposition in stems occurs early on in stem development. However, xylan epitope types representing substituted and unsubstituted sidechain regions on the xylan backbone (made up of β-(1,4)-linked xylose residues) and the strength of their integration into the final wall structure vary during stem maturation. These techniques used methods to comprehensively survey the differences in xylan epitope patterning and deposition occurring in stem development and thereby provide a robust tool for characterising altered xylan integration patterns in cell walls during the stem maturation process in diverse plant cell wall biosynthetic mutants. Our findings suggest that this approach could rapidly and reliably delineate xylan deposition patterns in the cell walls of plants belonging to diverse phylogenetic classes providing novel insights into the functional roles of xylans in overall plant growth and development.

2.1.1 Background

Cell walls perform a number of important roles in plant growth and development including: providing shape to different cell types, acting as an interface between adjacent cells, participating in intercellular communication, and being part of defence responses against pathogenic attack. Cell walls are divided into two categories, primary cell-walls and secondary cell-walls. Primary cell walls surround dividing and expanding cells (Keegstra, 2010). In dicots, the type I primary cell wall predominantly consists of equal amounts of cellulose and cross-linking xyloglucans (XGs), with various minor amounts of glucomannans, and galacto-glucomannans. The XG in type I walls have a repeating heptasaccharide unit structure that be substituted with galactosyl, fucosyl, and arabinosyl units. Type II primary cell-walls on the other hand, are the main primary cell-walls found in grasses. They contain cellulose microfibrils of the same structure as those of the Type I wall, but the main polymers that interlock the cellulose microfibrils are glucuronoarabinoxylans (GAXs). The attachment of arabinose and glucuronic acid side groups to the xylan backbone of GAXs prohibits the formation of hydrogen bonds, thereby diminishing the degree of cross-linking between two unbranched GAX chains or GAX to cellulose (Carpita, 1996). Additionally, Type II walls have small amounts of XyG, and these XyGs contain neither arabinose nor fucose units (Carpita, 1996). While xylans are typically not present in dicots, recent studies have demonstrated that a xylan specific to primary cell-walls was enriched in Arabidopsis. The structure has a β-(1,4)-Xyl backbone with a pentose linked 1–2 to the a-1,2-D-glucuronic acid (GlcA) side chains (Mortimer et al., 2015). This may lead us to infer if whether or not xylans are a crucial polysaccharide during primary cell-wall deposition. The type I and type II primary walls differ from the secondary cell walls of dicots

including *Arabidopsis*, where xylan is the major hemicellulosic polymer present in the wall where they are actively being biosynthesised (Carpita, 1996).

Secondary cell-walls are found in cells where cell division and elongation have ceased. (Keegstra, 2010). The major components of plant secondary cell-walls are cellulose, hemicelluloses, and lignin (Zhong and Ye, 2015). One of the major hemicellulose in secondary cell-walls is xylan, is a linear cell wall polymer that consists of a backbone made up of β-(1,4)-linked xylose residues that is generally substituted with arabinose, acetyl, glucuronic acid (GlcA), and 4-*O*-methylglucuronic acid residues to varying degrees depending on the plant species (Rennie and Scheller, 2014). Glucuronoxylan (GX), that is found in dicots consist of a linear backbone of β-(1, 4)-linked xylose (Xyl) residues that are substituted with α(1,2)-linked glucuronic acid (GlcA). These GXs occur as either: binding tightly to exposed faces of glucan chains in cellulose microfibrils, and spanning the distance between adjacent microfibrils; or with other GXs to space and lock cellulose microfibrils into place (Park and Cosgrove, 2012). Glucuronoarabinoxlyans (GAX), the abundant form of xylans in grasses are a backbone of β-(1, 4)-linked xylose (Xyl) residues that are linked with Ara*f* at either α-(1,2) or α-(1,3) positions (Rennie and Scheller, 2014, Busse-Wicher et al., 2014). GAX attach themselves to cellulose microfibrils in a similar fashion to type I walls (Carpita, 1996).

Along with cellulose and lignin, xylans represent one of the main structural components of the secondary cell-wall of dicots. They are typically deposited into xylem precursor cells and play are an important component when xylem precursor cells differentiate into xylem vessels. The deposition of xylans and other secondary cell-wall associated polysaccharides and phenolics allows xylem to transport water and solutes rapidly while simultaneously maintaining

its structural integrity despite the negative pressure that occurs in transpiration (Schuetz et al., 2013). In interfascicular fibres, xylans contribute to the thickness of the walls in fibre cells, which allow them to maintain the mechanical strength of the stem (Zhong et al., 2005, Persson et al., 2007). The importance of xylans as a major constituent of the secondary cell wall in stems is well-emphasised by xylan deficient mutants exhibiting weakened stems (Mortimer et al., 2010).

Xylans have been shown to exhibit varying structural features in plant cell walls throughout development. For example, in 7-day old wheat seedlings, arabinoxylan content changed from a high degree of arabinose substitution to a much lower degree of substitution at the start of day 4 and ceasing at day 7. Additionally, segments of 7-day old wheat seedlings had higher arabinose content in the upper 1/3 of the seedling segment (3.5% w/w) compared to the lower 1/3 segment (2.3% w/w) thereby highlighting the complex manner in which high and low substituted arabinoxylans are deposited in primary and secondary cell walls in different cell types and at different development stages (Obel et al., 2002). Other studies have also demonstrated changes in xylan content and substitution. In developing willow stems, it was observed that the xylan content and the degree of methylation in the GlcA side chains of xylan backbone polymers increases during stem maturation. In addition, immunolocalisation of xylan distribution using the LM10 monoclonal antibody demonstrated increased labelling of unsubstituted and substituted xylan epitopes as the secondary xylem in willow stems developed (Wan et al., 2014).

Since xylans are the second most abundant cell wall polysaccharide after cellulose, they are a major non-cellulosic component of plant biomass. The xylose monomer units in xylan

however, are incompatible for fermentation into biofuels and other bio-products by organisms such as yeast due to their pentose structure (Rennie and Scheller, 2014). Xylans also have a contributing role in cell wall recalcitrance by 1) cross-linking with lignin through ester bonds to GlcA and ether bonds with Xyl or Ara, and 2) the ferulic acid dimerisation in grass xylans results in cross-linking of adjacent xylan chains or to lignin (Imamura et al., 1994, Loque et al., 2015, Rennie and Scheller, 2014). Additionally, these ferulic acid esters negatively impact xylan and cellulose hydrolysis (Rennie and Scheller, 2014). Understanding xylan composition, structure and biosynthesis are of key significance in designing strategies for engineering xylans in plants with improved properties such as decreased recalcitrance for biofuel production.

Advances have been made in gaining insights into the co-expression analysis of genes directly or indirectly associated with xylan biosynthesis, including putative glycosyltransferases (Oikawa et al., 2010). In addition, several recent studies have focussed on xylan structural variations during primary and secondary cell wall formation in Arabidopsis [see review (Hao and Mohnen, 2014)]. However, there is only a handful of information on the structural dynamics of xylans in primary and secondary cell walls, especially as a function of developmental stages of plant organs (Mortimer et al., 2015). Moreover, despite early attempts to map the spatial and temporal distribution of xylans depending on developmental stages (da Costa et al., 2017, Wan et al., 2014), there are still no comprehensive studies on development-dependent variations pertaining to xylan sub-structures during stem maturation. Understanding the differentiation of xylan deposition in a developmental context would provide a clearer picture of spatiotemporal regulation of the xylan biosynthetic process and hence overall cell wall biosynthetic processes in plant organs.

Plant cell wall glycan-directed monoclonal antibodies (mAbs) are highly specific probes used in plant cell wall analyses (Lee et al., 2011, Pattathil et al., 2015). mAbs can bind monospecifically to glycan sub-structures, also known as glycan epitopes. This monospecificity feature provides mAbs with distinct advantages: they can bind to glycans whose structures are frequently repetitive and found in multiple macromolecular contexts (for example, arabinogalactan epitopes that are present in glycoproteins and pectic polysaccharides such as rhamnogalacturonan I) and more importantly, their epitope binding specificity can be determined unambiguously. These mAbs can be used for either: (1) *in vitro* detection through glycome profiling (Pattathil et al., 2012) and (2) *in situ* visualisation by immunohistochemical methods (Avci et al., 2012). Glycome profiling (GP) involves sequential extraction of cell wall samples using a series of reagents increasing in harshness and then ELISA-screening these isolated extracts with mAbs in order to determine and monitor the glycan-epitopes released by each extraction. Sequential extractions allow cell wall glycans to be isolated in extracts on the basis of the relative tightness with which they are integrated into the final wall structure. GP provides data regarding cell wall epitope composition as well as the differences in extractability of these components in the wall (thereby revealing the relative tightness of their integration to the wall) (Pattathil et al., 2012). GP has been extensively used in analysing cell walls for functional characterisation of genes involved in cell wall biosynthetic processes, pretreated and bio-converted plant biomass, and comparative glycomics of different plant phylogenies based on their cell wall composition (Biswal et al., 2015, Popper et al., 2011, DeMartini et al., 2011). However, the limitations with GP are that firstly, low-molecular-weight glycans released by cell

wall extractions do not bind to solid supports such as nitrocellulose, glass slides, or multiwell plastic plates that are used for the screening assays. The lower limit of the glycan size that can be retained on such solid supports, while not definitively determined, is greater than 10 kDa. Secondly, certain glycans may get modified by the later harsh alkaline extraction conditions, for example, the loss of acetylation or methylation (Pattathil et al., 2010). Lastly, because glycome profiling is reliant on chemical/enzymatic extractions, absolute quantification of epitope composition in biomass/cell wall samples is problematic. This is due to the extraction methods abovementioned being rarely complete in releasing glycan epitopes into solution (Pattathil et al., 2015).

In situ visualisation by immunolabelling techniques requires the fixation, embedding, and sectioning of biomass samples which are then probed by mAbs followed by a fluorescently tagged secondary antibody allowing an *in situ* visualisation of glycan epitope distribution under a fluorescence microscope (Avci et al., 2012). Immunolabelling has aided in determining epitope distribution in cell-wall biosynthetic mutants such as WRKY transcription factor knockouts, xylan-deficient mutants, and comparing distribution of glycan epitopes in plant biomass before and after various methods of pre-treatment to reduce cell wall recalcitrance (Wang et al., 2010, Petersen et al., 2012). A major disadvantage of *in situ* visualisation is that any glycan epitopes that are buried within the cell walls are not exposed by the sectioning process and therefore, cannot be visualised (Avci et al., 2012). Also, any modification of glycans (e.g., acetylation in xylan) will render the epitopes unavailable for recognition by their corresponding mAb despite being present in the cell-wall (Pattathil et al., 2015). *in situ*

immunolocalisation studies along with GP could thus be significantly more powerful as these two methods together provide complementary information (Pattathil et al., 2015).

Recent characterisation of xylan-directed mAbs using a library of xylan structural epitopes prepared by automated oligosaccharide synthesis provides detailed information about the epitopes recognised by these mAbs (Schmidt et al., 2015, Ruprecht et al., 2017). Therefore, with the use of different mAbs, it is now possible to monitor the abundances of xylans that vary in their structures based on their degree of polymerisation (DP), arabinosylation, acetylation and MeGlcA substitution (Schmidt et al., 2015, Ruprecht et al., 2017).

Studies using the complementary approaches of GP and immunolabeling, and incorporating the details of abovementioned recent advances in xylan epitope characterisations provide a powerful method for the study of patterning of xylan deposition in different stages of stem development. Our study, for the first time, describes xylan deposition and its spatiotemporal distribution over different stages of Arabidopsis stem development/maturation through GP, xylan epitope monitoring, and immunolabelling. Moreover, the xylan patterns that we identified are supported by *in silico* gene expression analysis. Our results from GP, xylan epitope monitoring, immunolabelling, and expression data show that xylans increase throughout stem development. Interestingly, the abundances of certain xylan epitope structures appear to correlate with certain developmental stages of the stem. Lastly, GP illustrated that xylan epitope abundance and distribution may also influence the patterning and distributions of non-xylan epitopes such as pectins and xyloglucans across stem development. Therefore, using epitope-directed approaches may be useful in further characterising xylan

biosynthetic mutants based on their specific xylan-epitope phenotypes across developmental gradients of organs.

2.2 Results:

2.2.1 Glycome profiling reveals differences in cell wall glycan epitope distribution and abundances among sequential extracts throughout Arabidopsis stem development

Arabidopsis thaliana plants grown under identical growth conditions (Figure 2.1) were used to perform a developmental gradient-dependent study to reveal dynamics in xylan structure and deposition during stem maturation. Arabidopsis inflorescence stems of 24 cm in height were divided into 4 equal sections that represented upper apical (D1), lower apical (D2), upper basal (D3), and basal (D4) stem sections (Figure 2.1) in order to obtain samples representing different points along the gradient of the stem maturation process. Cell wall materials were isolated from these segments, and sequential extracts from these cell walls were subjected to glycome profiling (see Methods section). A comprehensive suite of plant cell-wall glycan-directed mAbs capable of monitoring most major non-cellulosic cell wall glycans (Pattathil et al., 2010) were employed to perform this analysis (Figure 2.2, Appendix A). These mAbs, available as hybridoma culture supernatants, are monospecific probes for the glycan sub-structures (epitope) they recognise. The use of mAbs to monitor xylans present in the cell-walls of Arabidopsis during stem development is highly suitable as most xylans are repetitive and display different substructures (e.g. acetylation, arabinosylation, and methyl glucuronic acid substitution) (Busse-Wicher et al., 2014, Rennie and Scheller, 2014). Most of the carbohydrate material was recovered in the 1M KOH extract, followed by the 4M KOH, carbonate, and oxalate extracts with the exception of the apical (D1) developmental stage wherein the second

highest amount of material was recovered in the oxalate extract (potentially due to the higher proportion of primary walls in this stage of stem development). Glycome profiling revealed the presence of most major non-cellulosic cell-wall glycan-epitopes across the stem developmental gradient (D1 to D4 segments) mentioned above and how these epitope abundancies varied across various extracts from these segments (Figure 2.2). In the oxalate extracts from D1 through D4 segments, a significant abundance of pectic-arabinogalactan and arabinogalactan epitopes was observed, as indicated by the strong binding of mAbs belonging to the RG-I/AG and AG-1 through 4 clades (grouping based on the hierarchical clustering of ELISA binding of these mAbs to structurally-defined plant polysaccharides) (Pattathil et al., 2010). Rhamnogalacturonan-I (RG-I) backbone epitopes were abundant also, as indicated by the high binding of the RG-I backbone clade of mAbs. However, overall patterns of abundancies were subtly different across developmental stages. One notable difference was the reduced abundance arabinogalactan epitopes recognised by the AG-1 and AG-2 clades of mAbs in the D2 and D3 segments. Again, the highest amounts of oxalate-released carbohydrate material were recovered in the D1 segments, hinting a significantly higher proportion of primary cell walls in this apical segment causing the release of an increased proportion of pectic-components. In the carbonate extract, except for the trace amounts of non-fucosylated and fucosylated xyloglucans, all other non-cellulosic glycan epitopes detected (including xylan, homogalacturonan, RG-I backbone, pectic arabinogalctan and, arabinogalctan epitopes) exhibited a general trend of increasing abundance as the stem matures (D1 to D4). However, marginally increased amounts of carbohydrates were released from D1 cell walls compared to other segments potentially due to the higher proportion of pectic components originating from

the increased presence of primary walls in apical (D1) stems. Following a developmentally-dependent pattern, the relative proportions of pectic backbone, pectic arabinogalactan, and arabinogalactan epitopes were significantly reduced in the 1M KOH extract from the D4 segment and the 4M KOH extracts from the D2, D3 and D4 segments. Xyloglucan epitopes were detected in the 1M and 4M KOH extracts from all stem developmental regions. In 1M KOH extracts, a marginally reduced proportion of xyloglucans were observed in the D2 and D3 segments. However, significantly higher abundances of xyloglucan epitopes were detected in 4M KOH across all extracts from all segments (Figure 2.2). Since the focus of this study is delineating xylan composition, structure, extractability, and deposition in the wall as a function of stem development, our analyses was focused on the specific clades of xylan-directed mAbs (Xylan-2 to Xylan-7) in our whole glycome dataset (Figure 2.2), the results of which are described in the subsequent sections.

Figure 2.1 *Arabidopsis thaliana* Col-0 background stems grown to ~24cm for stem harvesting.

2.2.2 Xylan-focussed epitope profiling reveals varied patterns in deposition of xylan sub-structures across stem development in *Arabidopsis*

We specifically focussed on the patterns of xylan epitope abundance and extractabilities among the four cell wall extracts isolated from the different developmental regions of the stems, D1-D4. We wanted to take advantage of the detailed epitope information that is currently available for all xylan-directed antibodies belonging to the Xylan-2, and Xylan-4 through Xylan-7 clades (Schmidt et al., 2015, Ruprecht et al., 2017). This epitope information allowed detailed insights into changes in xylan structure along the developmental gradient.

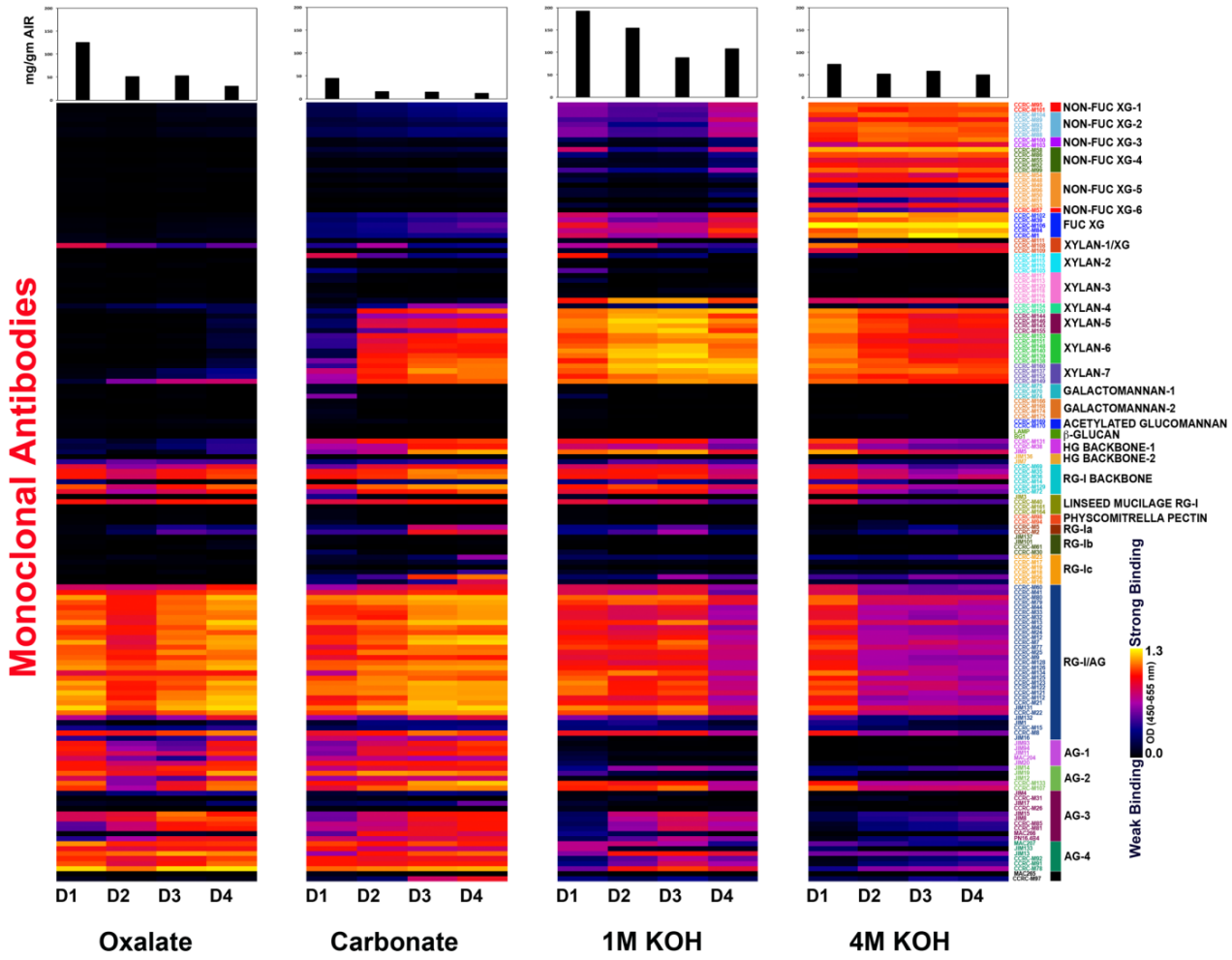

Figure 2.2: Glycome profiling of cell walls extracted from inflorescence stems at of *Arabidopsis* different development stages (D1-D4). These sequential extracts were screened using 155 mAbs against most major non-cellulosic plant cell wall glycans. The ELISA heat map depicts antibody binding strength where yellow, red, and black colours represent strong, medium, and no binding respectively. The groups of mAbs based on their reactivity to different cell wall glycans are identified in the panel at the right-hand side of the figure. The top bar graph shows the mg of soluble material (glucose equivalent) recovered per gram of biomass.

Figure 2.3 depicts the results of xylan epitope profiling of these developmental regions of the stem. Previous studies from our laboratory had broadly grouped xylan directed mAbs into 7 clades (Xylan-1 through Xylan-7 clades) based on the hierarchical clustering of ELISA binding response data of these mAbs against 55 structurally-defined plant polysaccharides (Pattathil et

al., 2010). More recent studies using an array of chemically synthesised , homogeneous oligosaccharides have delineated, in detail, the xylan structural features (epitopes) that are monospecifically recognised by antibodies belonging to the clades Xylan-4 through Xylan-7 (Schmidt et al., 2015, Ruprecht et al., 2017). In a broad sense, as depicted in Figure 2.3, we currently, have well-defined antibodies that detect xylan backbone epitopes with varying degrees of polymerization (DP = 3-8) (Xylan-6 and Xylan-7 clades), α-1,2-linked arabinosyl substituted xylan backbone region (CCRC-M110), α-1,3-linked arabinosyl substituted xylan backbone regions (CCRC-M154), glucuronic acid substituted xylan regions (CCRC-M150) and MeGlcA substituted xylan regions (Xylan-5 clade). Taken together, analyses using mAbs against this broad repertoire of xylan epitopes allows the monitoring of most major xylan structures present in higher plants.

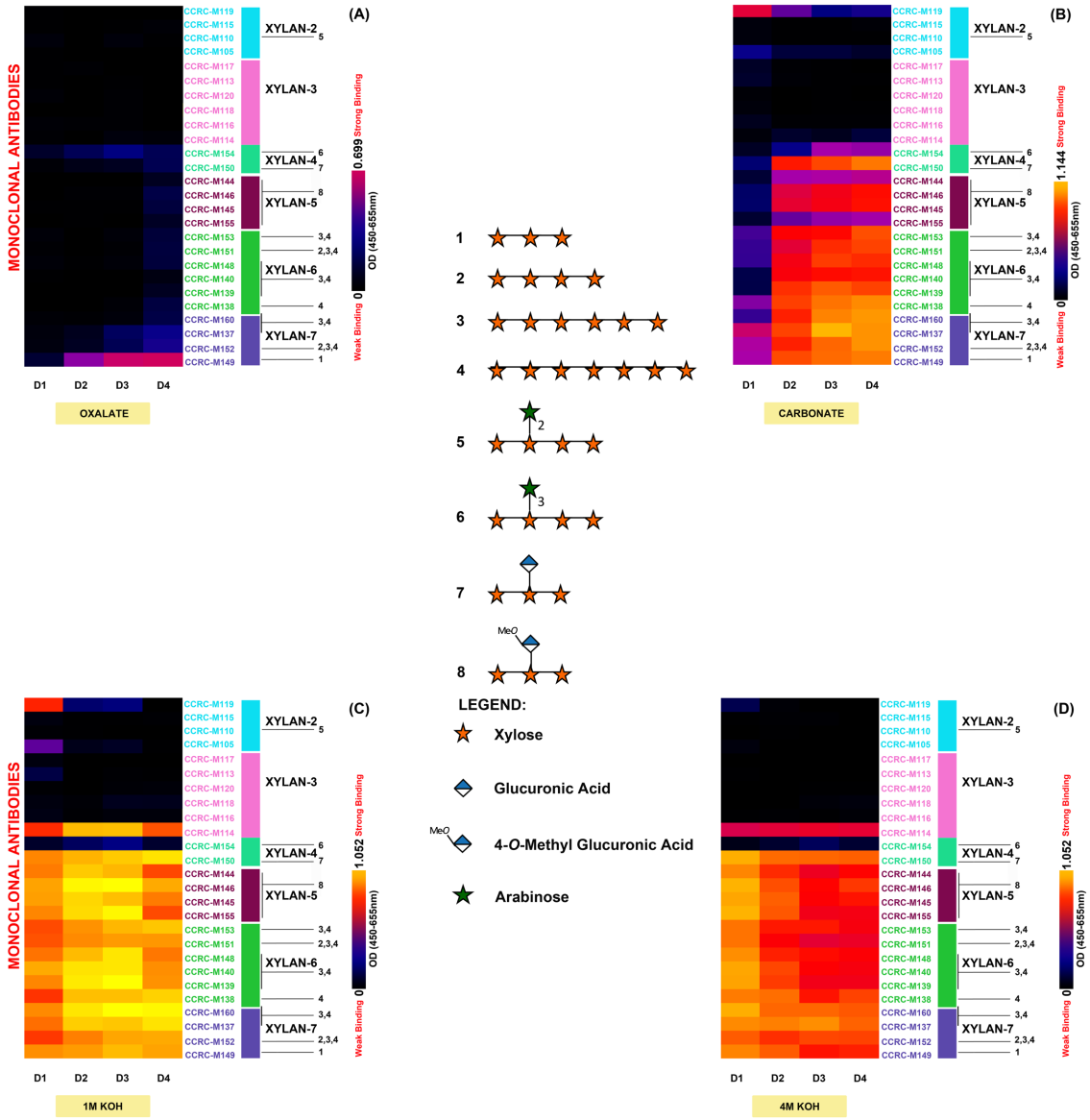

Figure 2.3: Xylan profiling of Col-0 inflorescence stems. ELISA binding signals specific to xylan epitope groups (Xylan-2 to Xylan-7) were taken from Figure 2.2 to depict specific xylans enriched at different stages of *Arabidopsis* stem development (D1-D4). The ELISA heat map depicts antibody binding strength, where yellow, red, and black colours represent strong, medium, and no binding respectively. The groups of mAbs based on their reactivity to different xylans are identified in the panels at the right-hand sides of each glycome profile. The middle illustration depicts the specific xylan structures recognised by specific mAbs (Schmidt et al., 2015, Ruprecht et al., 2017).

In the oxalate extracts from all segments, the only xylan epitope detected to a significant extent was the epitope recognised by CCRC-M149 (Xylan backbone DP=3) (epitope #1) (Figure 2.3). This epitope showed an increase in its abundance in oxalate extracts as the stem matures, thus maximum abundance is observed at the D4 segment stage. In carbonate extracts, however, xylan epitopes recognised by the Xylan-4 to Xylan-7 clades of antibodies first appeared in traces at the D1 stage, specifically, xylan backbone epitopes recognised by CCRC-M138, CCRC-M152, and CCRCM-149. At the D2 stage we observed a significant epitope abundance and increases as stem maturation occurs. However, exceptions occurred in the carbonate extracted glycan epitopes recognised by CCRC-M154 of the Xylan-4 clade and CCRC-M144 and CCRC-M155 of the Xylan-5 clade displaying lower abundances. Interestingly, xylan epitopes recognised by CCRC-M119 were present to a significant extent only in the apical stage of stem development.

In harsher extractions such as 1M and 4M KOH extracts, xylan epitopes recognised by CCRC-M114 of the Xylan-3 clade, CCRC-M150 of the Xylan-4 clade, and all antibodies belonging to the Xylan-5 through Xylan-7 clades were abundantly present. However, their patterns of extractability varied depending on the developmental regions. For instance, comparatively, the maximum mAb signal for xylan-directed mAbs in 1M KOH were from the D2 and D3 stages. In 4M KOH extracts, the maximum mAb signal for CCRCM-150 (Xylan-4) and Xylan-5 to Xylan-7 clades occurred at the D1 stage. This could be due to the increased formation of secondary walls through lignification in mature stems which could result in lower extractability of directly or indirectly lignin-associated cell wall components including xylan. In summary, based on oxalate, carbonate, and 1M KOH extracts, we observed an overall increase in xylan epitope

abundance in these extracts as the stem matures, suggesting enhanced biosynthesis and deposition of xylans. Alternatively, the degree of extractability of xylans are different depending on their stage of development. Where 1M KOH showed high extractability based on the mAb signal at a maximum in the D2-D3 (middle) part of stem and 4M KOH extracts display extractability only at the D1 stage of the Arabidopsis inflorescence stem.

2.2.3 Xylan immunolabelling of stems across different developmental stages

Arabidopsis inflorescence stems were sectioned, paraffin embedded, deparaffinised, treated with 0.1M KOH for 15 minutes, and followed by immunolabelling according to methods by Avci et al. (2012). The 0.1M KOH treatment was performed because untreated sections produced little or no signal in all sections of all the developmental stages sampled. Treatment with 0.1M KOH removes base-labile modifications on the glycan epitopes present *in vivo* to allow for detectable binding with the selected xylan-directed mAbs, all of which were generated against base-extracted xylan preparations (Pattathil et al., 2010). We selected these specific antibodies to be representative of the different groups of xylan-directed antibodies (Xylan-2 to Xylan-7) based on their abundance levels from the xylan-specific glycome profiles (Figure 2.3). Our immunolabelling results show that xylan epitopes display increasing abundance throughout stem development in Arabidopsis. However, certain xylan epitopes, particularly those recognised by CCRC-M119 and CCRC-M114 are only present at later stages of stem development, towards the basal portion of the stem (D4) (Figure 2.4). *in situ* visualisation of Arabidopsis stems using immunolabelling using the group of selected mAbs that bind to specific xylan epitope confirmed the results of our glycome profile revealing that hemicellulosic epitopes increase as stem development progresses.

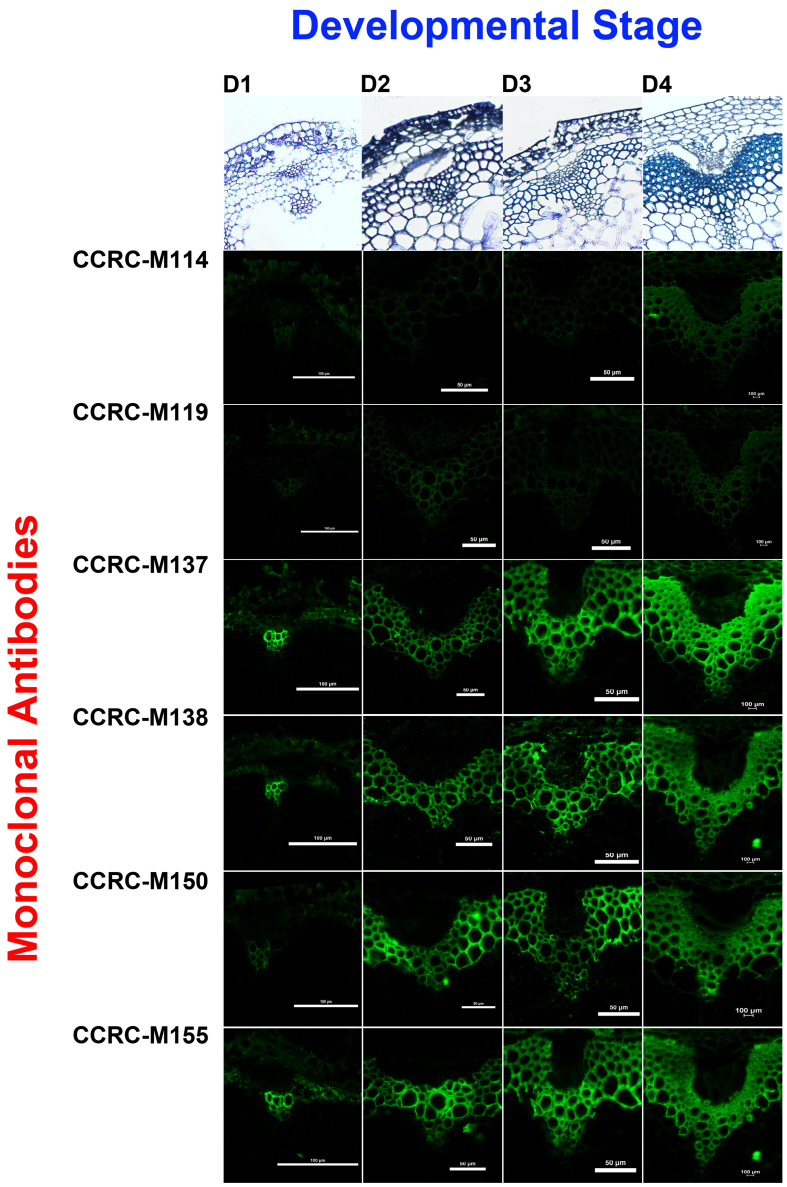

Figure 2.3: Immunolabelling of xylan epitopes of Col-0 stems at different development stages (D1-D4). Top row: toluidine blue-O staining of stems to show anatomical differences of vasculature tissue at different developmental stages. Equivalent sections were immunolabelled with xylan-directed mAbs CCRC-M114, CCRC-M119, CCRC-M137, CCRC-M138, CCRC-M150, and CCRC-M155. CCRC-M114 and CCRC-M119 show little to no signal and CCRC-M137 to CCRC-M155 show increasing signal throughout stem development.

2.2.4 *in silico* analysis of putative and proven xylan biosynthesis genes and enzymes reveals similar patterns of expression during development compared to glycome profiling using xylan-directed mAbs

To determine whether our observed glycome profiling and immunolabelling patterns were due to developmentally regulated differential expression of xylan biosynthetic genes or from developmentally regulated post-translational modification of enzyme products, we performed *in silico* expression analysis using a publicly available microarray database of proven and putative xylan biosynthesis genes and enzymes to determine whether or not their expression pattern share similarities with our xylan epitope profiles. We accessed the Expression Browser database from the Botany Array Resource and selected the AtGenExpress developmental dataset (Toufighi et al., 2005). From this, we selected the relative gene expression output option that used the average gene expression of replicate treatments relative to the appropriate control. We then surveyed the relative gene expression data of known xylan genes that were available in this dataset and created an output list of 20 xylan genes (Figure 2.4).

The gene expression data displayed overall patterns similar to the xylan-specific glycome profiles and immunolabelling data in that most genes increased throughout developmental stages with their relative expression strongly increased at later stages of stem development. However, we also observed that certain selected xylan genes do not display increasing patterns of expression towards later stages of stem development. For example, IRX9-L, GUX4/5, and GXM2 showed variable expression changes in all surveyed stages of stem developments. The expression patterns of these particular genes may not fully represent the

patterns obtained from our immunolabelling results because the list of chosen mAbs only represented a handful of xylan epitopes. Therefore, any of the mAbs that recognised xylan epitopes corresponding to the expression patterns of IRX9-L, GUX4/5, and GXM2 may not have been represented. IRX9-L is a functional homologue of IRX9 belonging to the glycosyltransferase (GT) 43 family and is known to play a minor redundant role in GX backbone biosynthesis when compared to IRX9 (Wu et al., 2010). A study by Wu et al. (Wu et al., 2010) demonstrated that *irx9-L* alleles displayed growth and secondary cell wall formation phenotypes similar to wild-type. Additionally, IRX9-L was indicated to perform non-essential redundant functions with IRX9. Hence, this may explain why the variable gene expression changes observed in the *in silico* analyses were not fully represented with the corresponding immunolabelling data. GUX1-GUX5 are GT 8 family proteins that may have putative roles in glucuronosyl substitutions onto the xylan backbone. Studies using GlcA transferase (GlcAT) assays demonstrated that GUX2 and GUX4 have GlcAT activities (Mortimer et al., 2015, Rennie et al., 2012). The mAb CCRC-M150 recognises GlcA substituted xylan epitopes (Schmidt et al., 2015, Ruprecht et al., 2017). Using this antibody, we were able to correlate our xylan-focussed epitope profiling and immunolabelling results with the developmental-dependent gene expression patterns of GUX2 and GUX4. Our results demonstrated that GUX2 expression patterns were highly correlated with the carbonate extracts from our xylan-focussed epitope profiling and immunolabelling. Further, we showed that GlcA-substituted xylan epitope abundance appeared early at the D2 stage (Figure 2.3 and Figure 2.4) and increased as stem maturation occurred and was concomitant to GUX2 developmental-dependent gene expression patterns (Figure 2.5). Interestingly, however, similar gene expression patterns between GUX2

and GUX4 were not observed and a weak correlation between GUX4 gene expression patterning and CCRC-M150-recognised epitope abundance occurred. Lastly, GXM2 is a DUF579 domain-containing proteins known to be implicated in glucuronoxylan methylation. Recent genetic and chemical analysis has revealed that GXM2, along with GXM1 and GXM3 are methyltransferases involved in 4-*O*-methylation of GlcA sidechains. Furthermore, the analyses demonstrated that GXM1, GXM2, and GXM3 are functionally redundant glucuronoxylan methyltransferases and among them, GXM3 is the predominant gene responsible for GlcA methylation (Lee et al., 2012). This may explain why the immunolabelling signal intensity of CCRC-M155, which specifically detects xylan epitopes containing 4-*O*-MeGlcA substitutions, corresponds to the expression pattern of GXM3. It should also be noted, however, that we cannot confirm whether or not the expression data of the xylan genes surveyed that correspond to our glycome profile and immunolabelling results are directly responsible for the observed distribution patterns of xylan epitopes.

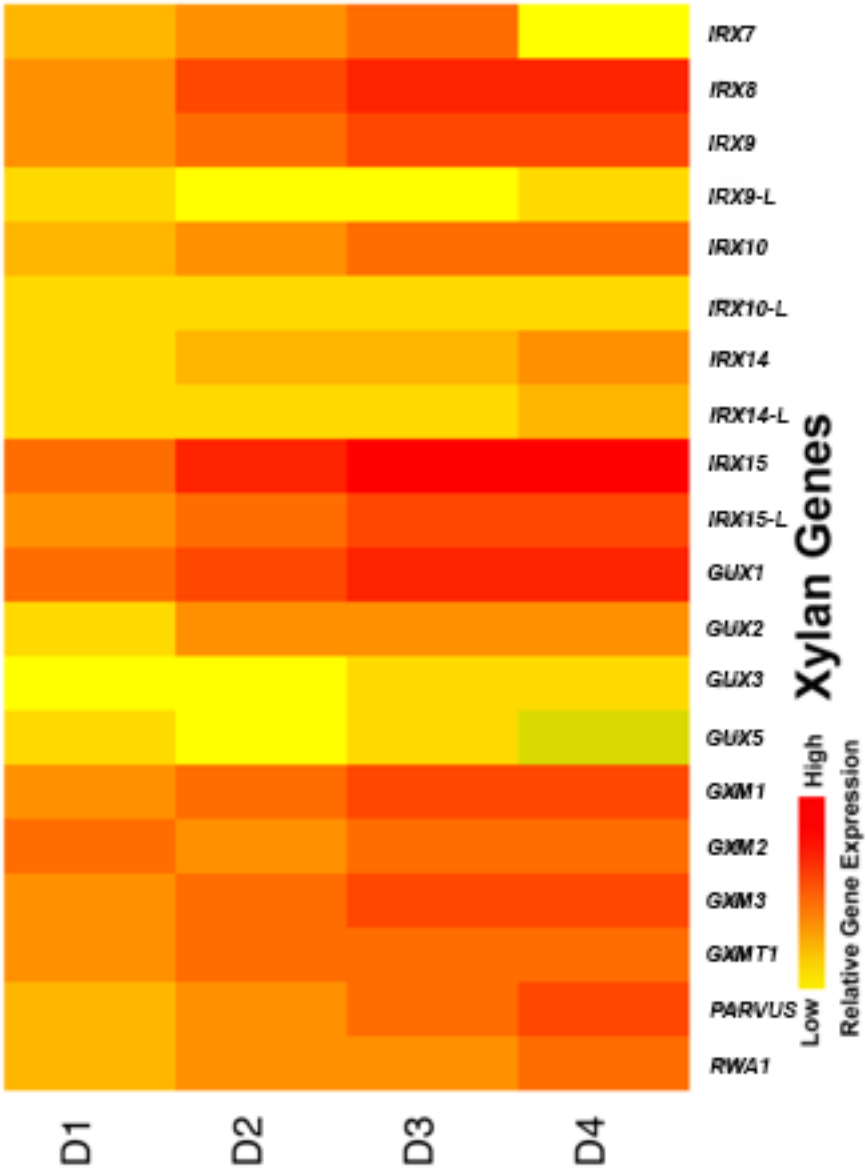

Figure 2.4: Heat map showing gene expression from publicly available microarray data (Toufighi et al., 2005) of xylan genes in different stages of Col-0 stem development from immature (D1), intermediate (D2-D3), and mature (D4) stems. Levels of low (white) and high expression (red) are shown on a log2 scale for each xylan gene

2.3 Discussion:

Plants cell walls are structurally highly complex, heterogeneous, and vary significantly across species, organs, and development. The studies herein analysed variations in cell wall makeup during stem maturation in Arabidopsis, focussing especially on xylan integration into stem cell walls. Previous studies have demonstrated organ development dependent variations in cell wall makeup in diverse phylogenetic classes of plants such as willow (*S. purpurea*) and switchgrass (Wan et al., 2014, da Costa et al., 2017). However, more comprehensive and rapid approaches employing advanced and reliable cell wall analytical tools that can operate in a medium to high throughput manner have always been in demand. In the current study, we developed, validated and report such an advanced immunological approach for higher plant xylan analyses employing a comprehensive collection of fully characterised xylan-directed mAbs. Agreeing with the abovementioned studies on willow and switchgrass, the whole glycome profiles (Figure 2.2) of cell walls isolated from different development stages of Arabidopsis stems revealed changes in the composition and extractability of most major non-cellulosic cell wall matrix glycans and revealed unique cell wall compositions for different developmental stages of this organ. Of the comprehensive suite of cell wall directed mAbs used in the glycome profiling analysis, detailed structural information about the epitopes recognised by most xylan directed antibodies is available (Schmidt et al., 2015, Ruprecht et al., 2017). Together, these xylan-directed antibodies can monitor seven distinct structural regions of xylans: 1) short, unsubstituted xylan backbone regions (DP = 3-4); 2-4) larger xylan backbone regions (DP > 4) with and without limited arabinose substitutions; 5-8) α-1,2-linked arabinosyl, α-1-3-linked arabinoxyl, GlcA, and 4-*O*-MeGlcA substituted regions. These antibodies,

therefore, allow monitoring of most major structural regions of complex xylans in higher plants, including unsubstituted, arabinosyl-substituted and glucuronosyl/methylglucuronosyl-substituted xylan structures (Schmidt et al., 2015, Ruprecht et al., 2017). Given this extent of detailed epitope structure information available for such a large group of xylan-directed antibodies, a unique opportunity opens up towards gaining a molecular level understanding of xylan formation and integration into cell walls under diverse spatiotemporal stages of plant organs. In this work, we took advantage of these well-characterised xylan-directed probes to study Arabidopsis stem development and developed an advanced tool for rapid and reliable characterisation of xylan formation and integration to the walls in higher plants.

Our results showed that in Arabidopsis, xylan incorporation is initiated early on in vascular tissue development; however, the integration of the different xylan epitopes surveyed vary across developmental stages of the stem. This is clearly demonstrated by the altered the extractability of specific xylan epitopes from cell walls isolated in different developmental regions. Summarising the glycome profile results of cell walls from D1 (youngest, apical) to D4 (most mature, basal) segments, we generated a table depicting detection of the eight (8) classes of xylan epitopes mentioned above amongst the stem cell wall extracts (Table 1).

Oxalate extracts contained only xylan backbone trisaccharide epitope with a DP of 3 in D2-D4 segments as indicated by the abundance of CCRC-M149 binding to these extracts. A possible explanation is that CCRC-M149 is recognising APAP1 instead of DP-3 xylan epitopes. Studies by Tan et al. (2013) demonstrated that CCRC-M149 exclusively showed strong binding to the domain of the purified APAP1 YS2 glycoconjugate. In addition, there is possible further evidence of CCRC-M149 binding to APAP1. The proposed structure of APAP1 showed that a

structural unit composed of a DP-3 xylan structure, this may provide supporting evidence to the hypothesis that APAP1 glycoconjugates exist not only in cell cultures but are also embedded in the cell-walls of tissues *in planta* (Tan et al., 2013). Unfortunately, more experiments are required to confirm our hypothesis.

In carbonate extracts, both substituted, unsubstituted xylan epitopes are barely present in the youngest tissue (D1) with exceptions such as CCRC-M137 and CCRC-M138, CCRC-M160, and CCRC-M149 all of which recognised linear xylan backbone structures with varying degrees of DP. We also observe that linear epitopes consisting of DP-4 to DP-8 xylan backbones are already embedded at the youngest stage of the stem (D1). Subsequently, GlcA and MeGlcA substituted xylans only start to appear at the start of the D2 stage and either increase or remain their xylan epitope signal abundance.

These results indicate that there exist sub-classes of xylans which are loosely-integrated xylans to the cell-walls because they are easily extracted by least harsh reagents such as oxalate and carbonate. Furthermore, the extractability and abundance depends on different xylan structures. For example, xylan epitopes recognised by CCRC-M138 and CCRC-M137 that are specific to xylan backbones appear as earlier in the D1 Stage and increase in signal as stem development progresses. In CCRC-M150, that recognises GlcA substitutions on xylan backbones, only appear at the start of D2 and increase in signal as well. These increasing signal trend is recapitulated in the *in situ* dataset (Figure 2.3) In terms of extractability, MeGlca substitutions vary in terms of their degree to which they are integrated into the wall. For instance, MeGlcA-xylan epitopes recognised by CCRC-M146 and CCRC-M145 are easily extractable from the D2 stage onwards. However, other mAbs recognising MeGlcA-xylan

epitopes are not so easily extractable using carbonate due to the weak signals observed (CCRC-M144, and CCRC-M155) from Figure 2.3B. Lastly, CCRC-M154 specifically recognises xylan epitopes with an α-1,3-arabinosyl substitution and is only present in the carbonate extract, suggesting that arabinosylation occurs in Arabidopsis despite being classified as a dicot where GX is the predominant form of xylan. However, as earlier mentioned, primary cell-wall in Arabidopsis do compose of xylan structures (Mortimer et al., 2015). The extent to which xylans occur in the primary cell-wall and arabinosylation of herbaceous dicots occur requires further investigation. These loosely integrated classes of xylan do exhibit variations across developmental stages. Furthermore, these classes of xylan seem to contain unsubstituted and substituted structural regions of xylan. However, loosely incorporated xylan in the apical (D2) region appear to consist predominantly of xylan backbone epitopes, GlcA substituted xylan epitopes, and, MeGlca substituted xylan epitopes. Lastly, a clear epitope signal abundance from the CCRC-M154 only appeared towards the later stages in stem maturation (D3-D4). Our study demonstrated that the degrees of variation in xylan epitope structure and integration are exhibited by loosely-bound xylan components across developmental stages of the stem based on carbonate extracts.

Table 1: Xylan epitope patterning observed in different extracts across developmental stages of Arabidopsis based on Figure 2. DP = degree of polymerisation; -, +, ++, and +++ refers to: absent, present, abundant, and highly abundant respectively.

Xylan Epitope	Oxalate				Carbonate				1M KOH				4M KOH			
	D1	D2	D3	D4	D1	D2	D3	D4	D1	D2	D3	D4	D1	D2	D3	D4
Xylan backbone DP-3	-	++	++	++	++	+++	+++	+++	+++	+++	+++	+++	+++	+++	++	++

Xylan backbone ≥ DP-4	-	-	-	+	+	++	+++	++	++	+++	+++	+++	+++	+	+	+
Xylan backbone ≥ DP-6	-	-	-	+	+	++	+++	+++	++	++	+++	+++	+++	++	++	++
Xylan backbone DP-8	-	-	-	+	+	++	+++	+++	++	+++	+++	+++	+++	++	++	++
α-1,2-linked arabinose	-	-	-	-	-	-	-	-	-	-	-	-	-	-	-	-
α-1,3-linked arabinose	-	+	+	+	-	+	++	++	-	-	-	-	-	+	-	-
Glucuronic acid	-	-	-	+	-	++	++	+++	++	++	+++	+++	+++	++	++	++
4-*O*-methyl glucuronic acid	-	-	-	+	-	++	++	++	++	++	+++	++	+++	++	++	++

The results of our glycome profiling demonstrates that all xylan epitope categories except for arabinosylated xylan backbones, specifically, α-(1,2)-Ara substitutions are significantly present in 1M and 4M KOH extracts of cell walls from all developmental regions. The xylan epitopes from concentrated alkali extracts are thereby termed as tightly-integrated xylan classes. These

tightly-integrated classes of xylan epitopes contain both unsubstituted and substituted regions (indicated by the binding of all Xylan-4 through 7 clades of mAbs).

Our observation with xylan backbone epitopes and MeGlcA substituted xylans in 1M KOH extract is that the increasing of epitope signal abundance peaks at the intermediate D2-D3 stem segments (maturing phase) and at the D4, mAb signals for these xylan backbone epitopes subsequently reverts back to its original signal abundance found in the apical D1 stage. For example, CCRC-M144, CCRC-M155, and CCRC-M145 mAb, which are specific for MeGlcA substituted xylans (epitope #8, Figure 2.3), demonstrate that these tightly-integrated MeGlcA substituted xylan epitopes display maximum extractability at the intermediate stages (D2-D3) (Figure 2.3C) based on their binding intensity. A possible reason for this pattern is that despite being tightly integrated into the cell-wall, variations in the degree to which they are integrated into the wall based on clades Xylan-4 to Xylan-7. Xylan biosynthesis for the tightly-bound sub-class, based on its patterning, occurs in a dynamic process. We speculate that the observed dynamics of xylan epitope extractability is possibly due to xylan remodelling i.e removal of substitutions, backbone elongation, and acetylation; however, this hypothesis is yet to be proven. On the other hand, an increase in mAb signal from CCRC-M150 that recognises GlcA substituted xylans (epitope #7, Figure 2.3) during stem maturation only from 1M KOH extracts (Figure 2.3C). This suggests that GlcA substituted xylans are only easily extracted at the basal portion of the stage.

Immunolabelling analysis conducted in our study largely agreed with our glycome profiling results. Both methods displayed an increased intensity of labelling during stem maturation. However, our results contradict those previously gathered by Kim and Daniel using

xylan-directed LM10 and LM11 mAbs. They obtained different xylan epitope distributions compared to our study (Kim and Daniel, 2012). Their study selected LM10, displaying specificity towards xylans that cannot be modified at the non-reducing end and its 2 and 3 positions; and LM11, which recognises a xylose disaccharide structure that cannot be modified at their 3 position(Ruprecht et al., 2017). Using these antibodies, their results displayed no differences in immunolabelling intensities in vessels and fibres at the apical and basal stem portions of Arabidopsis. Our results on the other hand clearly demonstrated that xylans with less restriction towards substitutions in the backbone (recognised by CCRC- CCRC-M138) and GlcA substituted xylan (CCRC-M150) displayed increasing intensities as stem development progressed. Additionally, xylan epitopes that bind to CCRC-M114 and CCRC-M119 mAbs are absent in early (D1) and intermediate (D2-D3) stages but barely appear in mature stem segments (D4). There are critical differences between these two studies. In our study, we surveyed a more comprehensive representation of stem developmental gradients including four regions: apical (D1), lower apical (D2), upper basal (D3), and basal (D4). In addition, we used a more comprehensive repertoire of xylan-directed mAbs whose epitopes are well-defined. Hence, a direct comparison between these two studies is not feasible. Our whole glycome profiling, xylan epitope-directed profiling, and *in silico* expression analysis of xylan genes (Toufighi et al., 2005) also contradict the transcriptomic studies of Arabidopsis performed by Minic et al (Minic et al., 2009), suggesting that xylan deposition starts to occur at the intermediate and late stages of stem development.

We represented the gravimetric amounts of material extracted out during each extraction step and the amounts of carbohydrate materials decreased with increasing stem

maturity. This is likely because, as the stem matures the secondary cell wall formation increases with increasing lignification processes. Hence, the extractability of non-cellulosic matrix glycans is reduced due to the increased abundance of more structurally rigid secondary walls. One of the main objectives of this study was to develop an optimised workflow for dissecting xylan epitope extractability from different developmental zones of the stem. However, in immunolabelling, epitope distributions are surveyed *in situ*. For example, this may be difficult wherein the distribution of the epitopes that we monitored are inaccessible (even after 0.1M KOH treatment) or are unrecognised by the antibody, hence we cannot directly correlate our glycome profiling and immunolabelling. Furthermore, subjecting the cell wall to chemical fractionation may cause modification/s of some glycans resulting in the loss of some epitope structures (Avci et al., 2012, Pattathil et al., 2012, Pattathil et al., 2015).

Our systematic approach allows the comprehensive monitoring of the spatial distribution of specific xylan structures that occured during stem development. We discovered using the available epitope structures and their corresponding mAb that xylans are embedded/biosynthesised in a developmental- and subclass-dependent manner. Summarising Figure 2.3, we discovered that in loosely integrated xylans from oxalate and carbonate extracts, APAP1 and/or APAP1-like epitope structures (Tan et al., 2013) appear at the earliest stage of stem development (D1), followed by xylan backbone epitopes, then GlcA- and MeGlcA substituted xylan epitopes, and lastly by α-1,3-arabinosylated xylan epitope. Tightly-bound xylans from alkali extracts display variations in their degree of extractability depending on the stage of stem development that was sampled. The observed decrease in 4M KOH extracts after the D1 stage shows that xylan epitopes are highly-integrated into the wall, preventing further

release despite using 4M KOH extract. All in all, combining glycome profiling, immunolabelling techniques, and the available xylan epitope characterisation data (Schmidt et al., 2015, Ruprecht et al., 2017), we can apply such an approach in order to explain certain behaviours in the formation of wood, an important potential source of raw materials for biofuel production (Gritsch et al., 2015, Zhong and Ye, 2015). Further, applying our approach to survey the structural and compositional differences observed in xylan biosynthetic mutants will reveal new insights into the functional characterisation of the complete spectrum of genes required for xylan biosynthesis/modification in the context of stem development (Brown et al., 2007). Lastly, our approach is a rapid, cost-effective, and is a high-throughput method to determine the effects of pretreatments on xylan and other hemicellulosic structures in biofuel crops without requiring time-consuming and sophisticated computational methods involved in NMR and FTIR approaches (Pena et al., 2007, Xu et al., 2013, Samuel et al., 2011).

2.5 Conclusion:

Our method of xylan epitope-directed glycome profiling complemented by *in situ* visualisation using immunolabelling provides a viable approach to examine specific structurally characterised xylan epitopes that are deposited in the cell wall at different stages of stem development. The overall pattern demonstrates that xylans increase during Arabidopsis stem maturation. Our approach also reveals that xylan epitope composition is dynamic as the stem matures with respect to its epitope abundance and degree of extractability. In relation, we present the existence of different sub-classes of xylan epitopes that vary in their degree of integration into the wall. These sub-classes also show different epitope abundance patterning where loosely-integrated xylans from oxalate and carbonate display specific xylan epitopes

early on and increases in epitope abundance as the stem matures. In addition, we show that arabinosylated xylans, specifically α-(1,2)-Ara substituted xylans exist in herbaceous dicots such as Arabidopsis and are weakly integrated into the primary cell-wall. Lastly, weakly-bound xylan epitope structures are integrated into the wall in a stepwise manner that is commensurate to the stem's maturation processes.

Tightly-integrated xylans from alkali extracts in contrast, demonstrated variations in their extractability of xylans as stem development progresses. Tightly-integrated xylan backbone epitopes and substituted xylan epitopes in 1M KOH extracts (Xylan- to Xylan-7 clades) show that maximum extractability of these epitopes occurs at the intermediate stage of the stem. Moreover, in 4M KOH extracts, decreases in xylan epitope extractability occur much earlier than in 1M KOH extracts due to the maximum signal abundance being present only at the apical portion of the stem (D1).

Therefore, our approach consequently opens up the feasibility of monitoring the changes in xylan epitope composition throughout stem development that are caused by specific mutations among xylan biosynthetic/modifying genes. The approach could also be a powerful tool in an evolutionary context in that phylogenetic analyses of variations in xylan structures across species, organ, and developmental stages can be performed in a rapid and medium to high throughput manner. Finally, our approach opens up the possibility to employ other cell wall glycan-directed mAbs for monitoring other important cell wall glycans such as pectins, arabinogalactans, and xyloglucans during development in diverse organs of plants.

2.6 Methods:

2.6.1 Growth and Harvesting

Thirty-two wild-type *Arabdopsis thaliana* ecotype Columbia plants were germinated on 0.8% w/v agar plates containing MS nutrients and B5 vitamins for 2 weeks prior to being transferred to compost containing vermiculite and perlite (10:1:1). Plants were subsequently grown at 22°C in controlled-environment cabinets using short-day (8 h light/ 16 h dark) followed by long-day (16 h light/ 8 h dark) conditions. Arabidopsis inflorescence stems were grown to a height of 22cm-25cm and were approximately divided into four equal segments from top to bottom to represent the different stages of stem development.

2.6.2 Biological material

24-cm inflorescence stems cut into 6-cm equal segments and were flash-frozen using liquid nitrogen. The segments were subsequently ground with a mortar and pestle. 200 mg ground tissue was then transferred to a 50 ml tube for Alcohol Insoluble Residues (AIR) were prepared as previously described (Pattathil et al., 2012). Glycome profiling of these AIR preparations were performed using the method described in Pattathil et al. (Pattathil et al., 2012). In brief, glycome profiling involved preparing cell wall extracts using increasingly harsh reagents (Ammonium oxalate, sodium carbonate, 1M KOH, 4M KOH) and subsequent enzyme-linked immunoabsorbent assay (ELISA) screening of these extracts using a comprehensive suite of plant cell wall glycan-directed monoclonal antibodies (mAbs). Plant glycan-directed mAbs were from laboratory stocks (CCRC, JIM, and MAC series) at the Complex Carbohydrate Research Center (available through CarboSource Services; http://www.carbosource.net) or were obtained from BioSupplies (Australia) (BG1, LAMP). Additional information about the mAbs employed in glycome profiling can be seen in Supplementary Table 1.

2.6.3 Histology

Inflorescence stem segments were fixed for 1 hour in ice-cold 100% acetone and rotated (20 rpm). The acetone was removed and replaced with fresh ice-cold 100% acetone and rotated (20 rpm) overnight at 4°C. Samples were then passed through 3:1, 1:1, and 1:3 gradients of acetone:histoclear for one hour each followed by an extra 100% histoclear change. Tissue samples were incubated at 57°C for paraplast (wax) infiltration. Tissue blocks with appropriate size and orientation were sectioning using a microtome in order to obtain 5μm thick sections, sections were subsequently placed on charged glass slides and dried at 45°C for 30 minutes. For anatomical observations, sections were stained with 0.025% toluidine blue (2 min). After staining, sections were dehydrated with 75% (v/v) ethanol. Sections were observed under a compound microscope with bright-field illumination.

2.6.4 Immunolabelling

Stem sections were treated with 0.1M KOH with 10mM $NaBH_4$ for 15 minutes and were rinsed with ddH2O three times. Immunolabelling was performed as described previously (Avci et al., 2012). Labelling was visualised using an Eclipse 80i light microscope (Nikon, Melville, NY) equipped with epifluorescence optics and Nikon B-2E/C filter. Images were captured using a Nikon DS-Ri1 camera head (Nikon, Melville, NY) and NISElements Basic Research software. Images were assembled without further processing using Adobe Photoshop (Adobe Systems, San Jose, CA)

2.7 References:

AVCI, U., PATTATHIL, S. & HAHN, M. G. 2012. Immunological approaches to plant cell wall and biomass characterization: immunolocalization of glycan epitopes. *Methods Mol Biol,* 908**,** 73-82.

BISWAL, A. K., HAO, Z., PATTATHIL, S., YANG, X., WINKELER, K., COLLINS, C., MOHANTY, S. S., RICHARDSON, E. A., GELINEO-ALBERSHEIM, I., HUNT, K., RYNO, D., SYKES, R. W., TURNER, G. B., ZIEBELL, A., GJERSING, E., LUKOWITZ, W., DAVIS, M. F., DECKER, S. R., HAHN, M. G. & MOHNEN, D. 2015. Downregulation of GAUT12 in Populus deltoides by RNA silencing results in reduced recalcitrance, increased growth and reduced xylan and pectin in a woody biofuel feedstock. *Biotechnol Biofuels,* 8**,** 41.

BROWN, D. M., GOUBET, F., WONG, V. W., GOODACRE, R., STEPHENS, E., DUPREE, P. & TURNER, S. R. 2007. Comparison of five xylan synthesis mutants reveals new insight into the mechanisms of xylan synthesis. *Plant J,* 52**,** 1154-68.

BUSSE-WICHER, M., GOMES, T. C., TRYFONA, T., NIKOLOVSKI, N., STOTT, K., GRANTHAM, N. J., BOLAM, D. N., SKAF, M. S. & DUPREE, P. 2014. The pattern of xylan acetylation suggests xylan may interact with cellulose microfibrils as a twofold helical screw in the secondary plant cell wall of Arabidopsis thaliana. *Plant J,* 79**,** 492-506.

CARPITA, N. C. 1996. Structure and biogenesis of the cell walls of grasses. *Annual Review of Plant Physiology and Plant Molecular Biology,* 47**,** 445-476.

DA COSTA, R. M. F., PATTATHIL, S., AVCI, U., LEE, S. J., HAZEN, S. P., WINTERS, A., HAHN, M. G. & BOSCH, M. 2017. A cell wall reference profile for Miscanthus bioenergy crops highlights compositional and structural variations associated with development and organ origin. *New Phytologist,* 213**,** 1710-1725.

DEMARTINI, J. D., PATTATHIL, S., AVCI, U., SZEKALSKI, K., MAZUMDER, K., HAHN, M. G. & WYMAN, C. E. 2011. Application of monoclonal antibodies to investigate plant cell wall deconstruction for biofuels production. *Energy & Environmental Science,* 4**,** 4332-4339.

GRITSCH, C., WAN, Y., MITCHELL, R. A., SHEWRY, P. R., HANLEY, S. J. & KARP, A. 2015. G-fibre cell wall development in willow stems during tension wood induction. *J Exp Bot,* 66**,** 6447-59.

HAO, Z. & MOHNEN, D. 2014. A review of xylan and lignin biosynthesis: foundation for studying Arabidopsis irregular xylem mutants with pleiotropic phenotypes. *Crit Rev Biochem Mol Biol,* 49**,** 212-41.

IMAMURA, T., WATANABE, T., KUWAHARA, M. & KOSHIJIMA, T. 1994. Ester linkages between lignin and glucuronic acid in lignin-carbohydrate complexes from Fagus crenata. *Phytochemistry,* 37**,** 1165-73.

KEEGSTRA, K. 2010. Plant cell walls. *Plant Physiol,* 154**,** 483-6.

KIM, J. S. & DANIEL, G. 2012. Immunolocalization of hemicelluloses in Arabidopsis thaliana stem. Part I: temporal and spatial distribution of xylans. *Planta,* 236**,** 1275-88.

LEE, C., TENG, Q., ZHONG, R., YUAN, Y., HAGHIGHAT, M. & YE, Z. H. 2012. Three Arabidopsis DUF579 domain-containing GXM proteins are methyltransferases catalyzing 4-o-methylation of glucuronic acid on xylan. *Plant Cell Physiol,* 53**,** 1934-49.

LEE, K. J., MARCUS, S. E. & KNOX, J. P. 2011. Cell wall biology: perspectives from cell wall imaging. *Mol Plant,* 4**,** 212-9.

LOQUE, D., SCHELLER, H. V. & PAULY, M. 2015. Engineering of plant cell walls for enhanced biofuel production. *Curr Opin Plant Biol,* 25**,** 151-61.

MINIC, Z., JAMET, E., SAN-CLEMENTE, H., PELLETIER, S., RENOU, J. P., RIHOUEY, C., OKINYO, D. P., PROUX, C., LEROUGE, P. & JOUANIN, L. 2009. Transcriptomic analysis of Arabidopsis developing stems: a close-up on cell wall genes. *BMC Plant Biol,* 9**,** 6.

MORTIMER, J. C., FARIA-BLANC, N., YU, X., TRYFONA, T., SORIEUL, M., NG, Y. Z., ZHANG, Z., STOTT, K., ANDERS, N. & DUPREE, P. 2015. An unusual xylan in Arabidopsis primary cell walls is synthesised by GUX3, IRX9L, IRX10L and IRX14. *Plant J,* 83**,** 413-26.

MORTIMER, J. C., MILES, G. P., BROWN, D. M., ZHANG, Z. N., SEGURA, M. P., WEIMAR, T., YU, X. L., SEFFEN, K. A., STEPHENS, E., TURNER, S. R. & DUPREE, P. 2010. Absence of branches from xylan in Arabidopsis gux mutants reveals potential for simplification of lignocellulosic biomass. *Proceedings of the National Academy of Sciences of the United States of America,* 107**,** 17409-17414.

OBEL, N., PORCHIA, A. C. & SCHELLER, H. V. 2002. Dynamic changes in cell wall polysaccharides during wheat seedling development. *Phytochemistry,* 60**,** 603-610.

OIKAWA, A., JOSHI, H. J., RENNIE, E. A., EBERT, B., MANISSERI, C., HEAZLEWOOD, J. L. & SCHELLER, H. V. 2010. An integrative approach to the identification of Arabidopsis and rice genes involved in xylan and secondary wall development. *PLoS One,* 5**,** e15481.

PARK, Y. B. & COSGROVE, D. J. 2012. A revised architecture of primary cell walls based on biomechanical changes induced by substrate-specific endoglucanases. *Plant Physiol,* 158**,** 1933-43.

PATTATHIL, S., AVCI, U., BALDWIN, D., SWENNES, A. G., MCGILL, J. A., POPPER, Z., BOOTTEN, T., ALBERT, A., DAVIS, R. H., CHENNAREDDY, C., DONG, R., O'SHEA, B., ROSSI, R., LEOFF, C., FRESHOUR, G., NARRA, R., O'NEIL, M., YORK, W. S. & HAHN, M. G. 2010. A comprehensive toolkit of plant cell wall glycan-directed monoclonal antibodies. *Plant Physiol,* 153**,** 514-25.

PATTATHIL, S., AVCI, U., MILLER, J. S. & HAHN, M. G. 2012. Immunological approaches to plant cell wall and biomass characterization: Glycome Profiling. *Methods Mol Biol,* 908**,** 61-72.

PATTATHIL, S., AVCI, U., ZHANG, T., CARDENAS, C. L. & HAHN, M. G. 2015. Immunological Approaches to Biomass Characterization and Utilization. *Front Bioeng Biotechnol,* 3**,** 173.

PENA, M. J., ZHONG, R. Q., ZHOU, G. K., RICHARDSON, E. A., O'NEILL, M. A., DARVILL, A. G., YORK, W. S. & YE, Z. H. 2007. Arabidopsis irregular xylem8 and irregular xylem9: Implications for the complexity of glucuronoxylan biosynthesis. *Plant Cell,* 19**,** 549-563.

PERSSON, S., CAFFALL, K. H., FRESHOUR, G., HILLEY, M. T., BAUER, S., POINDEXTER, P., HAHN, M. G., MOHNEN, D. & SOMERVILLE, C. 2007. The Arabidopsis irregular xylem8 mutant is deficient in glucuronoxylan and homogalacturonan, which are essential for secondary cell wall integrity. *Plant Cell,* 19**,** 237-55.

PETERSEN, P. D., LAU, J., EBERT, B., YANG, F., VERHERTBRUGGEN, Y., KIM, J. S., VARANASI, P., SUTTANGKAKUL, A., AUER, M., LOQUE, D. & SCHELLER, H. V. 2012. Engineering of plants with improved properties as biofuels feedstocks by vessel-specific complementation of xylan biosynthesis mutants. *Biotechnol Biofuels,* 5**,** 84.

POPPER, Z. A., MICHEL, G., HERVE, C., DOMOZYCH, D. S., WILLATS, W. G., TUOHY, M. G., KLOAREG, B. & STENGEL, D. B. 2011. Evolution and diversity of plant cell walls: from algae to flowering plants. *Annu Rev Plant Biol,* 62**,** 567-90.

RENNIE, E. A., HANSEN, S. F., BAIDOO, E. E., HADI, M. Z., KEASLING, J. D. & SCHELLER, H. V. 2012. Three members of the Arabidopsis glycosyltransferase family 8 are xylan glucuronosyltransferases. *Plant Physiol,* 159**,** 1408-17.

RENNIE, E. A. & SCHELLER, H. V. 2014. Xylan biosynthesis. *Current Opinion in Biotechnology,* 26**,** 100-107.

RUPRECHT, C., BARTETZKO, M. P., SENF, D., DALLABERNADINA, P., BOOS, I., ANDERSEN, M. C. F., KOTAKE, T., KNOX, J. P., HAHN, M. G., CLAUSEN, M. H. & PFRENGLE, F. 2017. A Synthetic Glycan Microarray Enables Epitope Mapping of Plant Cell Wall Glycan-Directed Antibodies. *Plant Physiol,* 175**,** 1094-1104.

SAMUEL, R., FOSTON, M., JIANG, N., ALLISON, L. & RAGAUSKAS, A. J. 2011. Structural changes in switchgrass lignin and hemicelluloses during pretreatments by NMR analysis. *Polymer Degradation and Stability,* 96**,** 2002-2009.

SCHMIDT, D., SCHUHMACHER, F., GEISSNER, A., SEEBERGER, P. H. & PFRENGLE, F. 2015. Automated synthesis of arabinoxylan-oligosaccharides enables characterization of antibodies that recognize plant cell wall glycans. *Chemistry,* 21**,** 5709-13.

SCHUETZ, M., SMITH, R. & ELLIS, B. 2013. Xylem tissue specification, patterning, and differentiation mechanisms. *J Exp Bot,* 64**,** 11-31.

TAN, L., EBERHARD, S., PATTATHIL, S., WARDER, C., GLUSHKA, J., YUAN, C., HAO, Z., ZHU, X., AVCI, U., MILLER, J. S., BALDWIN, D., PHAM, C., ORLANDO, R., DARVILL, A., HAHN, M. G., KIELISZEWSKI, M. J. & MOHNEN, D. 2013. An Arabidopsis cell wall proteoglycan consists of pectin and arabinoxylan covalently linked to an arabinogalactan protein. *Plant Cell,* 25**,** 270-87.

TOUFIGHI, K., BRADY, S. M., AUSTIN, R., LY, E. & PROVART, N. J. 2005. The Botany Array Resource: e-Northerns, Expression Angling, and promoter analyses. *Plant J,* 43**,** 153-63.

WAN, Y., GRITSCH, C., TRYFONA, T., RAY, M. J., ANDONGABO, A., HASSANI-PAK, K., JONES, H. D., DUPREE, P., KARP, A., SHEWRY, P. R. & MITCHELL, R. A. 2014. Secondary cell wall composition and candidate gene expression in developing willow (Salix purpurea) stems. *Planta,* 239**,** 1041-53.

WANG, H., AVCI, U., NAKASHIMA, J., HAHN, M. G., CHEN, F. & DIXON, R. A. 2010. Mutation of WRKY transcription factors initiates pith secondary wall formation and increases stem biomass in dicotyledonous plants. *Proc Natl Acad Sci U S A,* 107**,** 22338-43.

WU, A. M., HORNBLAD, E., VOXEUR, A., GERBER, L., RIHOUEY, C., LEROUGE, P. & MARCHANT, A. 2010. Analysis of the Arabidopsis IRX9/IRX9-L and IRX14/IRX14-L pairs of glycosyltransferase genes reveals critical contributions to biosynthesis of the hemicellulose glucuronoxylan. *Plant Physiol,* 153**,** 542-54.

XU, F., YU, J. M., TESSO, T., DOWELL, F. & WANG, D. H. 2013. Qualitative and quantitative analysis of lignocellulosic biomass using infrared techniques: A mini-review. *Applied Energy,* 104**,** 801-809.

ZHONG, R., PENA, M. J., ZHOU, G. K., NAIRN, C. J., WOOD-JONES, A., RICHARDSON, E. A., MORRISON, W. H., 3RD, DARVILL, A. G., YORK, W. S. & YE, Z. H. 2005. Arabidopsis fragile fiber8, which encodes a putative glucuronyltransferase, is essential for normal secondary wall synthesis. *Plant Cell,* 17**,** 3390-408.

ZHONG, R. & YE, Z. H. 2015. Secondary cell walls: biosynthesis, patterned deposition and transcriptional regulation. *Plant Cell Physiol,* 56**,** 195-214.

CHAPTER 3: GLYCOME PROFILING OF VASCULAR TISSUES IN WILD-TYPE AND MUTANT ARABIDOPSIS STEMS[1]

[1] Angelo G Peralta, Sivakumar Pattathil, Sivasankari Venketachalam, Joseph Dahlen, Michael G Hahn. To be submitted to *Plant Physiology*

3.1 Abstract:

Glycome profiling is a powerful tool for understanding plant cell-wall structure and composition, and for monitoring changes in plant cell walls during growth and differentiation. However, current glycome profiling protocols utilise whole plants, plant organs, or aggregate plant biomass, and do not allow for analysis of wall composition and heterogeneity within different plant cell types. Here, we report a novel, sensitive, and reproducible method of glycome profiling that can be applied to this purpose. We have used laser capture microdissection to isolate individual vascular cell types, namely those derived from the vascular bundles and interfascicular fibres. A simplified extraction procedure allowed the reproducible determination of glycome profiles of the cell-walls in these vascular cell types from wild-type Arabidopsis stems and from plants carrying mutations in genes that regulate secondary cell-wall deposition in vessels. We are able to show that cell-wall extracts from these cell types displayed varying glycan epitope contents, particularly with regard to xyloglucan and xylan epitope compositions, depending on the genetic background of the plants being studied. These results demonstrate that it is possible to immunotype cell walls from specific cells in selected plant tissues and open up the opportunity to examine the structure and composition of the walls of selected plant cell-types along developmental gradients.

Background: 3.1.1

Plant secondary cell-walls significantly differ in their structure and composition depending on their environmental conditions, the species of origin, stage of development, and tissue or cell type. Variations occurring in the relative composition and proportion of different secondary cell-wall components include (but are not limited to) cellulose and hemicellulose polysaccharides as well as phenolics that constitute lignin. Currently, information regarding the cell-wall structure and glycan epitope composition are obtained relying primarily on whole-tissue extracts comprising a mixture of cell types. For tissues comprising of different cell types, the cell-wall polysaccharide compositions found in one or a handful of cell types tends to be diluted if whole tissues are assayed (Pattathil et al., 2015b).

Cell-walls play a diverse function in plants. For example, load-bearing walls withstand the forces of gravity while simultaneously maintaining a degree of flexibility in order to withstand large tensile and compressive forces. In contrast, many walls are subjected to further forces from within the cell, where internal osmotic pressure requires considerable strength to be imparted on the affected walls. In juvenile xylem cells, cell-walls must be porous to allow water and low-molecular-weight nutrients to diffuse between cells and tissues. In most tissues, cell-walls are required for intercellular adhesion as well. It clear that the various functional needs of plant cells are achieved by the accumulation of different cell-wall polysaccharides.

Steps towards understanding the genetic and biochemical bases of the biosynthesis of the cell-walls and their functional role(s) in plants have advanced

throughout the years (Lee et al., 2011). Precise methods for delineating the process and dynamics of cellulose deposition and its interaction with other polysaccharides have been made through the use of analytical methods such as Solid-state NMR (Haghighat et al., 2016, Zhong et al., 2008). In parallel, advancements have been made in identifying transcriptional factors involving the regulation of cell wall thickening and the deposition of secondary cell walls (Taylor-Teeples et al., 2015, Zhong et al., 2008, Kubo et al., 2005). In relation to all these biochemical and genetic approaches toward understanding the genes and proteins involved in cell wall biosynthesis and modification, there is still a significant need for the generation of robust and tractable methods to analyze and generate detailed inventories of polysaccharides at the level of tissues, cell types, cell status, and cell-wall architecture at a high-resolution. In other words, we are lacking a developmental atlas of the cell-wall polysaccharide architectures for various cell-types. Since it is increasingly evident that cell walls within plant organs are mosaics of complex heterogeneous structures (Burton et al., 2010, Lee et al., 2011, Leroux et al., 2015), the next prudent step would be to describe and comprehend this molecular pattern and to elucidate what specific types of polysaccharides are synthesized by specific cell-types and why.

Because of the structural complexity present in plant cell-walls, it still remains a challenge to analyze their composition and structure, especially using high-throughput methods. Most plant cell-wall analytical workflows involve the preparation of cell-wall extracts followed by analytical methods such as chemical derivatizations coupled with gas chromatography, mass spectroscopy (Biswal et al., 2017), and nuclear magnetic

resonance (NMR) spectrometry (Pena et al., 2008, Wang and Hong, 2016, Haghighat et al., 2016). Unfortunately, the limitations of these experimental approaches include the fact that they are time-consuming, often require expensive equipment, and are low-throughput, and frequently only provide information regarding a single polysaccharide of interest (Obel et al., 2009, Pidatala et al., 2017, Li et al., 2013). However, over the last decade, immunological approaches geared towards cell-wall and biomass analyses are tools that have broad applications towards cell-wall and biomass research have made considerable advancements (Moller et al., 2008, Larson et al., 2014, Shinohara et al., 2015, Xiao et al., 2014).

Cell-wall glycan-directed monoclonal antibodies (mAbs) are the best characterised and most widely used probes for immunological analyses of plant cell-wall structure and composition (Manabe et al., 2011, Pattathil et al., 2015b, Crowe et al., 2017, Xue et al., 2013). This is because mAbs are monospecific with regards to the epitopes they detect; thereby making them crucial for studying plant cell-wall glycans, which possess repetitive substructures that often are located in different macromolecular contexts (e.g. arabinogalactans in rhamnogalacturonan I and glycoproteins). Most importantly, a worldwide collection of mAbs is now available (over 200) consisting of mAbs recognising specific structural features of a large diversity of non-cellulosic glycan epitopes (Pattathil et al., 2010, Pattathil et al., 2015b, Ruprecht et al., 2017, Schmidt et al., 2015, Dallabernardina et al., 2017, Rydahl et al., 2018).

One such immunological approach is Glycome Profiling (GP), the sequential extraction of cell-wall samples using a series of increasingly harsh reagents followed by

an ELISA-based screening of the resulting extracts using cell wall glycan-directed mAbs. This approach permits the determination and monitoring of the cell-wall glycan epitopes that are released by each extraction. The use of sequential extractions allow cell wall glycans to be released from the walls based on their relative tightness with which they are integrated into the final wall structure and detected in a high-throughput manner (Pattathil et al., 2012). However, sequential extractions are limited because they do not completely release all glycans from the cell-wall material nor are they quantitative, making absolute quantification of epitope abundance in the intact wall difficult [see review by (Pattathil et al., 2015a). Despite these limitations, GP has been extensively applied in the analysis of cell walls for functional characterisation of genes involved in cell wall biosynthesis (e.g. comparing mutants vs. wild-type), pretreated and bio-converted plant biomass, stem developmental-dependent glycan epitope changes, and comparative glycomics of different plant phylogenies based on their cell wall composition (Biswal et al., 2015, Popper et al., 2011, DeMartini et al., 2011, Peralta et al., 2017, Crowe et al., 2017, Wilson et al., 2015, Leroux et al., 2015).

However, there are limitations to the GP approach. Firstly, low-molecular-weight glycans released by cell wall extractions do not bind to solid supports such as nitrocellulose, glass slides, or multiwell plastic plates, and thus are not detected by GP. The lower limit of the glycan size that can be retained on such solid supports, while not definitively determined, is greater than 10 kDa for most cell wall glycan examined to date. Secondly, certain glycans may get modified by the harsh alkaline extraction conditions, which lead, for example, to the loss of acetylation or methylation (Pattathil

et al., 2010). Third, because glycome profiling is reliant on chemical/enzymatic extractions, absolute quantification of epitope composition in biomass/cell wall samples is problematic.

An alternative immunological approach is *in situ* visualisation by immunolabelling techniques. This approach employs fixation, embedding, and sectioning of biomass samples, followed by probing of the sections with glycan-directed mAbs as the primary antibody that binds to the glycan epitope and then by a fluorescently tagged secondary antibody to detect the bound primary antibody. This approach allows an *in situ* visualisation of glycan epitope distributions in a particular sample under a fluorescence microscope (Avci et al., 2012, Verhertbruggen et al., 2017). Immunolabelling has provided valuable insights regarding glycan epitope distribution patterns in cell-wall biosynthetic mutants such as WRKY transcription factor knockouts, xylan-deficient mutants, and compared distribution of glycan epitopes in plant biomass before and after various methods of pre-treatment for reducing cell wall recalcitrance (Wang et al., 2010, Petersen et al., 2012, Pattathil et al., 2015b). One major disadvantage of *in situ* visualisation is that any glycan epitopes that are buried within the cell wall matrix are not exposed by the sectioning process thereby rendering them inaccessible to mAbs and hence preventing the visualisation of epitopes of interest (Avci et al., 2012). Also, any *in vivo* modifications to glycans [such as acetylation in xylans] can render the epitopes unavailable for recognition to their corresponding mAb despite being present in the cell-wall (Pattathil et al., 2015a). Thus, combining immunological approaches towards cell-wall glycan analyses, for example by combining GP with *in situ*

immunolocalisation, can be significantly more powerful, as these two methods together provide complementary information.

Recent advances in epitope characterization using defined synthetic oligosaccharides (Bartetzko et al., 2015, Schmidt et al., 2015, Dallabernardina et al., 2017, Ruprecht et al., 2017) have provided detailed information about the binding specificities of a large number of the available plant glycan-directed mAbs now enabling the monitoring of specific cell-wall glycan epitope structures, diverse substitution patterns and their abundance in a given cell type. This is particularly true for xylan, xyloglucan, and some arabinogalactan substructures recognised by a diverse set of mAbs.

The Arabidopsis genome sequence has provided an important tool towards accurately identifying and providing systematic functional analysis of cell-wall related biosynthetic genes (McCann and Carpita, 2008, Liepman et al., 2010, The Arabidopsis Genome, 2000). About 10% of the genes in Arabidopsis are estimated to play roles in cell-wall functions. Arabidopsis has served effectively to discover and elucidate cell-wall related genes such as those involved in cellulose and hemicellulose biosynthesis (Brown et al., 2011, Brown et al., 2005, Brown et al., 2009). Specifically, the inflorescence stem, a load-bearing organ is ideal for studying cell type-specific secondary cell-wall formation (Strabala and Macmillan, 2013). This is because the inflorescence stem makes thickened lignified secondary cell-walls in abundance (Zhong et al., 2002). Despite the absence of a well-defined vascular cambium, clear parallels exist between the developmental programs underlying secondary growth processes in the stems of herbaceous plants like

Arabidopsis and woody plants (Wang et al., 2011). More importantly, however, the stem of Arabidopsis shows only primary growth in the apical region and secondary growth in its basal region, closer to the rosette. As a consequence, we have distinct areas for sampling the transition in the stem between primary cell-wall formation and growth and secondary cell-wall formation (Altamura et al., 2001, Ragni and Greb, 2018). Lastly, the inflorescence stems grown using long-day conditions can be produced in a few weeks compared to stems grown in short-day conditions (MacMillan et al., 2013, Chaffey et al., 2002). Thus, the developing Arabidopsis influorescence stem provides an accessible model for studying cell-wall composition within individual cell types.

Studies in Arabidopsis have also led to the identification of regulatory genes and networks that control secondary wall formation. NAM/ATAF/CUC (NAC) domain transcription factors were demonstrated to play important roles in secondary cell wall biosynthesis. One such family of genes are the *VASCULAR-RELATED NAC DOMAIN1-7* (*VND1-7*) genes (Demura and Fukuda, 2007, Yamaguchi et al., 2010b). These transcription factors were originally discovered when because their expression levels were increased during trans-differentiation of *Zinnia elegans* suspension-cultured cells into treachery elements (Kubo et al., 2005, Yamaguchi et al., 2008). Studies have shown that overexpression of *VND6* and *VND7* induced ectopic differentiation of metaxylem-like and protoxylem-like tissues in roots and leaves (Endo et al., 2015, Yamaguchi et al., 2008, Yamaguchi et al., 2010a, Zhou et al., 2014), respectively. On the other hand, suppression of VND6 and VND7 activity is known to cause defects in treachery element formation in Arabidopsis (Kubo et al., 2005). Therefore, these results suggest *VND6* and

VND7 are the main regulators of xylem differentiation. Plants carrying T-DNA insertional mutations in individual genes presented no detectable defects in morphology suggesting functional redundancy for these genes. Studies by Zhou et al. (2014) were able to support the gene redundancies for *VND6* and *VND7* by demonstrating that VND1 to VND5 are vessel-type specific, and their overexpresion (OE)-lines activated secondary cell wall biosynthesis genes and programmed cell death. Moreover, VND1 to VND5 and VND7 rescued the secondary wall defects in fibres of the *nac secondary wall thickening promoter factor1 nst1 nst3* double mutant (Zhou et al., 2014, Yamaguchi et al., 2011)

Most studies on *VND6* and *VND7* function were carried out by overexpression (Kubo et al., 2005, Yamaguchi et al., 2008, Yamaguchi et al., 2010b) or by dominant repression using the SRDX repression system. SRDX repression is accomplished by fusing a target TF to a modified Ethylene-responsive element binding factor-associated amphiphilic repression (EAR) motif to form a chimeric repressor (Mitsuda and Ohme-Takagi, 2009) in order to repress its normal function. EAR motifs are the most predominant form of transcriptional repression motif identified in plants known to date (Kagale and Rozwadowski, 2011). *VND6* and *VND7* loss-of-function phenotypes were only demonstrated by the SRDX repression system (Kubo et al., 2005). This is problematic because SRDX repression systems suppress the targeted TF and related functionally redundant TFs. Hence, chimeric repressors like SRDX exhibit a phenotype similar to the loss-of-function phenotype of the target TF and other related TFs that have redundant functions (Mitsuda and Ohme-Takagi, 2009).

We focussed on T-DNA insertion lines, since a number of studies have already focused on VND6 and VND7 overexpression lines by means of genetics and biochemistry (Kubo et al., 2005, Yamaguchi et al., 2008, Endo et al., 2015, Ohashi-Ito et al., 2010) (Figure 3.1, Table 3.1). *vnd6* and *vnd7* single mutants were reported to lack morphological and growth phenotypes. However, these results do not rule out that loss-of-function of *vnd6* and *vnd7* could still exhibit aberrant phenotypes, specifically cell-wall related phenotypes, which might not be visible at the morphological level. Loss-of-function studies are more suited for gene function analysis (Mitsuda and Ohme-Takagi, 2009). T-DNA inserts still prove to be useful and relevant for such studies, despite new methods for targeted mutagenesis using the CRISPR and TALEN systems (Mali et al., 2013, Christian et al., 2013). The latter has issues related to specificity towards the target gene-of-interest and gene off-targeting that still requires refining in order to be a standard laboratory technique (Bogdanove and Voytas, 2011, Mali et al., 2013). *Agrobacterium tumefaciens* transfer-DNA (T-DNA) is the insertion of a T-DNA fragment into a plant host's genome and results from a natural transformation process wherein Agrobacterium infection results in the transfer of a DNA fragment (T-DNA) and deleting genes in the process.

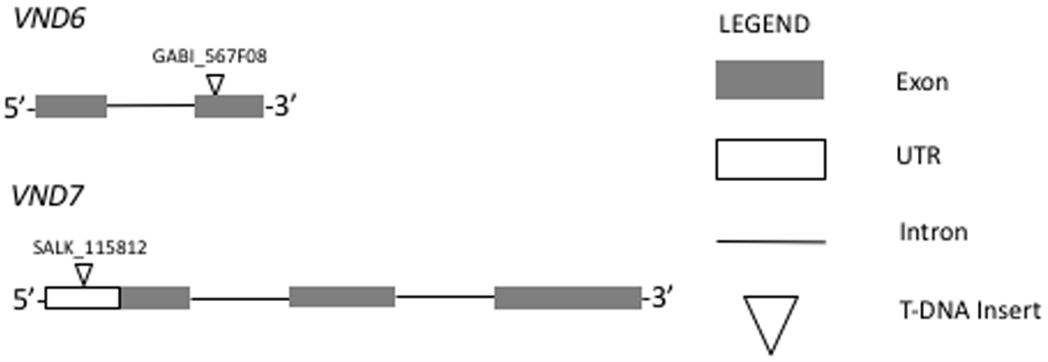

Figure 3.1: Schematic diagram *VND6* and *VND7* genes and the location of t-DNA insertion in *vnd6* and *vnd7* mutants. Legend depicts gene structural components.

As previously mentioned, *VND* TFs are tier 1 master regulators that can activate tier 2 MYB transcription factors and cell-wall biosynthetic genes through feed-forward mechanisms (Hussey et al., 2013, Taylor-Teeples et al., 2015). *VND6* and *VND7* regulate secondary cell-wall biosynthesis and programmed cell death in metaxylem and protoxylem respectively (Endo et al., 2015). Therefore, these genes are highly probable to produce changes in cell walls due to their broad regulation of secondary cell-wall transcription factors and biosynthesis genes (Hussey et al., 2013). This, in turn, makes them highly attractive candidate genes for mutational studies that would lead to cell-type specific changes in glycan epitope composition of cell walls that could be detected immunologically using approaches described above.

Table 3.1: Description of *VND6* and *VND7* genes in *A. thaliana*

Gene	Annotation	Insertion	Stem Phenotype	Reference
VND6	At5g62380 NAC-domain transcription factor involved in xylem formation	GABI_567F08	No detectable defects in morphology. However, SRDX lines showed defects in growth and vessel formation in roots	(Yamaguchi et al., 2011, Kubo et al., 2005)
VND7	At1g71930 NAC-domain transcription factor involved in xylem formation	SALK_115812	No detectable defects in morphology. However, SRDX lines showed defects in growth and vessel formation in roots	(Yamaguchi et al., 2011, Kubo et al., 2005)

Laser capture microdissection (LCM) is an efficient tool to collect and harvest single cell populations found in diverse plant tissues. LCM has been successfully employed to study Arabidopsis cell type-specific expression at the RNA and protein levels (Schad et al., 2005, Shinozaki et al., 2018, Kerk et al., 2003). In the current study, we developed a tissue processing method to independently isolate cells from vascular bundles and interfascicular fibres and coupled this with the well-established immunological-based glycome profiling technique (Pattathil et al., 2012) for carrying out a comprehensive glycomic analysis of cell-walls from different cell types at a high resolution. We demonstrate that glycome profiling performed at a cell type-specific level possesses the ability detect cell-type specific wall immunotypes. Furthermore, using T-DNA insertional mutants of transcriptional regulators in xylem formation, *VND6* and *VND7* (Kubo et al., 2005), we demonstrate that clear differences in glycan epitope compositions can be detected in selected cell types that were undetectable using whole

Arabidopsis stem glycome profiling approaches. Our findings suggest that a shift from whole organ-based examinations of cell-wall biosynthesis, modification, and structures to a cell type-specific level is now within reach. Additionally, glycome profiling at a cell-specific level may support direct correlations between glycan epitope compositional data and transcriptional data at the cell-type specific level rather than at the bulk tissue levels currently employed.

3.2 Results:

3.2.1 Glycome Profiling of Arabidopsis Inflorescence Stems at the Organ Level

Glycome profiling has been used to analyse cell wall material from various plant species, different plant organs, and comparative studies between native/genetically modified, and variously pre-treated and enzymatically converted biomass. We chose to apply this approach to *vnd* loss-of-function mutants that have previously been shown not to have any observable phenotypes (Kubo et al., 2005). It is possible however, that analysis of cell walls will reveal a phenotype, since the mutations are in genes whose products regulate secondary cell wall formation. We analysed the morphology of the inflorescence stems of Arabidopsis Col-0, *vnd6*, *vnd7*, and *vnd6 vnd7* T-DNA mutants that were grown under the same growth conditions (See Methods) (Figure 3.2). *VND6* had its T-DNA insert at the second exon which would result in a knock-out of this gene and *VND7* T-DNA insert was located at the 5' UTR region which causes a knockdown in this gene (Figure 3.1 and Table 3.1.) (Alonso et al., 2003). In terms of stem growth, no obvious differences in the gross architecture of stems was observed between Col-0 and *vnd* mutants; however, we noticed that the double mutant, *vnd6 vnd7*, was significantly

shorter (Figure 3.2A). This was supported by the growth height distribution represented by box plots (Figure 3.2B) and statistical analysis using one-way ANOVA. The ANOVA resulted in a p-value of 2.00^{-16}, and the null hypothesis is therefore rejected ($p = 0.05$) (n=30), (Sum of Squares =62.10), (Mean Square = 20.70), (F-Value = 45.36).

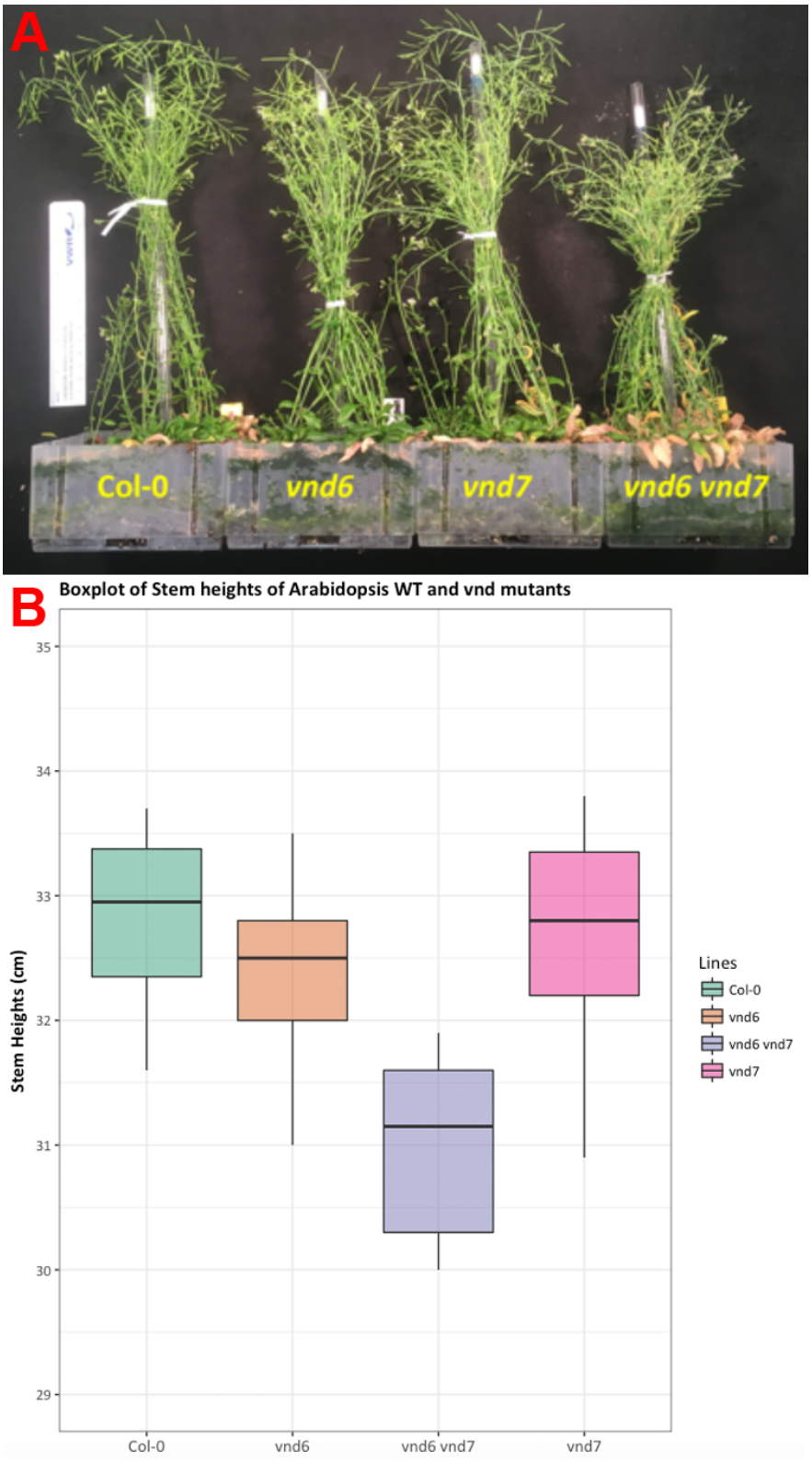

Figure 3.2: Growth of *Arabidopsis thaliana* Col-0, *vnd6*, *vnd7*, and *vnd6 vnd7* double mutants. (**A**) Appearance of 8-week old plants. (**B**) Distribution of plant heights (cm) for each genotype displayed as boxplots (n=30)

We carried out the glycome profiling of whole stems from plants that were grown under identical conditions to a height of 13-15 cm (Figue 3.21). This height range was chosen because clear distinct xylem differentiation and SCW formation already occurs at this growth stage, shortening the time of harvest (Ko et al., 2004). These plants were then harvested at the apical portion: 1 cm of stem that was located 1 cm away from the inflorescence was cut and stored till a pool of 10 stems per genotype were obtained. Similarly, the basal portion involved harvesting the 1 cm of stem that was located 1 cm away from the rosette (See methods, Figure 3.22). The rationale was to sample the most juvenile stage of the stem while simultaneously avoiding harvesting the peduncle. The basal portions were chosen to avoid parts of the stems directly attached to the rosette where biological activities have been completed which would complicate our analyses as to whether or not any observable glycan epitope differences are due to *vnd* knock-outs or a result of stem senescence. Col-0 and *vnd* mutants were subjected to ELISA-based glycome profiling at the whole stem level with plant glycan-directed mAbs to establish a baseline of the glycan epitope compositions of Col-0 and the *vnd* mutants in order to have a point of reference when examining vascular tissues. In terms of epitope abundance and patterning, whole stem glycome profiles of Col-0 and *vnd* stems displayed distinct immunotypes (Figure 3.3). In the walls from apical segments, the oxalate and 4M KOH extracts displayed similar antibody binding patterns in Col-0 and *vnd6 vnd7* for the xyloglucan-binding antibodies and these patterns were distinct from those exhibited by the single mutants (Figure 3.3). Xylan epitopes were more abundant in *vnd* mutants as compared to Col-0, particularly for the Xylan-7 mAbs,

which recognise short, unmodified regions of xylan backbones (Ruprecht et al., 2017). Whole apical stems from the *vnd6 vnd7* double mutant also exhibited the presence of acetylated galactomannan epitopes recognised by CCRC-M169 and CCRC-M170. Increases in signals from RG-Ia and RG-Ib antibody clades were also observed in the 4M KOH extracts of the *vnd* mutants; conversely, faint to no signals were observed with most of these antibodies for Col-0 apical stems. Pectin epitopes recognized by the mAbs from the RG-I/AG clade revealed different signatures between Col-0 and *vnd* mutants; however, no obvious trends could be easily identified except for enhanced signals for all of these antibody clades in the 4M KOH extracts of *vnd7* single mutant apical stems. mAbs recognising S-lignin epitopes (GLIM6 and GLIM10) showed differences between Col-0 and the *vnd* mutants in apical stem extracts. GLIM10 binding was present in oxalate and 4M KOH extracts from Col-0 but was absent in the *vnd* mutant lines. Conversely, epitopes recognised by GLIM6 were detected in the oxalate extracts of apical stems from all of the *vnd* mutants.

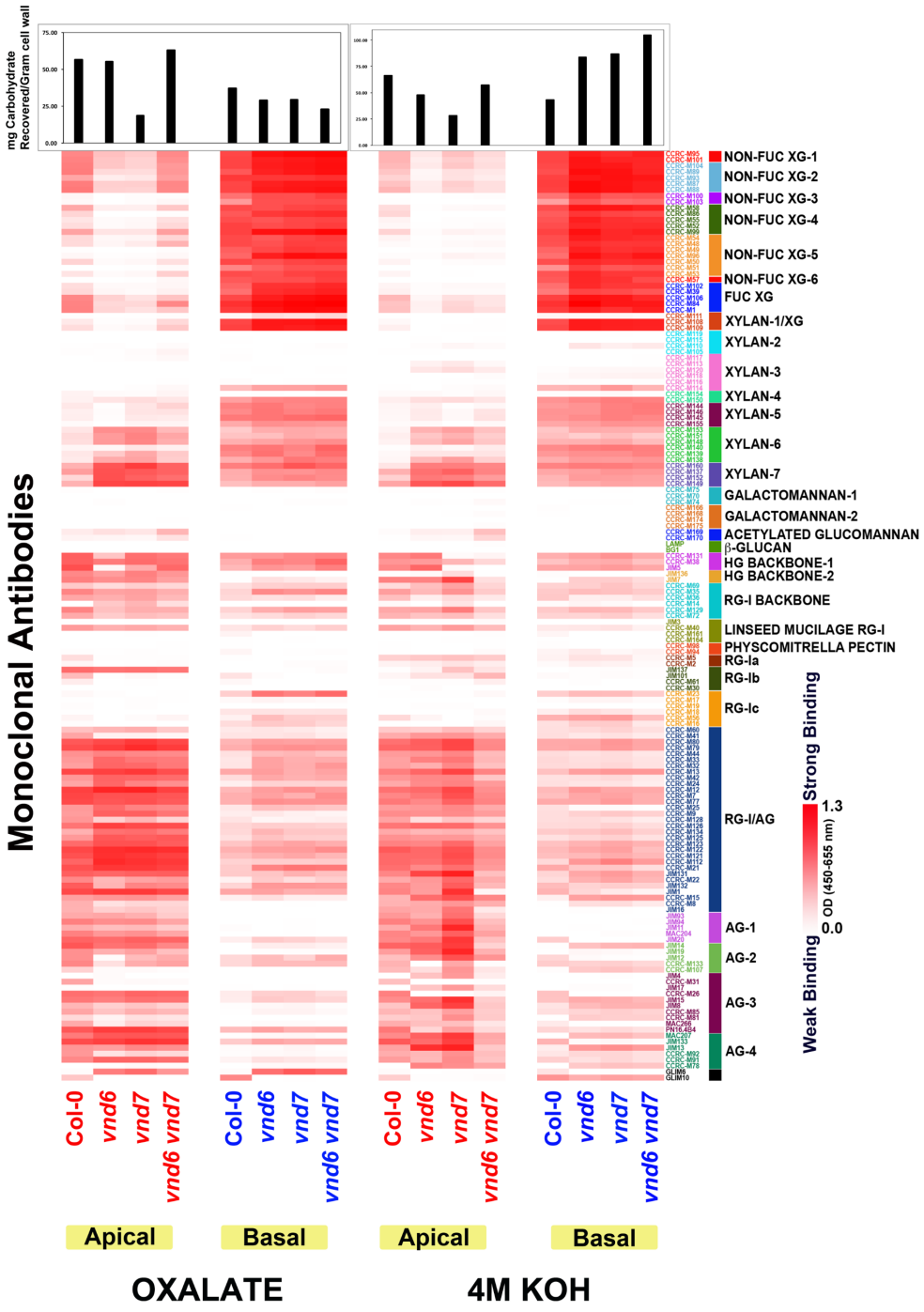

Figure 3.3 Glycome profile of Arabidopsis inflorescence stem apical and basal sections sequentially extracted with 50 mM ammonium oxalate and 4M KOH as explained in the Methods section. Antibody binding strength based on optical density (OD) is presented as a colour gradient ranging from white (no binding) to red (strongest binding) (OD=1.3). Binding intensities represent a pool of 10 stems of each genotype studied here. Black bars on the top indicate the average amount of sugars recovered in the solubilised extracts g^{-1} cell wall (mg g^{-1})

The oxalate and 4M KOH extracts from basal portions of Col-0 and *vnd* stems displayed only subtle variations in binding patterns compared to the corresponding extracts from apical stem segments. For xylan epitope-directed mAbs, all extracts of basal stem segments displayed similar epitope abundances and more comprehensive coverage of xylan epitopes as compared to extracts from apical stem segments. Interestingly, xylan epitopes that were abundant in the extracts of basal stem segments but scarce in apical stem segments were the GlcA and Me-GlcA substitutions recognized by CCRC-M150 and the Xylan-5 mAb clade. Pectin epitopes from the basal segments of the Col-0 and *vnd* mutant stems also displayed similar signature patterning as the apical segments albeit at lower abundances as demonstrated by decreased mAb signals. Lastly, S-lignin epitopes patterning in the oxalate extracts of basal stems were similar to those of apical segments. The GLIM6 epitope was abundant in the *vnd* mutants but absent in Col-0; conversely GLIM10 was present in Col-0 basal stems and absent in *vnd* basal stems. In 4M KOH extracts, the GLIM10 epitope is abundant in all lines in basal segments of the inflorescence stems. In summary, we for the first time, demonstrate immunotypic differences in the non-cellulosic wall glycomes of loss-of-function *vnd* mutants, even though these mutants lack stem morphological and growth phenotypes (Kubo et al. (2005). Glycome profiling therefore, is a powerful approach for detecting cell-wall epitope differences despite an absence of standard cell-wall phenotypic effects such as pendant stems, collapsed xylem phenotypes, and stem dwarfism.

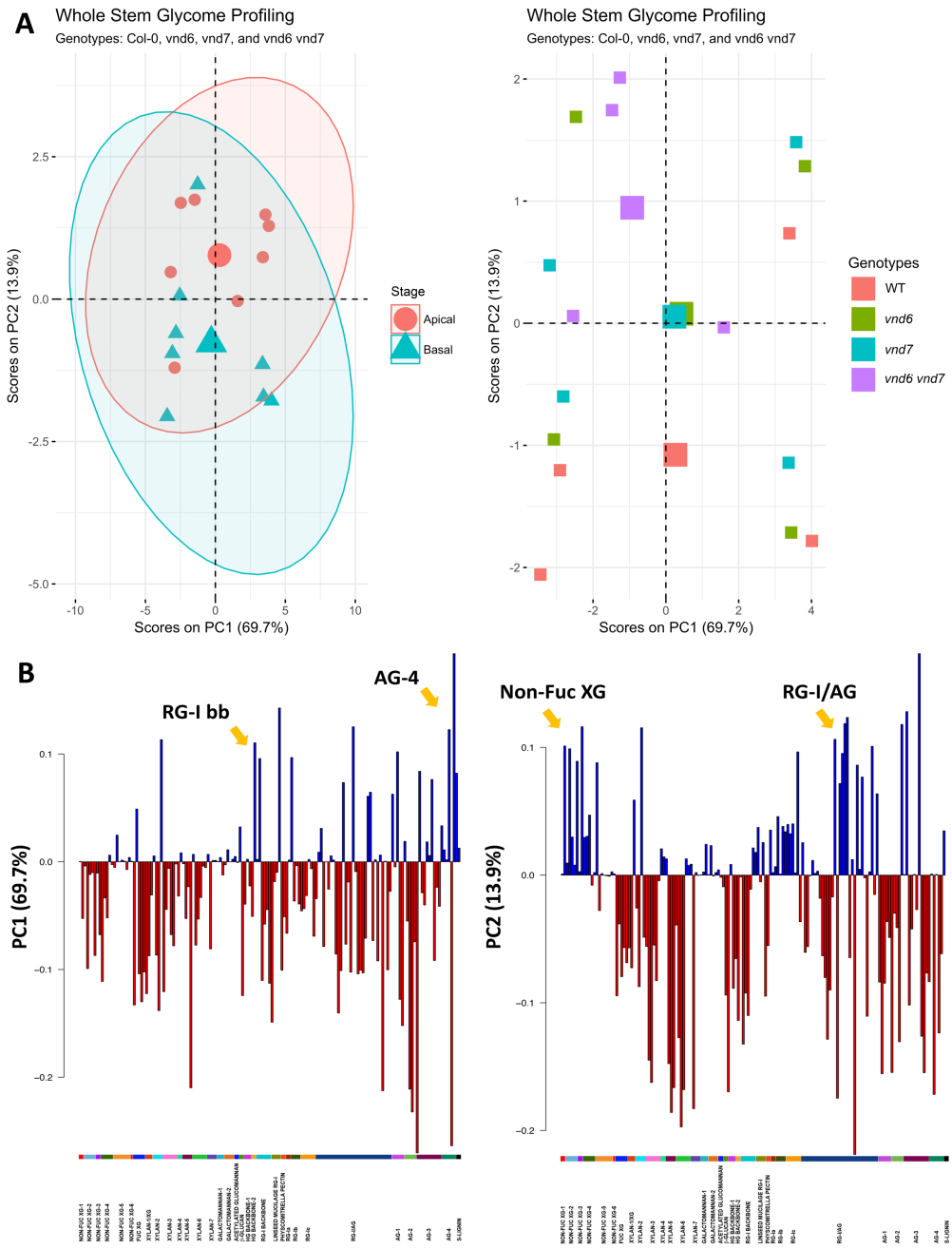

Figure 3.4: Principal components analysis of whole stem glycome profiling data (A). Plot of principal component one (PC1) and principal component two (PC2) scores and corresponding loadings plots of the PC along which clusters emerged (B). Data points are presented for all samples from the two fractions obtained during the sequential extraction. Gold arrows depict the mAb signals that contributed the most variance (blue) for PC1 and PC2.

3.2.2 Glycome profiling from whole stem reveals differences in-cell wall glycan epitope distribution and abundancies among sequential extracts throughout Arabidopsis stem development:

Oxalate extracts from whole stems demonstrated distinct glycan epitope abundances. Non-fuc XG, fucosylated XG, XG epitopes, and AG epitopes (RG-I/AG and AG-1 to 4) were less abundant in Col-0 than *vnd6 vnd7* stems. Xylan-directed mAb signals, however were stronger in the *vnd* mutants when compared to Col-0, a possible reason for this is the sub-class of weakly integrated xylan as described by Peralta et al. (2017) are present in apical stem portions of *vnd* mutants. Moreover, these weakly integrated xylans are more abundant in *vnd* mutants compared to Col-0. Pectin epitopes had an increase in abundance from apical stem portions and then decreased in the basal portions. This could be explained by the concomitant increase in the hemicellulose XG similar to the results found in Peralta et al. (2017). Glycan epitopes from the oxalate extract of basal sections displayed similarities from its 4M KOH extracts in mAbs specific for xylans, acetylated glucomannans, and to an extent, pectin epitopes. Also in both oxalate extracts, pectin epitopes were more abundant in the apical portion and decreased once xylan and XG epitopes started to be more abundant in the basal portion of the stem. Interestingly, *vnd7* had stronger pectin mAb signalling from pectin epitopes belonging to RG-I/AG and AG-1 to 4 clades. We also observed that tightly integrated xylan epitopes were more abundant in the *vnd* mutants than Col-0, specifically in apical 4M KOH extracts. Lastly, whole glycome profiling of *vnd* mutants demonstrated increased variation in glycan epitopes from apical stems in both oxalate

and 4M KOH extracts. Contrastingly, basal stems displayed more consistent in epitope abundance amongst the genotypes, especially XG and xylan epitopes.

3.2.3 Trimethylsilyl (TMS) compositional analysis of Arabidopsis inflorescence stems:

Total monosaccharide compositions of cell walls isolated from apical and basal stem segments were determined in order to determine if there were any differences between Col-0 and *vnd* mutant stems (Figure 3.5).

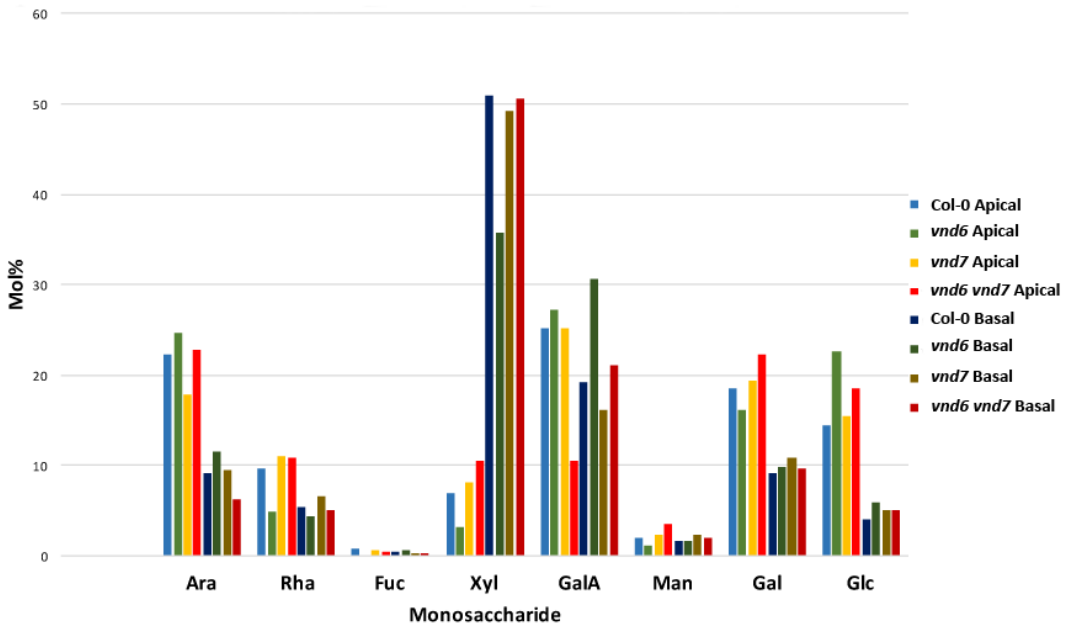

Figure 3.5: Monosaccharide composition analysis from TMS hydrolysis followed by GC-MS in mol% of Col-0, *vnd6*, *vnd7*, and *vnd6 vnd7*. Thirty pooled Apical (A) and Basal (B) stem portions for each genotype were analysed using two technical replicates (1 and 2).

3.2.4 Method Optimisation for Laser Microdissection-Based Glycome Profiling:

Standard glycome profiling (GP) methods provide an immense challenge in order to be suited for cell populations that are in the Nano gram range. Firstly, the standard harvesting and grinding of tissues is replaced by laser capture microdissection to harvest cell populations of interest instead of simple sample harvesting and grinding (Figure 3.7). The typical chemical extraction process involves the sequential extraction using Oxalate and(or) Carbonate that releases pectin glycan, followed by 1M and 4M KOH for the extraction of hemicellulose and pectin glycans. Sodium chlorite is then used to remove lignin and ended by another extraction round of 4M KOH for lignin-bound polysaccharides. The complete extraction process is not recommended for small-scale GP as each extraction step requires the collection of the supernatant followed by ddH_2O rinses. Applying this same process for minute samples prevents reproducibility between extracts as it increases the chances of the cell material being pipetted out in unknown amounts. As a result, inconsistencies between biological replicates will occur. Because of these challenges we modified the standard glycome profiling workflow (Figure 3.8):

1. Laser capture microdissection methods for harvesting different cell populations (Figure 3.7)
2. Removal of AIR step
3. Reducing the number of sequential extractions to just oxalate and 4M KOH
4. Eliminated dialysis and sugar estimation steps
5. Removal of the lyophilisation step
6. Loading of extracts were based on LCM surface area (800,000 μm^2)

Table 3.2: Glycosyl residue composition of apical and basal stem portions from Col-0 and *vnd* lines. 1 and 2 are technical replicates from AIR material

	Arabinose (Ara)	Rhamnose (Rha)	Fucose (Fuc)	Xylose (Xyl)	Galacturonic Acid (GalA)	Mannose (Man)	Galactose (Gal)	Glucose (Glc)
Col-0 Apical 1	22.2	9.7	0.8	7	25.1	2.1	18.6	14.5
Col-0 Apical 2	19.3	9.1	0.5	6.5	26.8	1.9	20.1	15.8
Col-0 Basal 1	9.14	5.4	0.5	50.9	19.2	1.6	9.1	4.1
Col-0 Basal 2	10.5	5.6	0.4	47.6	19	1.9	10.9	4.1
vnd6 Apical 1	24.7	4.9	0	3.2	27.3	1.1	16.1	22.6
vnd6 Apical 2	20.7	8.2	0.7	7.3	26.3	2.2	19.5	15.2
vnd6 Basal 1	11.6	4.3	0.6	35.7	30.6	1.6	9.8	5.9
vnd6 Basal 2	9.7	3.8	0.2	59.5	6.8	2.6	10	7.4
vnd7 Apical 1	17.8	11.1	0.6	8.1	25.1	2.3	19.4	15.5
vnd7 Apical 2	21.2	4.3	0.4	3.6	34.2	1.4	16.8	18.2
vnd7 Basal 1	9.5	6.5	0.3	49.3	16.1	2.4	10.9	5.1
vnd7 Basal 2	6.1	4.5	0.3	63.0	13.3	1.8	7.5	3.6
vnd6 *vnd7* Apical 1	22.8	10.8	0.5	10.5	10.5	3.43	22.3	18.5
vnd6 *vnd7* Apical 2	18.1	3.6	0.1	4.1	40.7	1.46	14.7	17.2

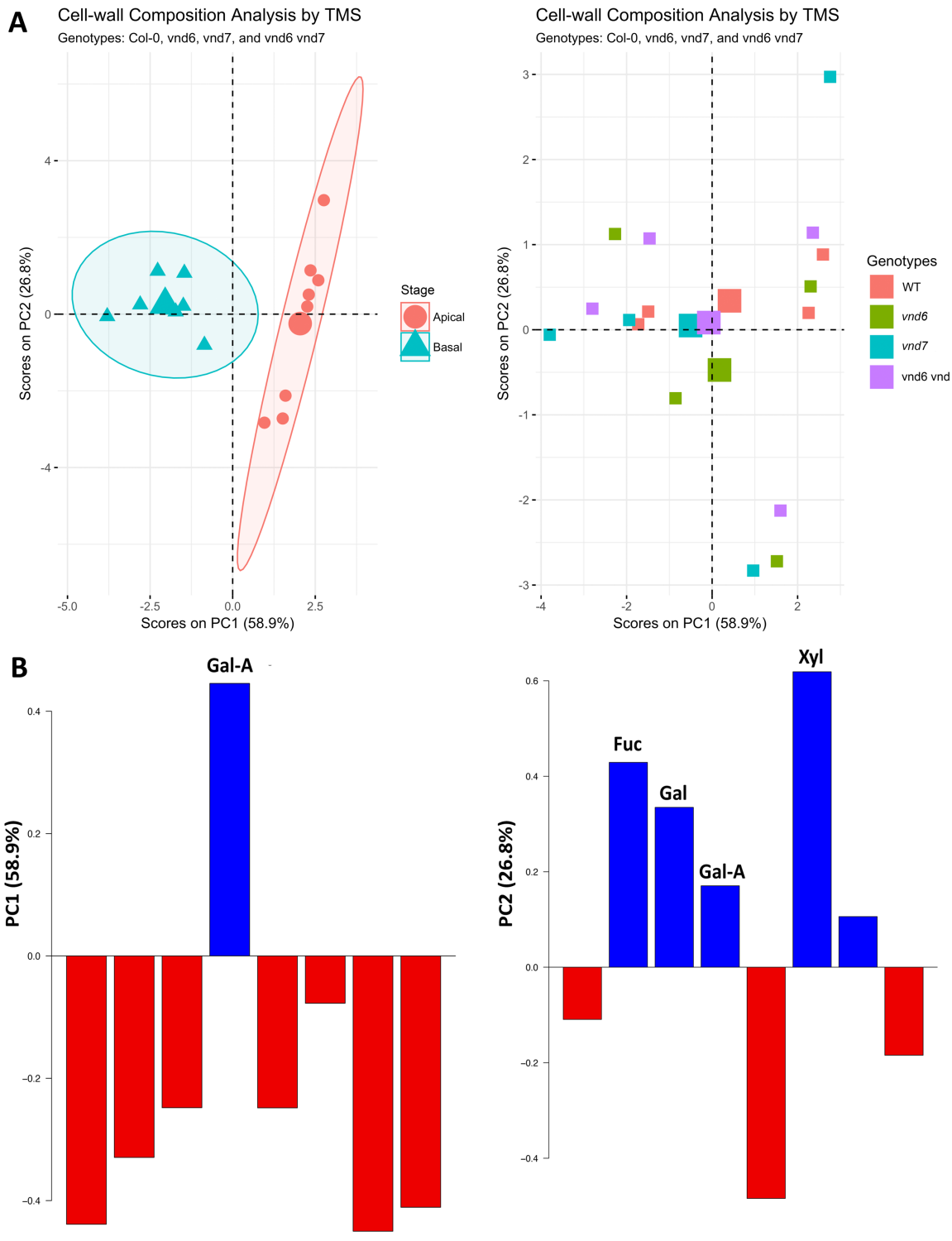

Figure 3.6: Principal components analysis of total monosaccharide composition using TMS methods (A). Plot of principal component one (PC1) and principal component two (PC2) scores and corresponding loadings plots of the PC along which clusters emerged (B). Data points are presented for all samples from the two fractions obtained during the sequential extraction.

Implementation of of LCM-GP in specific cell types/populations found in the vascular bundles (VB) and interfascicular fibres (IFF); and at the apical and basal region of Arabidopsis stems requires proper fixation process, ensuring anatomical features remain intact and clearly visible after subsequent histological processing. To do so, fixation was carried out using the method of Gautam et al. (2016), involving a series of acetone changes and using vacuum infiltration. Typical fixation reagents such as Farmer's fixative (3:1 EtOH:acetic acid) or formalin-acetic acid-ethanol (FAA) (Kerk et al., 2003) is not recommended because acidic solutions have the potential to cleave labile pentoses such as fucose, xylose, and, which are substituents XG. Additionally, xylose can be subject to acid hydrolysis which is a key residue in arabinoxylan (Aspinall et al., 1966, Elsayed, 1982). Subsequently, dehydration steps to ensure proper embedding of hydrophobic paraplast wax were carried using the standard method of ethanol (EtOH) and histoclear gradients. Embedding stems in paraplast was recommended over London Resin- (LR) because LR-White resin sections cracks during laser beam dissection (Angeles et al., 2006, Joseleau and Ruel, 1997). Although polyethylene glycol (PEG) would also be a good alternative, the catapulting of the selected cells would be difficult since PEG retains moisture (Angeles et al., 2006). Sectioning of paraplast blocks embedded with Arabidopsis stems were sectioned transversely using a microtome (Lipshaw Manufacturing, Michigan) to a thickness of 11 µm because too thin sections, would result in more time-consuming process of collecting material, and too thick sections result in the need for higher laser power settings which could thermo-alter the

polysaccharide composition of the cells collected (Jin Nakashima, personal correspondence 2016).

Laser dissection was performed using the LMD 7000 (Leica Microsystems) to harvest VB and IFF from apical and basal stem sections individually (Figure 3.6) (see Methods). The traditional workflow described by Pattathil et al. (2012) involved extraction of soluble components, such as soluble sugars, proteins, lipids, pigments, DNA, and RNA; this step was eliminated, because the fixation process described above included similar steps, particularly EtOH washes.

It is important to note that the reduction in the number of extracts compared to standard glycome profiling (Pattathil et al., 2012) was because additional rinses, which required pipetting in and out ddH2O, resulted in a lot of variation in our biological replicates due to loss of cell material. Therefore, we selected ammonium oxalate and 4M KOH solutions to extract primary cell wall and secondary cell wall glycans respectively. This results in a reduction of pipetting steps during ddH2O rinses and a more robust amount of cell-wall material available to subsequent 4M KOH fractionation. Moreover, the extracts were spun at 13,500 rpm for 30 min to ensure vascular cells form a pellet. The supernatant is carefully removed and stored or neutralised to pH7 with glacial acetic acid for 4M KOH extracts. Dialysis using 3,500 Da molecular weight cut-off tubing and subsequent lyophilisation, purification steps included in the original work flow, caused considerable loss of glycans (data not shown), and were omitted as inappropriate to the extremely small amount of material resulting from laser capture microdissection. Similarly, standard quantitation of total sugars using phenol-sulphuric

acid extraction cannot be performed, (data not shown) therefore, the loading of glucose equivalent glycan solutions for the ELISA-based assay techniques based on sugar estimation was eliminated. Without sugar quantitation, normalisation in the amounts of carbohydrate material coated on to ELISA 384-well plates proved challenging. We were able to approximate by using the same total area harvested (~800,000 μm^2) from Arabidopsis stem sections of equal thickness (11 μm). This total represents half the area of a whole section taken from the basal portion of an Arabidopsis inflorescence stem.

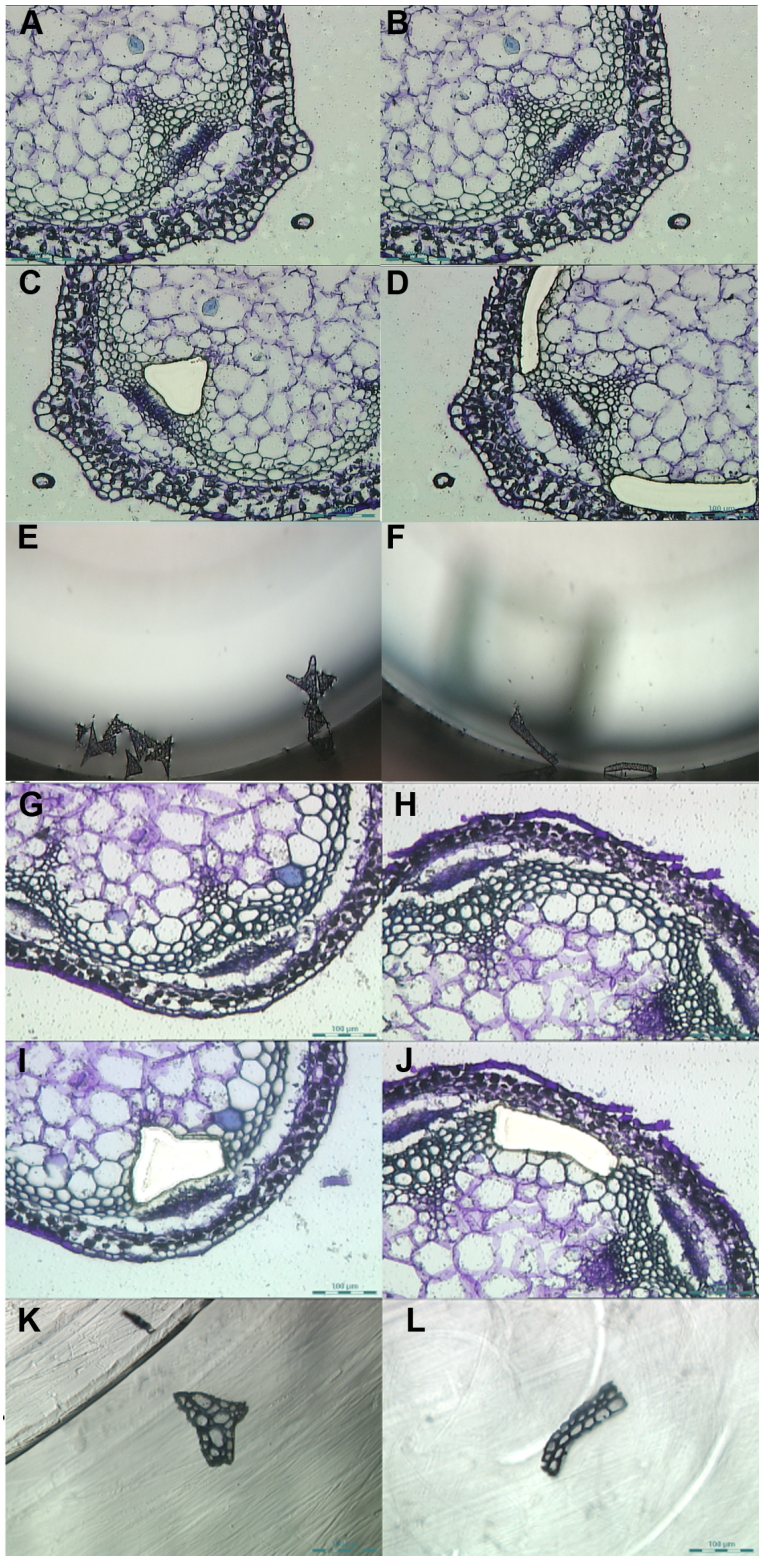

Figure 3.7: Vascular bundles and Interfascicular fibres subjected to laser capture microdissection. Apical portions (A, B), and basal (G, H) of VB and IFF post dissection (C, D, I, J) and, dissected tissue in microcentrifuge cap (E, F, K, L)

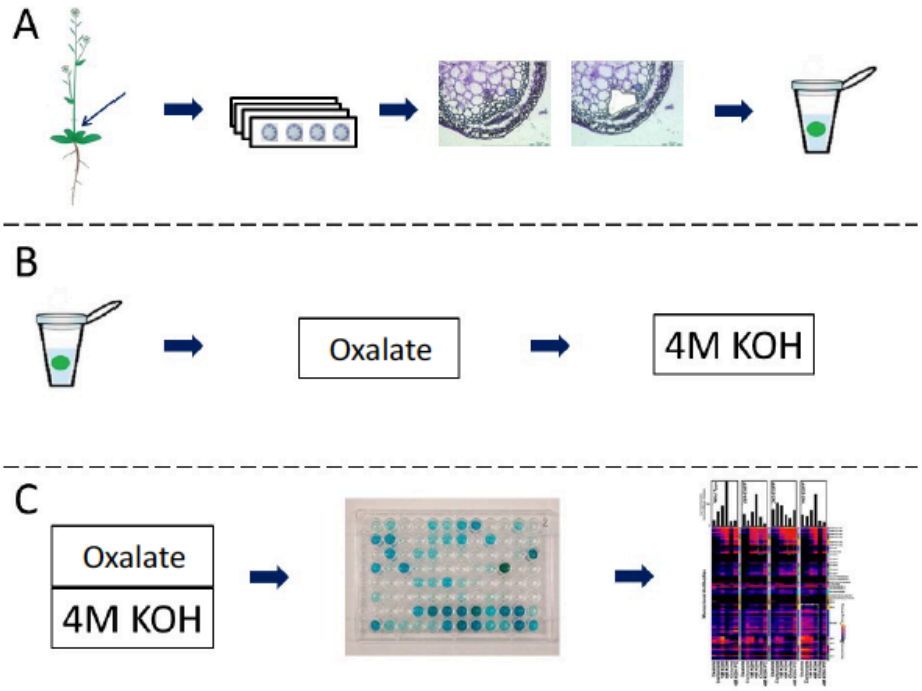

Figure 3.8: Method for tissue specific glycome profiling of Arabidopsis vascular cells from inflorescence stems. A) Stem harvest, stem processing and microtome sectioning, laser capture microdissection. B) Sequential fractionation of LCM harvested vascular tissues. C) Fractions were subjected to ELISA-based glycome profiling according to Pattathil et al. (2012) with modifications.

3.2.5 Laser Capture Microdissection-Glycome Profiling of Vascular Bundles and Interfascicular Fibres in Arabidopsis Stems:

Once the samples were optimised for LCM-based Glycome Profiling, we carried out analyses of the VB and IFF found at the apical and basal portion of Arabidopsis Col-0 *vnd6*, *vnd7*, and *vnd6 vnd7* stem oxalate and 4M KOH extracts. Choosing these t-DNA mutants has several advantages: these mutants there were no morphological phenotypes of observed, resulting in the need for further cell-wall compositional analyses being performed. SRDX repression lines were generated as an alternative to t-DNA which revealed vessel-type specific aberrant phenotypes, however, as mentioned, SRDX suppresses the expression of target genes of both the transcription factors and their redundant genes, resulting in phenotypes from multiple gene knockouts instead of a single target transcription factor(s) (Abe and Ichikawa, 2016). Moreover, using SRDX repressor systems under constitutive promoters induces aberrant phenotypes where the endogenous gene function is normally observed (Mitsuda and Ohme-Takagi, 2009). Therefore, this work provided the first attempt at comprehensively immunotype the glycan composition of these mutants using a collective suite of mAbs at a whole organ, and cell type-specific level.

3.2.5.1 LCM-based glycome profiling provides higher-resolution of immunotyping *vnd* mutants as compared to whole stem analyses:

ELISA optical density (OD) values from glycome profiling and % mol for 8 sugars using TMS GC-MS methods were analysed using principal component analysis (PCA) as a discriminant tool. In whole stem glycome profiling (Figure 3.4A), Col-0 and the *vnd* mutants clustered in an overlapping manner around the point of origin when comparing ELISA OD values from apical and basal sections of the stem. However, for the monosaccharide composition (in mol %), the apical and basal stem data clustered separately (Figure 3.6A), where the basal section compositions positioned towards the negative side and the apical section compositions in the positive side of the PC1 graph respectively. Separation of apical and basal data points in the PC1 axis displayed the most variance (58.9%) in total sugar composition. On the other hand, total sugar composition from apical stem portions contributed to PC2. This is observed from the greater vertical variation in the apical cluster while the basal shows tighter vertical clustering. Apical stems possibly contribute to most of the 26.8% variance in PC2. Therefore, the monosaccharide composition data could distinguish apical stem segments from basal stem segments, while glycome profiling did not. A possible reason for such variation between the two methods is that glycome profiling is an epitope-directed approach (Pattathil et al., 2015b) while the monosaccharide composition involves the hydrolysis of the wall polysaccharides and conversion of the resulting monosaccharide into TMS-methyl glycosides to quantify monosaccharide composition (Sweeley et al., 1963). Therefore, a correlation of the data between the two methods in

terms of stem development should not be expected. However, in comparing epitope and monosaccharide compositions in the different genotypes using GP and TMS methods, respectively, the whole stem segments failed to show any clustering or observable patterns between genotypes in their respective PCA plots (Figure 3.4A and Figure 3.6A). This implies that epitope variation amongst the genotypes cannot be distinguished at the whole organ level using these two orthogonal techniques.

3.2.5.2 Oxalate extraction of cell harvested revealed little changes in glycan epitope composition between Col-0 and *vnd* mutants

Oxalate extracts of LCM-GP (Figure 3.9A) revealed that no changes in epitope abundances occurred in the apical and basal VBs of Col-0 stems. However, changes in epitope abundance in IFFs during stem maturation occurred. Specifically, we observed that the presence of XG and xylan epitopes diminished as the parenchymal cells differentiated into fibre cells in the interfascicular region (purple dotted rectangle). In the single mutants, we see a clear reduction in these glycans as the VB differentiates, and no changes in glycan epitope composition during IFF differentiation. *vnd7* showed an absence of the aforementioned glycan epitopes (as highlighted by purple dashed lines) except for the presence of CCRC-M150 in the basal portion of *vnd7* IFF (orange dashed inlet). Also, mAb signalling from AG-1 to AG-3 clades were not detected in *vnd7* (green dotted rectangle). The double mutant, *vnd6 vnd7* showed epitope abundances similar to Col-0 except for HG-backbone-1 clades where there were increases in mAb signals from differentiated cells located at the basal VB and IFF (black dashed and dotted rectangle). Interestingly, the glycan epitope recognised by CCRC-M119 in the

Xylan-2 clade remained present in all genotypes and all stages of VB and IFF differentiation.

PCA of oxalate extracts displayed differences between cells harvested at different stem development stages and different cell types as demonstrated by the clusters being perpendicular to each other. Furthermore, we observed that VB cells from the basal segment of the stem significantly contributed to the PC1 variance (59.4%) and IFF cells from the segment only contributed to 19.9% of the variance (PC2). Interestingly, however, we observed no difference in the sample clustering between the genotypes in the oxalate extract (Figure 10). To further investigate the underlying causes for the clustering patterns observed in the oxalate extract, we produced loading plots for PC1 and PC2 (Figure 11A). These plots allowed us to determine which changes in mAb epitopes were responsible for the variances in the two PCs. Oxalate PC loading plots demonstrated that significant changes in mAbs recognising Xylan-2 and pectin backbones (bb), however only a scarce amount of mAbs from these groups contributed to variance in PC1. Similar patterns were observed in the oxalate PC2 loading plots: only one mAb in Xylan-2 and in Linseed Mucilage RG-I significantly contributed to the variance in PC2. Therefore, the lack of clustering in LCM-GP of oxalate extracts results from a lack of detectable contributions in mAb variations.

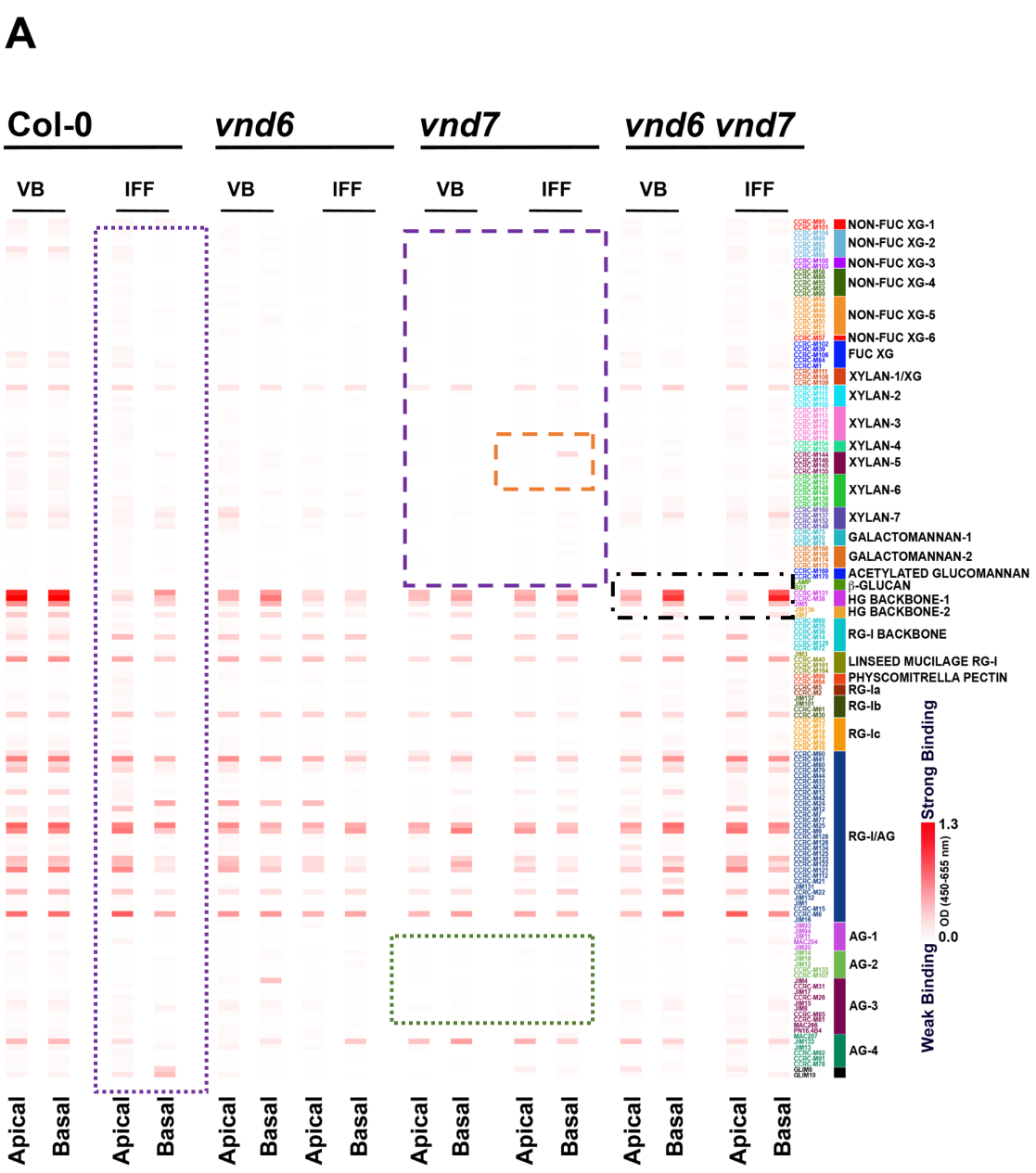

Figure 3.9A: Glycome profile from laser capture microdissected cells extracted using 50mM Ammonium Oxalate as explained in the Methods section. Corresponding vascular tissue location of cells laser dissected and from different plant genotypes are labelled above (VB = vascular bundle; IFF = interfascicular fibre). Developmental stages are labelled below. Each extracted was probed against a repertoire of plant glycan-directed monoclonal antibodies (for a list of all mAbs see Appendix A). Antibody binding strength is represented as a white-red gradient ranging from white (no binding) to red (strongest binding) (OD= 1.3).

3.2.5.3 4M KOH extracts revealed significant changes between Col-0 and *vnd* mutants and within *vnd* mutants

4M KOH extracts of LCM harvested cells subjected to GP revealed numerous changes between Col-0 and *vnd* mutants and within *vnd* the mutants (Figure 3.9B). In Col-0, no changes in glycan epitopes were observed between apical and basal portions of cells harvested from either the VB or IFF region (highlighted by blue dotted rectangles). Interestingly, however, was the mAb signal patterns of XG clades and Xylan-1/XG clades: *vnd6* and *vnd7* single mutants showed a significant reduction in these clades, and in contrast, *vnd6 vnd7* displayed near exact Xylan-1/XG mAb signal patterning with Col-0 (purple dashed rectangle) were observed. mAbs belonging to the Xylan-4 and 5 clades displayed reductions in all samples from the *vnd6* mutant. On the other hand, *vnd7* mutants only showed reduced epitope presence at the apical portion for both VB and IFF regions. For the *vnd6 vnd7* double mutant displayed a significant reduction in mAb signals from antibodies belonging to the Xylan-4 to 7 clades in basal cells from both the VB and IFF region (blue solid rectangles). Additionally, a unique pattern was observed in this genotype where there were increased abundance in epitopes recognised by CCRC-M31 and CCRC-M36 belonging to the AG-3 clade (black dotted and dashed inlet). Lastly, we observed a lack in epitopes recognised by mAbs from the AG-1 to 4 clades in all *VND* T-DNA mutants as compared to Col-0 (green dashed rectangle).

Results from the PCA of 4M KOH extracts displayed no differences between harvested material from different stem developmental stages or cell types. This is evident based on the overlapping clusters in the PCA plots from LCM-harvested

samples. However, a clear difference was detected in the PCA plot that compared the different genotype samples. Here we observed that *vnd6* and *vnd7* single mutants clustered towards the negative side of the plot, in contrast Col-0 and *vnd6 vnd7* double mutants clustered in the positive area of the plot. This showed that the largest variance is contributed by the differences *vnd6*, *vnd7* single mutants and Col-0 and the *vnd6 vnd7* double mutant (83.4% of the variance in PC1) (Figure 10). The loading plot for PC1 in the 4M KOH displayed that non-fucosylated xyloglucan and RG-I/AG mAb signals were responsible for the observed variance in PC1 (Figure 11B). The difference in sample clustering between Col-0 and *vnd6 vnd7* double mutants are due to the variances in PC2 (Figure 10). Variances in this PC resulted from mAbs recognising xylan epitopes as exhibited in the PC2 loading plot (Figure 11B). In summary, we observed that the largest variances are between *vnd6*, *vnd7* single mutants and Col-0 and *vnd6 vnd7* double mutants as a result of differences in xyloglucan epitope abundances. Variances between Col-0 and *vnd6 vnd7* double mutants are caused by the changes in xylan epitope abundances.

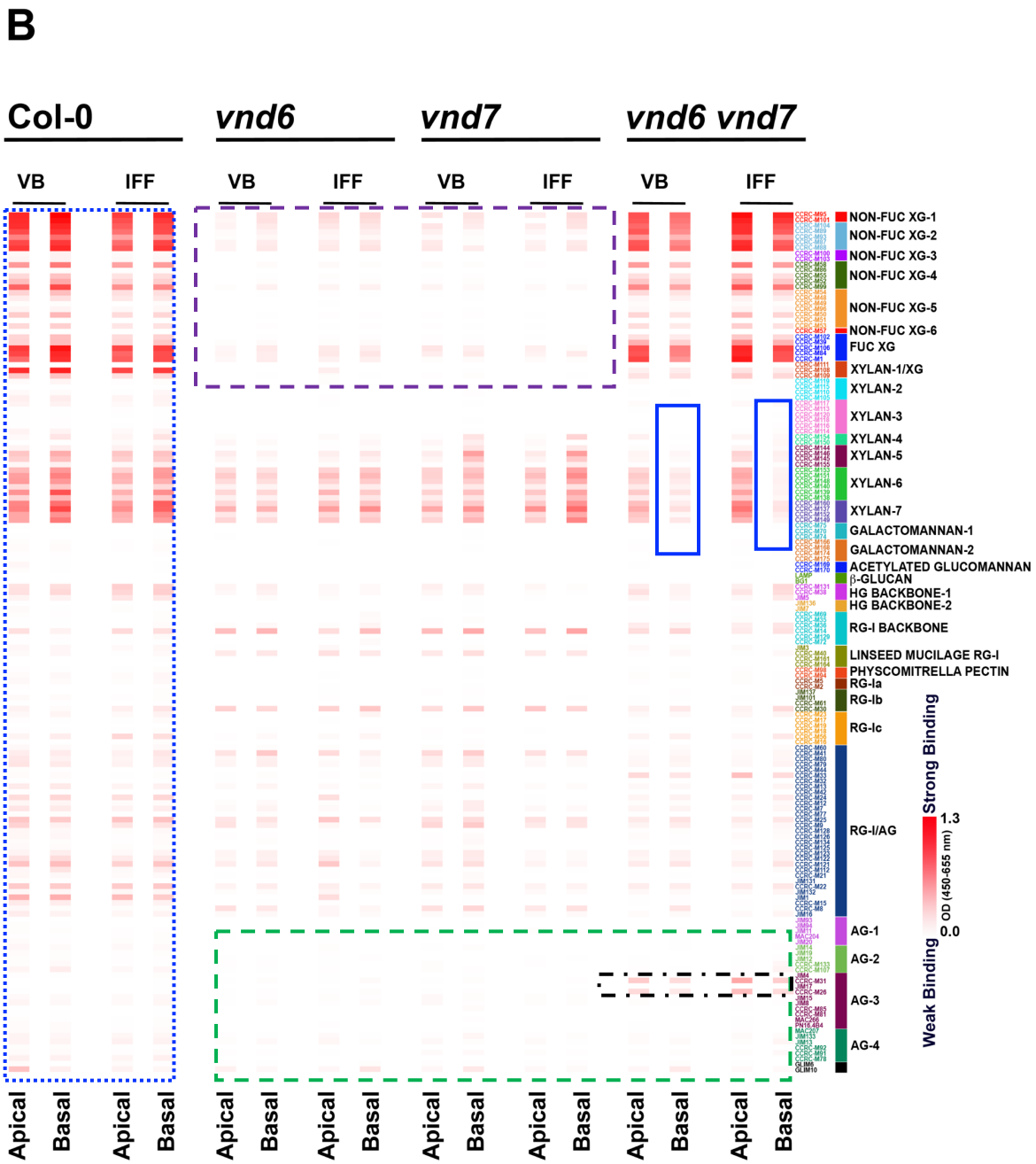

Figure 3.9B: Glycome profile from laser capture microdissected cells extracted from 4M KOH as explained in the Methods section. Corresponding vascular tissue location of cells laser dissected and from different plant genotypes are labelled above (VB = vascular bundle; IFF = interfascicular fibre). Developmental stages are labelled below. Each extracted was probed against a repertoire of plant glycan-directed monoclonal antibodies (for a list of all mAbs see Appendix A). Antibody binding strength is represented as a white-red gradient ranging from white (no binding) to red (strongest binding) (OD= 1.3).

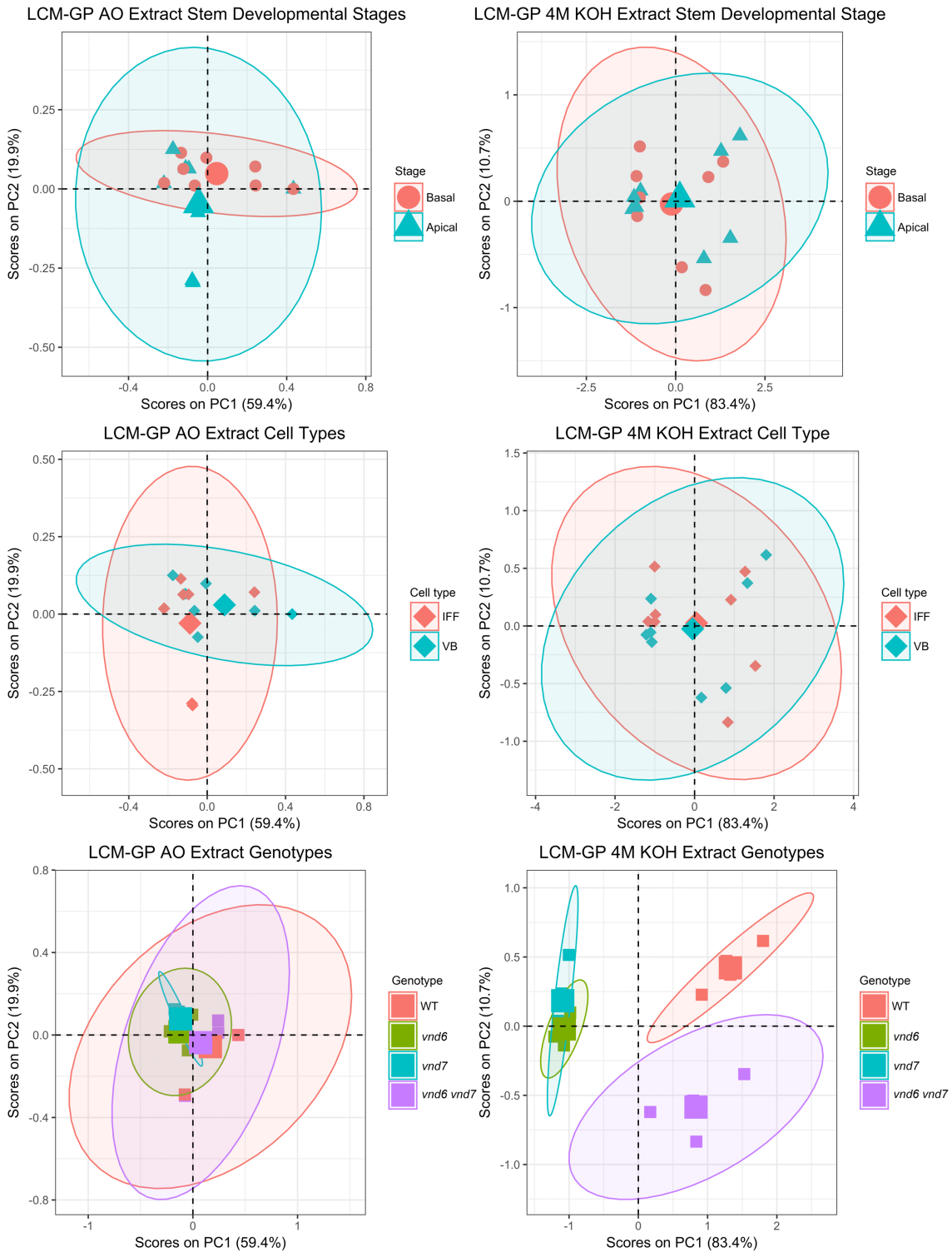

Figure 3.10: Principal components analysis of LCM-Glycome profiling. Data points are presented for all samples from the two fractions obtained during sequential extraction.

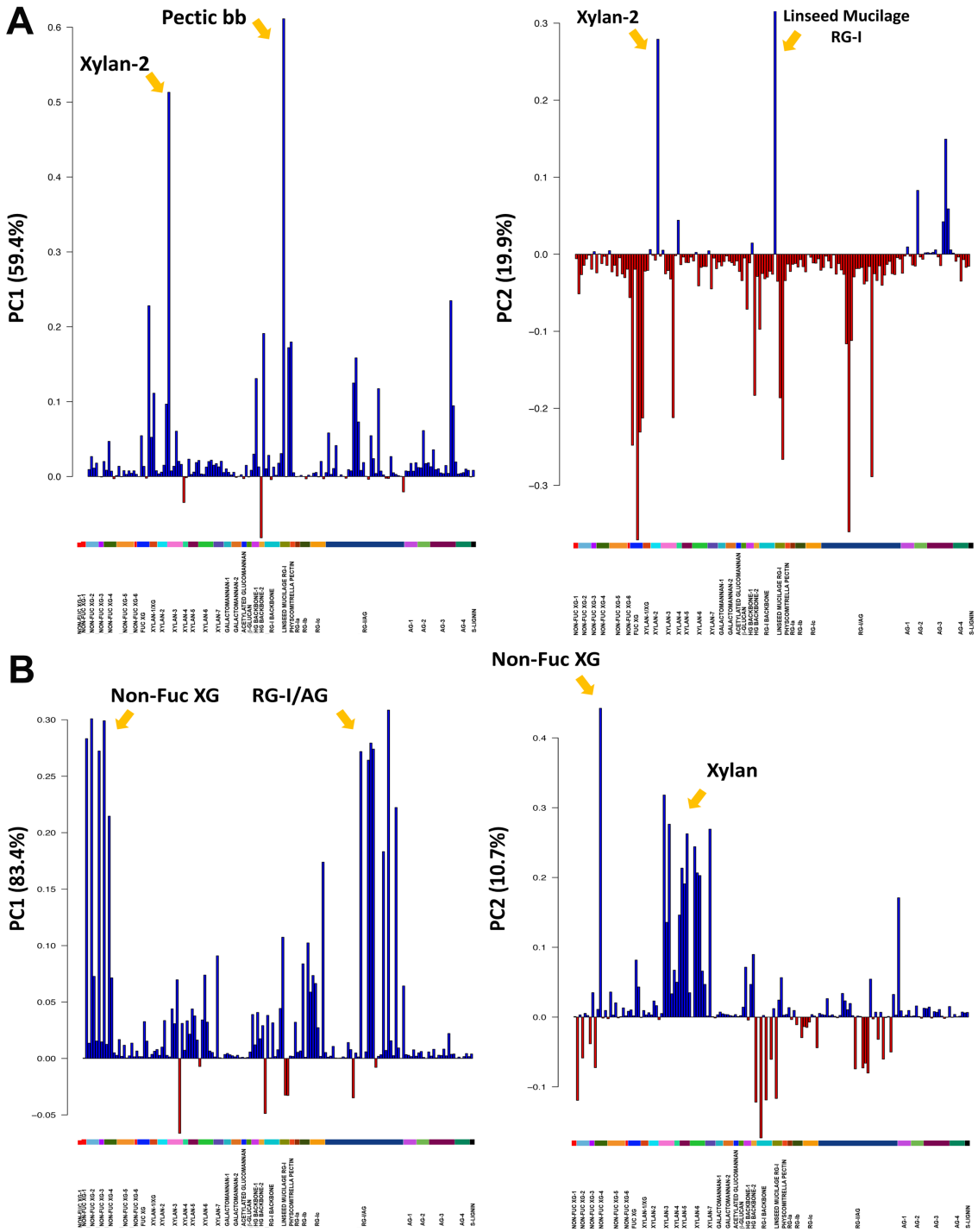

Figure 3.11: Loading plots of oxalate (A) and 4M KOH fractions of LCM-GP. PC1 and PC2 are shown along which clusters emerged. Bottom shows the mAb key from glycome profiling. Gold arrows depict the mAb signals that contributed the most variance (blue) for PC1 and PC2. bb = backbone.

3.2.5.4LCM-GP cell-type/population demonstrated glycan differences amongst Col-0 and *vnd* mutants:

Ammonium oxalate extracts that are probed with mAbs shows a majority of pectin epitopes abundance. There are variations, such as the increase in signals of CCRC-M36 and CCRC-M131 that recognise rhamnogalacturonan-I backbone (Ruprecht et al., 2017) and de-esterified homogalacturonan backbone with > DP 4 (Pattathil et al., 2010), respectively, that are observed from cell-types harvested from the basal VB and IFF of the *vnd6 vnd7* double mutant. Concomitantly, these antibodies are significantly reduced in the cells harvested from VB and IFF of *vnd6* and *vnd7* single mutants. Studies by (Hussey et al., 2013), Manfield et al. (2004) demonstrated that homogalacturonan possessing low amounts of esterification were increased in the cell-wall compensate for a lack of cellulose elicited by either cellulose inhibitor treatments or by reducing cellulose synthase expression. Studies of *IRX8* a galacturonosyltransferase showed that homogalacturonan in higher plants are essential for cell-wall integrity by cross-linking with xylans (Persson et al., 2007). The increase in these epitopes that are present in the basal VB and IFF may compensate for the reduction of xylan epitopes and possibly of cellulose content due to *vnd6 vnd7* loss-of-function mutations. We cannot confirm the latter as there are no currently available mAbs specific to cellulose and no alternative methods for quantifying cellulose on a cellular or tissue scale. In addition, epitope(s) recognised by CCRC-M119 were present in all samples of LCM-GP. CCRC-M119 recognises *Phorium cookanium* xylans with the structure resolved in its leaves using 13C NMR, in which the xylan backbone with a structural unit containing both 2-O- and 3-O-acetyl groups and its sidechains contain α-d-GlcA and are terminated by β-d-Xyl*p* and α-

l-Ara*f* units (Sims and Newman, 2006). This proves that through LCM-GP methods we can uncover new xylans such as the abovementioned epitope possibly specific to CCRC-M119 in the PCW. It also demonstrates that our understanding of xylan deposition in PCWs are incomplete. Lastly, in oxalate extracts, the VB glycan epitope signature remained the same throughout cell differentiation. However, in the IFF, there were significant glycan epitope changes during the transition of parenchymatous cells composed of the primary cell wall to fully differentiated fibre cells. There were reductions in XG, xylan, galactomannan, acetylated glucomannan as differentiation when parenchyma cells differentiate to IFF cells.

LCM-based GP shows a reduction in diverse xylan epitopes in basal vascular bundles and interfascicular fibers collected from *vnd* single mutants. The *vnd6 vnd7* double mutant displays an even more severe reduction in xylan epitopes, particularly in the substituted xylans recognized by the Xylan-4 and -5 mAb clades. These mAbs specifically recognize xylan side-chains of α-1,3-Ara*f*, GlcA, and Me-GlcA (Schmidt et al., 2015). Therefore, it would be prudent to investigate the expression levels of *GUX1* and *GUX2* (GlcA substitutions) (Bromley et al., 2013), GXMT1 (MeGlcA substitution) (Urbanowicz et al., 2012), and those arabinosyltransferases (AraT) in Arabidopsis that play a role in α-1,3-Ara*f* substitution (Faik, 2010, Held et al., 2021) as possible targets of VND transcriptional regulators. Homogalacturonan-I-directed mAbs recognising low methyl-esterified homogalacturonan also show reduced binding to cell-type specific extracts in the *vnd* mutants as compared to Col-0 (Figure 8B). This further supports a role for pectin in SCW formation, possibly by VND regulation of *IRX8*. The loss of xylans

in interfascicular fibers of the *vnd6 vnd7* double mutant also calls to question the degree to which these regulators are expressed in a cell type-specific manner. Brady et al. (2007) demonstrated that Arabidopsis root cell type-specific TFs have broader expression patterns than previously assumed. Also, *WAT1* expression patterns are also in conflict with the idea that signals regulating the master regulators are themselves cell-type specific (Ranocha et al., 2010). However, a more likely scenario is maybe that VND6 and SND1 share common downstream targets for SCW biosynthesis (Ohashi-Ito et al. (2010). Therefore, decreases in xylan epitopes could be due to the decrease in downstream SCW-related genes that are targets of both VND6 and SND1.

Another striking pattern is observed in 4M KOH extracts of wild-type Col-0 xylem cells. LCM-based GP shows that in 4M KOH extracts, Col-0 glycans remain unchanged in vascular bundles and interfascicular fibers during differentiation from juvenile to mature cells. A possible reason for this is that we sampled apical vascular bundle cells that were fully differentiated at the point where we harvested them. Interfascicular fiber cells on the other hand demonstrated changes in glycan epitopes in ammonium oxalate extracts that points to potential remodelling of primary cell-walls into secondary cell walls. This could be achieved by decreasing primary cell wall-associated glycans, as evidenced by the observed reduction in their epitope abundances in the oxalate extracts of basal interfascicular fibers (Figure 3.8B vertical dotted rectangle). Another reason could be that Arabidopsis is a poor model for surveying glycan epitope changes in xylem and fibre differentiation in stems. Our apical and basal samples are only 12-cm apart pointing to the possibility that within this sample range, PCW to SCW changes during differentiation

are minute. In summary, the data obtained through LCM-based GP suggests that we lack full comprehension of plant cell wall differentiation processes at a cell type-specific resolution.

The lack of glycan epitope changes in cell walls of vascular bundles and interfascicular fibers of Col-0 stems during their differentiation leads to the hypothesis that changes in glycan epitope composition is not responsible for the helical or pitted patterns in vascular bundle cell walls and the smooth patterns observed in cell walls of fibres. Other factors such as glycoproteins or kinesin and Rho GTPases complex could then be responsible for these wall differentiation patterns. The *MIDD1* Kinesin13A complex is an example of such an alternative regulatory network controlling vessel shape by promoting cortical microtubule depolymerisation to form secondary cell-wall pits (Oda and Fukuda, 2013). Moreover, Yamaguchi et al. (2011) and Zhou et al. (2014) showed that *SND1*:*VND1-5* and *SND1*:*VND7* are able to rescue secondary cell-wall deposition in fibres from *snd1 nst1* mutants, but with vessel-like secondary cell-wall patterning. These experiments show that other proteins and/or protein complexes regulated by VNDs are responsible for vessel secondary cell-wall deposition patterns, which make compositional changes or abundances of glycans epitopes deposited in the secondary cell wall an unlikely factor in determining how SCW polymers are deposited in these cell types.

3.2.6 Data Correlation Analyses to Determine Reproducibility and Robustness of ELISA data from LCM harvested samples:

In order to confirm the reproducibility of our ELISA data from LCM harvested material. We generated a correlation heat map by from experimental datasets. Reference datasets from Col-0 basal VBs extracted with 4M KOH were compared to themselves and to the average values derived from three biological replicates of the same extract and stem developmental stage representing a test dataset. The datasets of ELISA OD values screened using 155 antibodies were subsequently transformed into a correlation matrix in which each element is a dot product of a row vector in the reference matrix with a row vector of the average test vector similar to the methods described in Pattathil et al. (2010). A correlation heat map analysis was generated using R (Figure 3.12). In this heat map, the order of rows from the reference matrix and columns from the test matrix are the same. Therefore, each off-diagonal element in the correlation matrix corresponds to the correlation of the ELISA OD value for a mAb (i.e., a row vector *i* from the reference) with the ELISA OD value for another mAb (row vector *j* from the test averages). If there is perfect reproducibility, the heat map will display all diagonal elements equal to 1.0 (brightest yellow) and perfect symmetry about the diagonal. Additionally, this should be the result if the data were compared to itself (Figure 3.12A). The adjacent heat map (Figure 3.12B) was derived from the ELISA response pattern of all 155 mAbs used in our repertoire from the reference dataset and compared against the average ELISA response pattern of three individual biological replicates (test dataset). The similarities of all diagonal elements equalling 1.0 and

symmetry of the diagonal confirmed the reproducibility of our ELISA data obtained from LCM-dissected material (Figure 3.12).

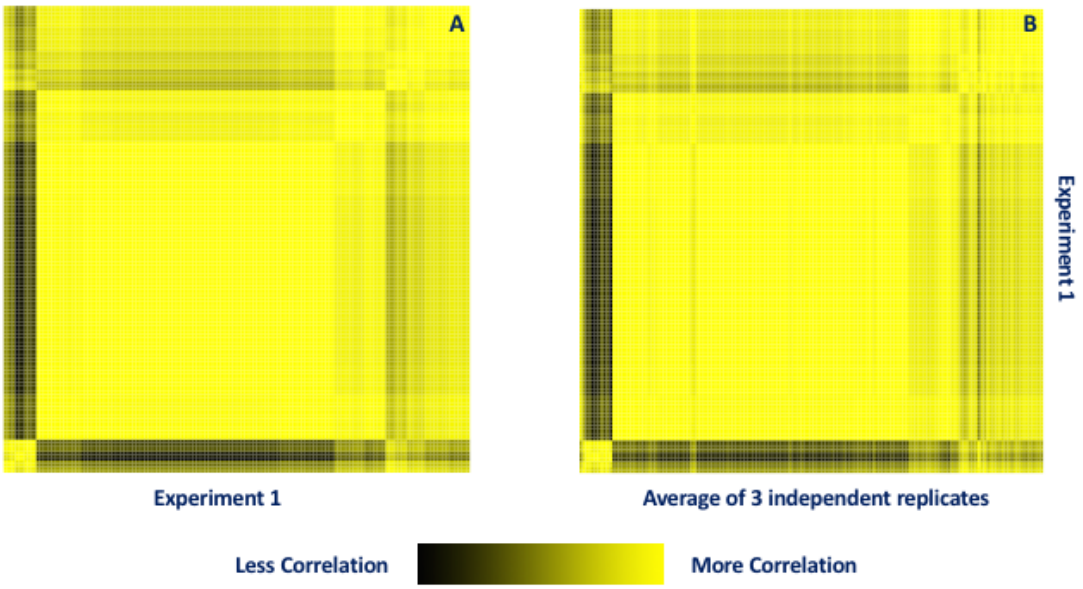

Figure 3.12: Reproducibility of LCM-harvested ELISAs. Data correlation heat maps were generated by comparing one ELISA dataset with itself (A) and with the average of three ELISA replicates (B). Within each square in this heat map, increasing yellow colour indicates a greater correlation between two mAb-binding patterns. The bright yellow diagonal elements depict the high degree of correlation of specific mAb-binding patterns between replicates. The high colour intensity of the diagonal and high degree of symmetry of the diagonal in (B) indicated high reproducibility among independently performed ELISA replicates.

In relation to the reproducibility of our test dataset, we tested the robustness of our method. To do so, we harvested an additional set of Arabidopsis basal stems that were grown at a separate time points after the previous test dataset under the same conditions. Additionally, samples from the previous test dataset were sectioned and laser dissected to harvest cells from VBs basal stem portions. Although our new correlation map (Figure 3.13) does not exactly recapitulate the correlation patterns in the previous heat map (Figure 3.12), similar trends in correlation symmetry were observed. Data correlation heat maps from the comparison of the new ELISA dataset

with itself (Figure 3.9A) and with an average of six independent replicates (three from samples derived from the original test dataset and the other three from the new set of stems harvested at different time points) showed correlation patterns similar to Figure 3.12. Here we observed similar diagonal elements equalling 1.0 and symmetry of the diagonal with our new dataset, thereby the robustness method of ELISA-based glycome profiling at a cell type-specific resolution using laser microdissection was verified (Figure 3.13).

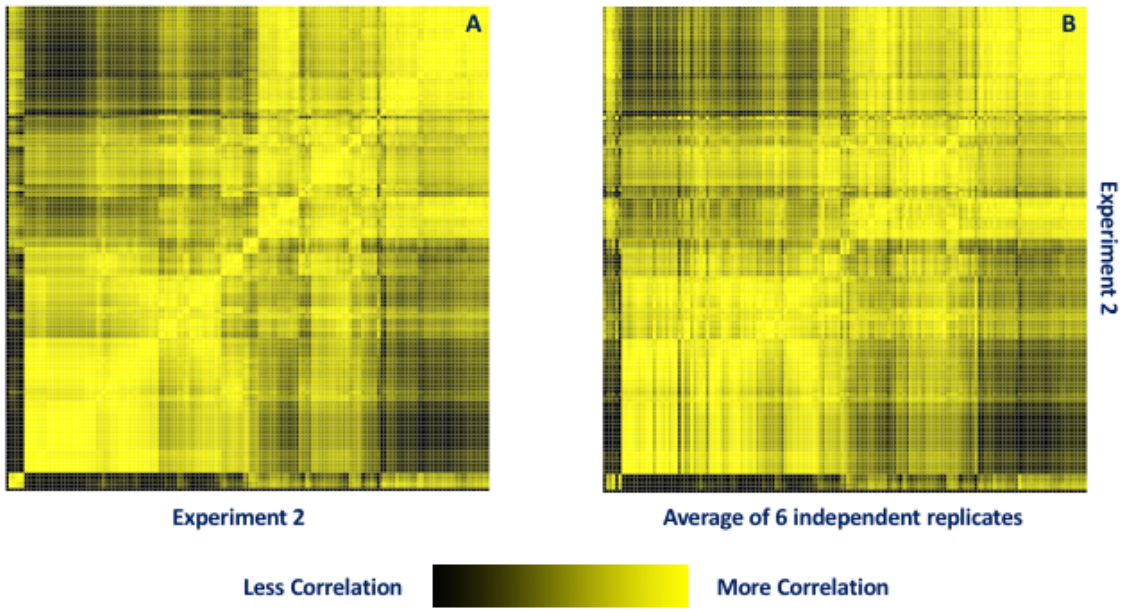

Figure 3.13: Robustness of LCM-harvested ELISAs. Data correlation heat maps were generated by comparing one ELISA dataset with itself (A) and with an average of six ELISA replicates (B). Within each square in this heat map, increasing yellow colour indicates a greater correlation between two mAb-binding patterns. The bright yellow diagonal elements depict the high degree of correlation of specific mAb-binding patterns between replicates. The high colour intensity of the diagonal and high degree of symmetry of the diagonal in (B) indicated high reproducibility among independently performed ELISA replicates

3.2.7 *in situ* immunolabelling revealed cell- and developmental-specific patterns of distribution of cell-wall glycan epitopes in Col-0 and *vnd* mutants:

We carried out immunohistochemical analysis with a subset of the antibodies used in Glycome Profiling on cross-sections of the same paraffin embedded blocks of Arabidopsis inflorescence stems used for LCM harvesting. This will diminish any batch variations in stem growth, harvesting, and histochemical processing. A panel of antibodies was selected (Table 3.3) derived from different glycan-directed antibody clades in order to compare their correlation with the LCM-based ELISA heat map (Figure 3.9). Fluorescence from non-vascular cells i.e. cells belonging to the pith, cortex, phloem and epidermal tissue was blacked-out using Photoshop image software to eliminate unwanted and background signals. This allowed a more convenient comparison of vascular tissues-of-interest namely the vascular bundle and interfascicular fibres of the different genotypes. Furthermore, it permitted us to compare the mAb signal patternings between *in vitro* GP and *in situ* immunolabelling. The original unprocessed images can be found in Appendix B. *In situ* visualisation using the mAbs from Table 3.3 demonstrated differences in glycotypes *in situ* that supports differences resulting from T-DNA inserts in *vnd6* and *vnd7* observed previously.

Table 3.3: Selected list of glycan-directed mAbs for *in situ* visualisation and comparison with LCM-based Glycome Profiling

Antibody	Epitope	Clade	Reference
CCRC-M101	XG with L side chain	Non-Fuc XG-1	Dallabernadina et al., 2017
CCRC-M87	XG with L side chain	Non-Fuc XG-2	Dallabernadina et al., 2017
CCRC-M100	XG with L side chain	Non-Fuc XG-3	Ruprecht et al., 2017
CCRC-M55	XG with L side chain	Non-Fuc XG-4	Dallabernadina et al., 2017, Tuomivaara et al., in prep

CCRC-M50	XG with L side chain	Non-Fuc XG-5	Tuomivaara et al., in prep
CCRC-M1	Fuc side chain XG	Fuc XG	Puhlmann et al., 1994
CCRC-M84	Double Fuc side chain XG		Dallabernadina et al., 2017
CCRC-M108	α-1,2-Ara substituted Xylan	Xylan-1	Ruprecht et al., 2017, Schmidt et al., 2015
CCRC-M110	α-1,2-Ara substituted Xylan	Xylan-2	Ruprecht et al., 2017, Schmidt et al., 2015
CCRC-M154	α-1,3-Ara substituted Xylan	Xylan-4	Ruprecht et al., 2017, Schmidt et al., 2015
CCRC-M150	GlcA substituted Xylan	Xylan-4	Ruprecht et al., 2017, Schmidt et al., 2015
CCRC-M146	4-*O*-MeGlcA substituted Xylan	Xylan-5	Ruprecht et al., 2017, Schmidt et al., 2015
CCRC-M145	4-*O*-MeGlcA substituted Xylan	Xylan-5	Ruprecht et al., 2017, Schmidt et al., 2015
CCRC-M139	Xylan Backbone	Xylan-6	Ruprecht et al., 2017, Schmidt et al., 2015
CCRC-M38		HG Backbone-1	
CCRC-M14		RG-I Backbone	
CCRC-M30		RG-Ib	
CCRC-M56		RG-Ic	
CCRC-M24		RG-I/AG	
CCRC-M26		AG-3	
JIM133	Nonreducing ends of the β-1,3-linked galactan backbone	AG-4	Ruprecht et al., 2017

Non-Fuc XG: NonFucosylated Xyloglucan, Fuc XG: Fucosylated Xyloglucan, HG: Homogalacturonan, RG: Rhamnogalacturonan, AG: Arabinogalactan

Immunolabelling analysis of specific XG epitopes probed with CCRC-M101, CCRC-M87, CCRC-M55, CCRC-M50, CCRC-M1, and CCRC-M84 demonstrated distinct labelling patterning (Figures 14-15). These antibodies recognised galactosylated or fucosylated xyloglucan backbones. Apical sections displayed mAb signals in all genotypes and that were localised in the protoxylem. While basal sections displayed decreased xyloglucan

directed mAb signalling in all *vnd* mutants as compared with Col-0. Xylan-directed mAbs displayed patterns that classified them as weak or strong signals. Weak signals were observed with epitopes recognised by CCRC-M108, CCRC-M110, CCRC-M114, CCRC-M145, CCRC-M139, and CCRC-M140. Contrastingly, strong signals from xylan-directed mAbs were from CCRC-M154, CCRC-M150, CCRC-M146, and CCRC-M137 (Figures 16-18) which recognise arabinosylated, GlcA substituted, 4-*O*-MeGlca substituted, and unsubstituted DP 4 xylan backbones respectively. Overall, the labelling patterns xylan-directed mAbs showed an overall decrease in signal intensity. Similarly, results from pectin-direct mAbs demonstrated varying labelling patterns. Overall, *vnd6 vnd7* mutant displayed weaker epitope presence at the basal portion of the stem (Figure 20). Interestingly, we found that CCRC-M56 showed weak to no signalling in all genotypes and stem developmental stages. On the other hand, we observed the contrary in JIM133 labelling were it was present in all genotypes. Lastly, CCRC-M24 displayed stronger labelling in *vnd* t-DNA mutants compared to Col-0. In summary, our results confirm *in vivo*, that glycomic differences caused by T-DNA insertions in *VND6* and *VND7* transcription factors and are not a result of epitope modifications when subject to the chemical fractionation process involved in GP

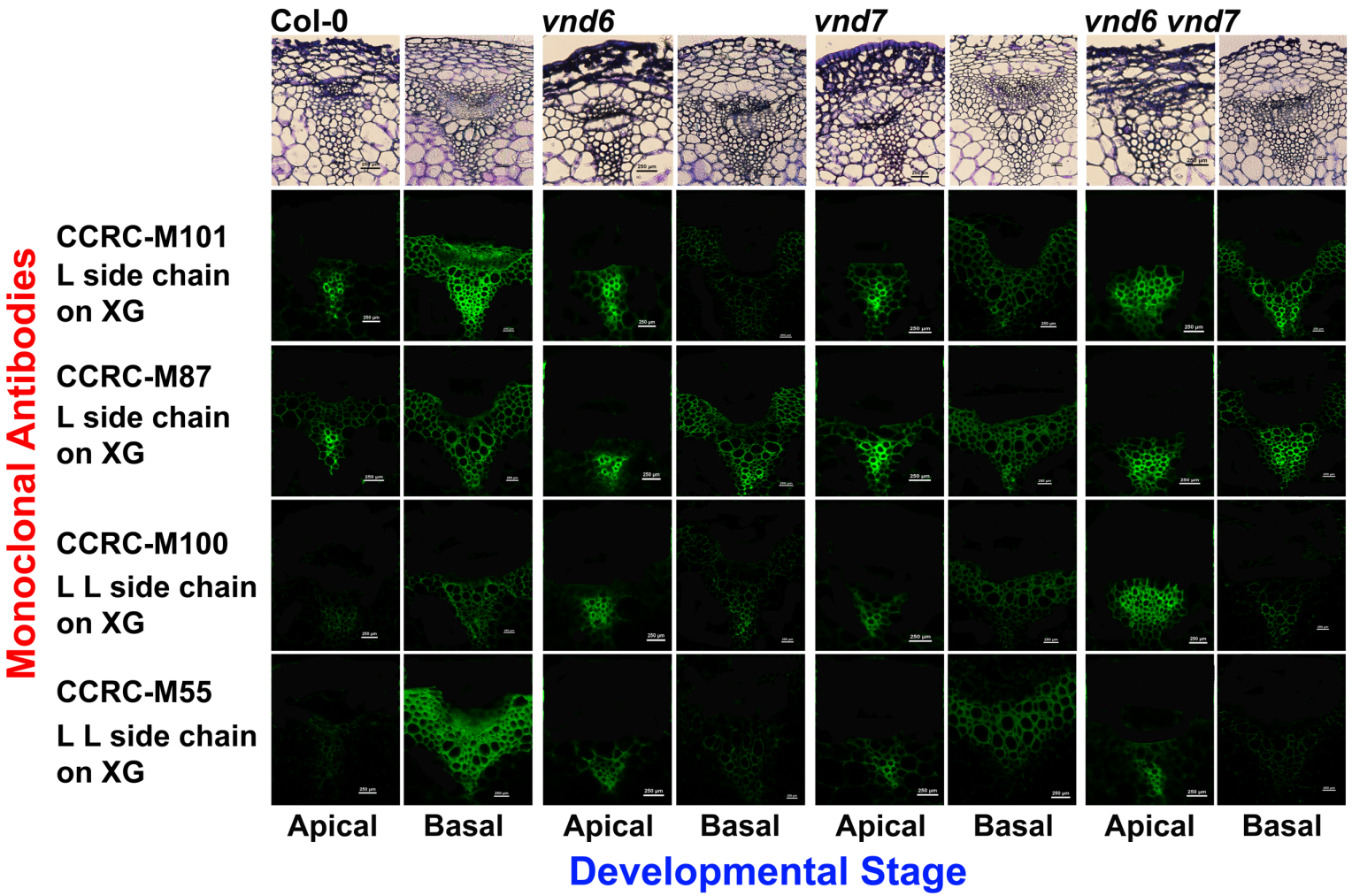

Figure 3.14: Immunofluorescent labelling of cell wall glycan XG epitopes in transverse sections of inflorescence stems from Arabidopsis (Col-0, *vnd6*, *vnd7*, *vnd6 vnd7*) taken from apical and basal segments of the stem. Immunolabelling studies were preceded by microscopic inspection of sections using toluidine blue-O staining (top row of images). Bar = 200 µm.

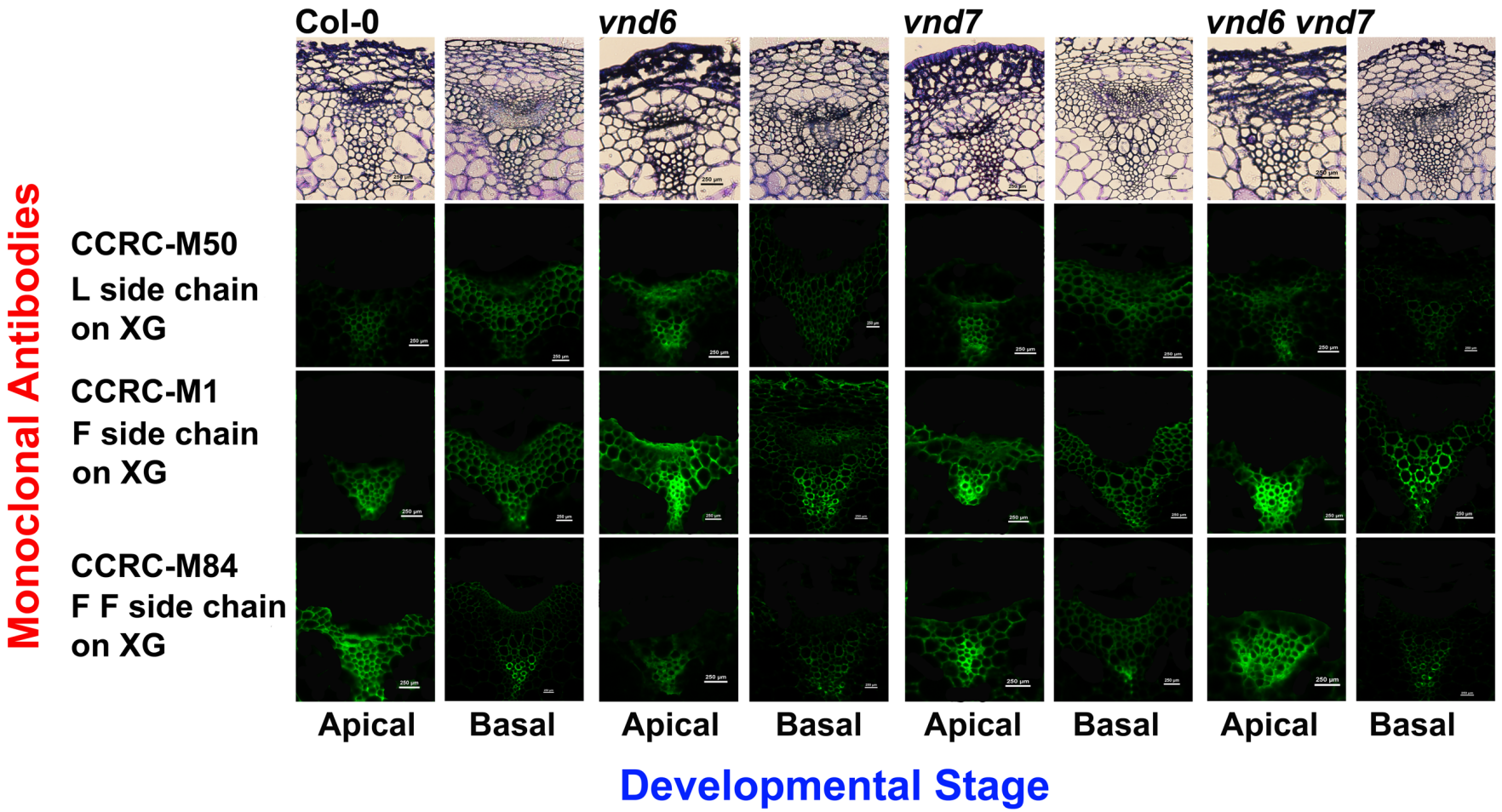

Figure 3.15: Immunofluorescent labelling of cell wall glycan XG epitopes in transverse sections of inflorescence stems from Arabidopsis (Col-0, *vnd6*, *vnd7*, *vnd6 vnd7*) taken from apical and basal segments of the stem. Immunolabelling studies were preceded by microscopic inspection of sections using toluidine blue-O staining (top row of images). Bar = 200 µm.

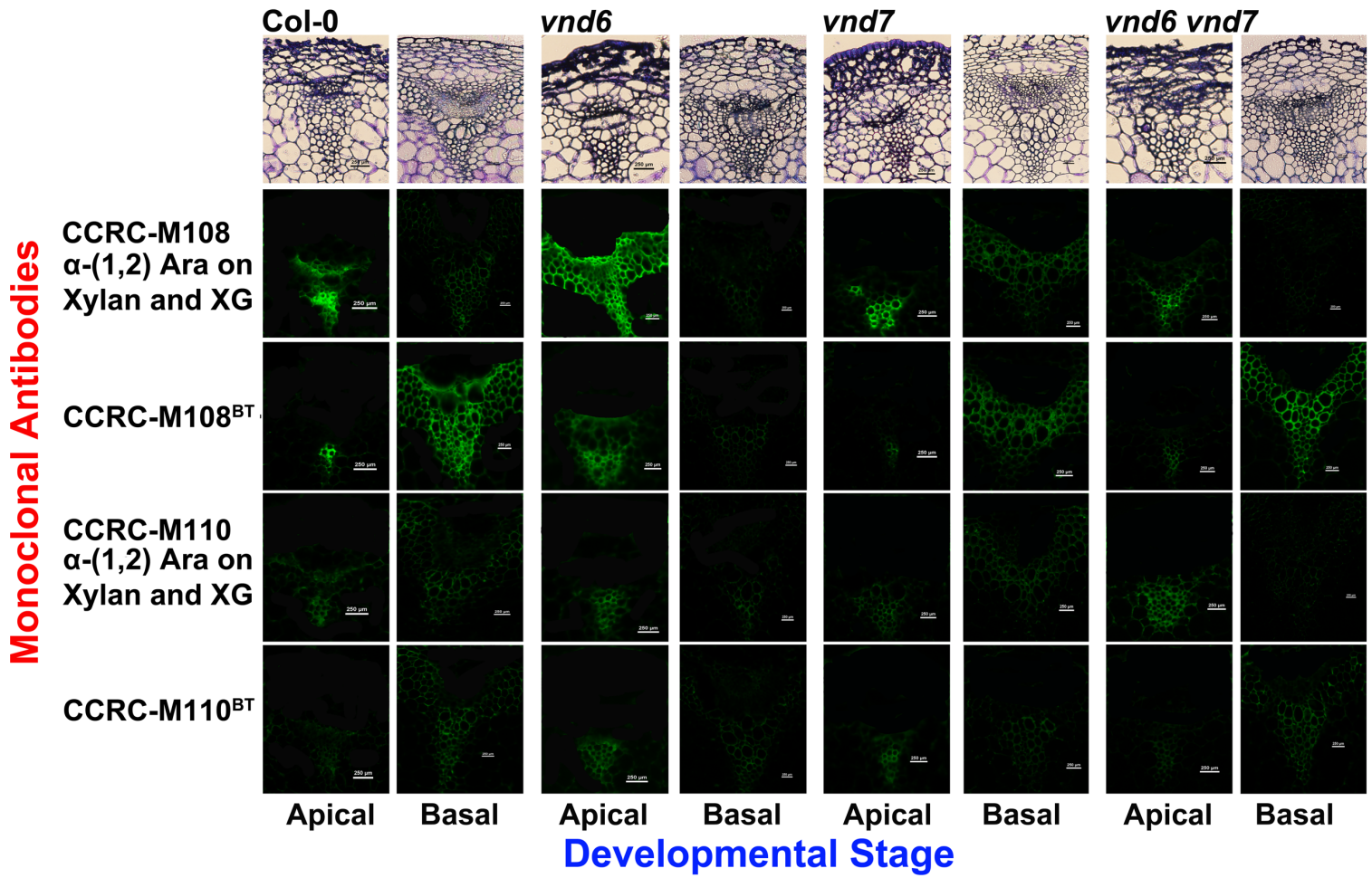

Figure 3.16: Immunofluorescent labelling of cell wall glycan Xylan/XG epitopes in transverse sections of inflorescence stems from Arabidopsis (Col-0, *vnd6*, *vnd7*, *vnd6 vnd7*) taken from apical and basal segments of the stem. Immunolabelling studies were preceded by microscopic inspection of sections using toluidine blue-O staining (top row of images). Bar = 200 µm. BT = base treated.

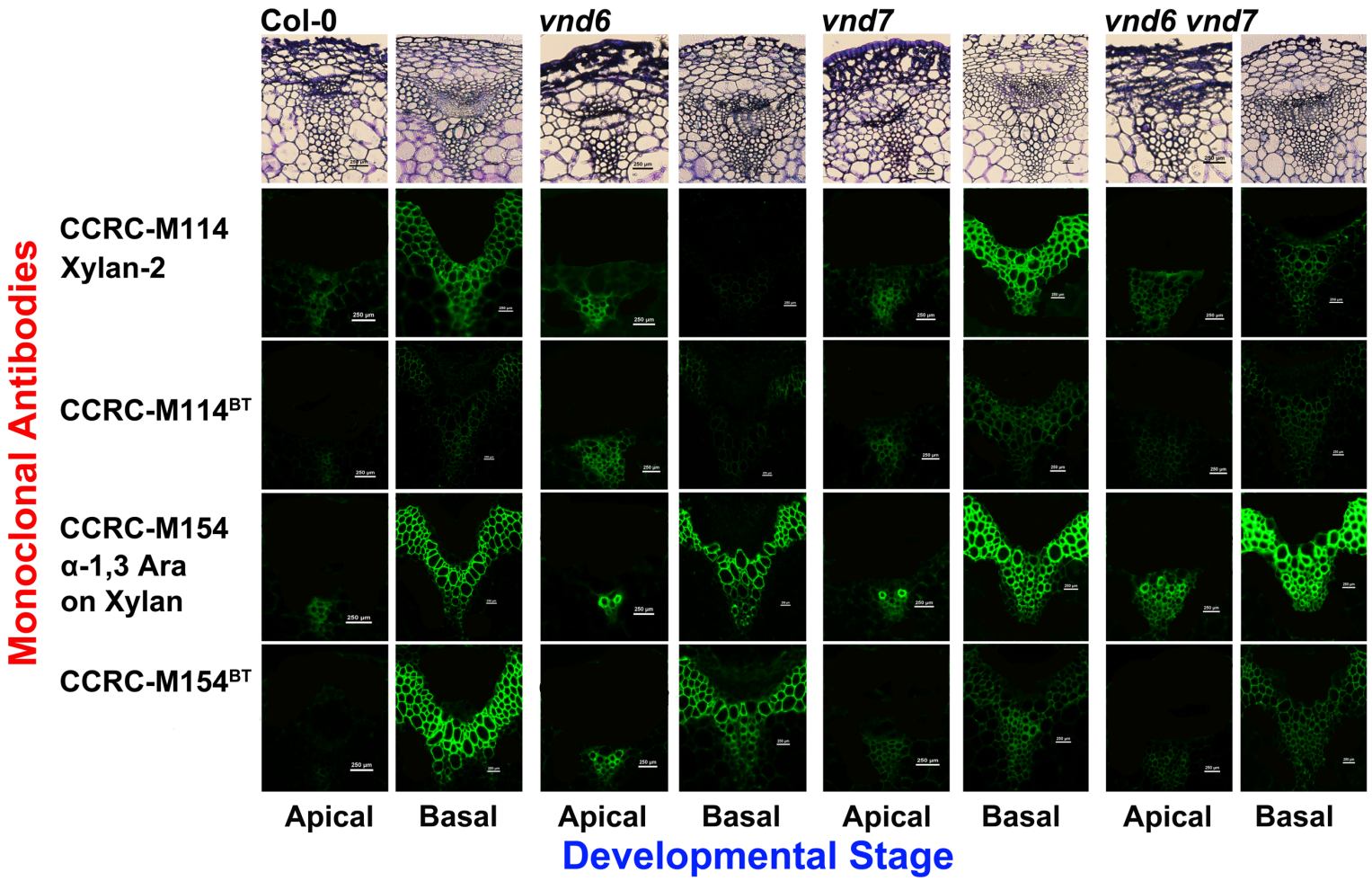

Figure 3.17: Immunofluorescent labelling of cell wall glycan Xylan epitopes in transverse sections of inflorescence stems from Arabidopsis (Col-0, *vnd6*, *vnd7*, *vnd6 vnd7*) taken from apical and basal segments of the stem. Immunolabelling studies were preceded by microscopic inspection of sections using toluidine blue-O staining (top row of images). Bar = 200 µm. BT = base treated

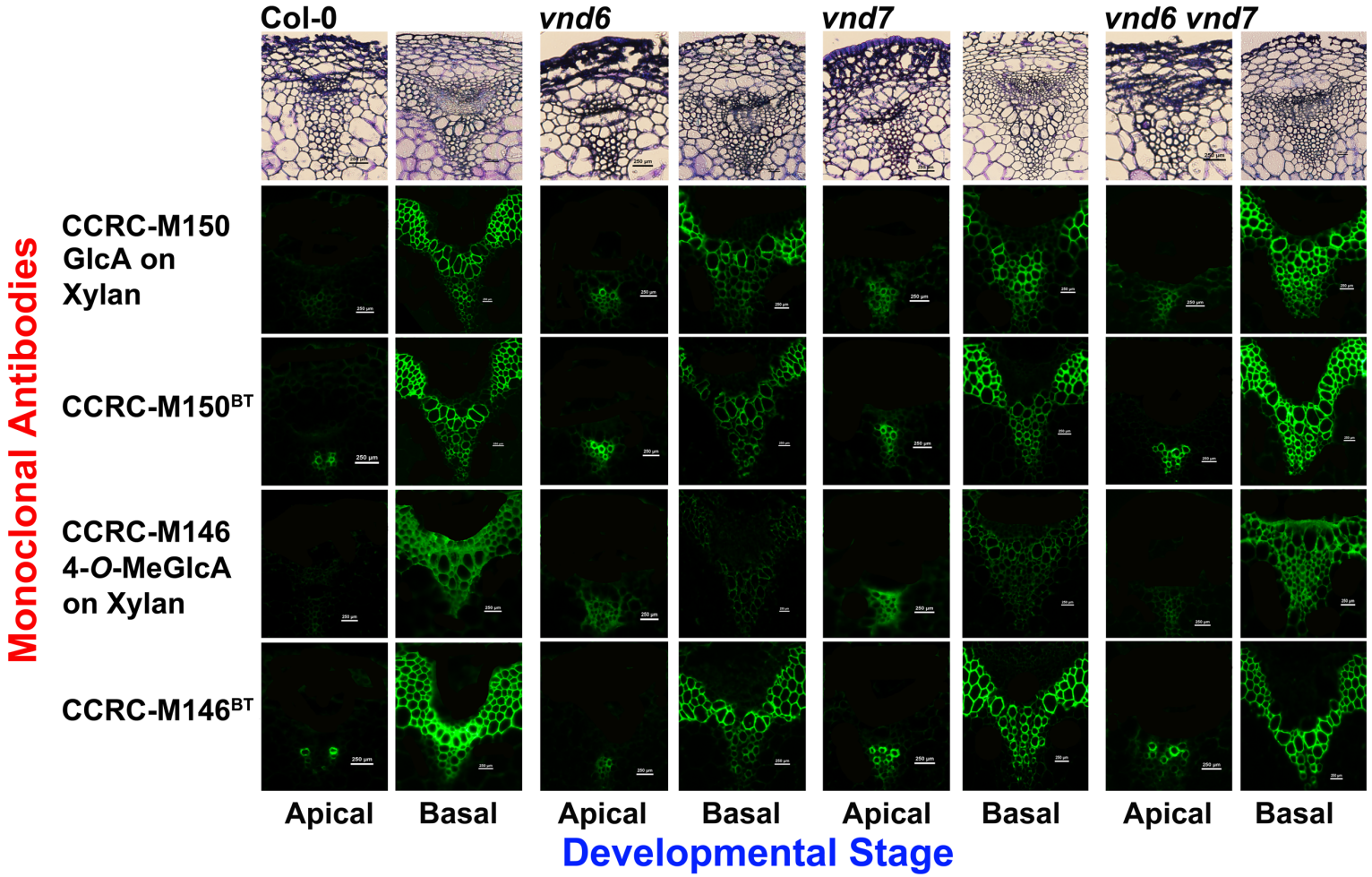

Figure 3.18: Immunofluorescent labelling of cell wall glycan Xylan epitopes in transverse sections of inflorescence stems from Arabidopsis (Col-0, *vnd6*, *vnd7*, *vnd6 vnd7*) taken from apical and basal segments of the stem. Immunolabelling studies were preceded by microscopic inspection of sections using toluidine blue-O staining (top row of images). Bar = 200 µm. BT = base treated.

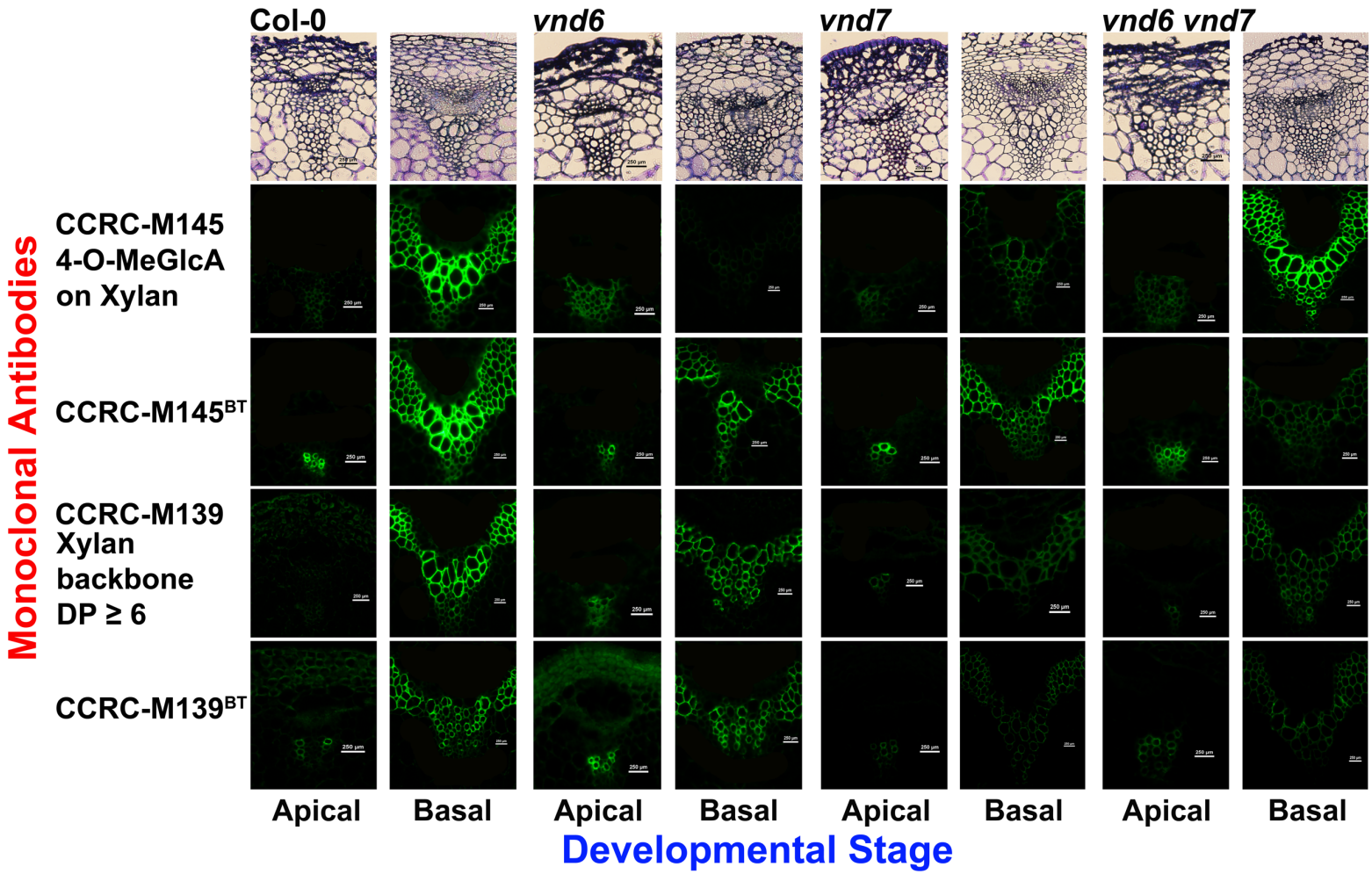

Figure 3.19: Immunofluorescent labelling of cell wall glycan Xylan epitopes in transverse sections of inflorescence stems from Arabidopsis (Col-0, *vnd6*, *vnd7*, *vnd6 vnd7*) taken from apical and basal segments of the stem. Immunolabelling studies were preceded by microscopic inspection of sections using toluidine blue-O staining (top row of images). Bar = 200 µm. BT = base treated.

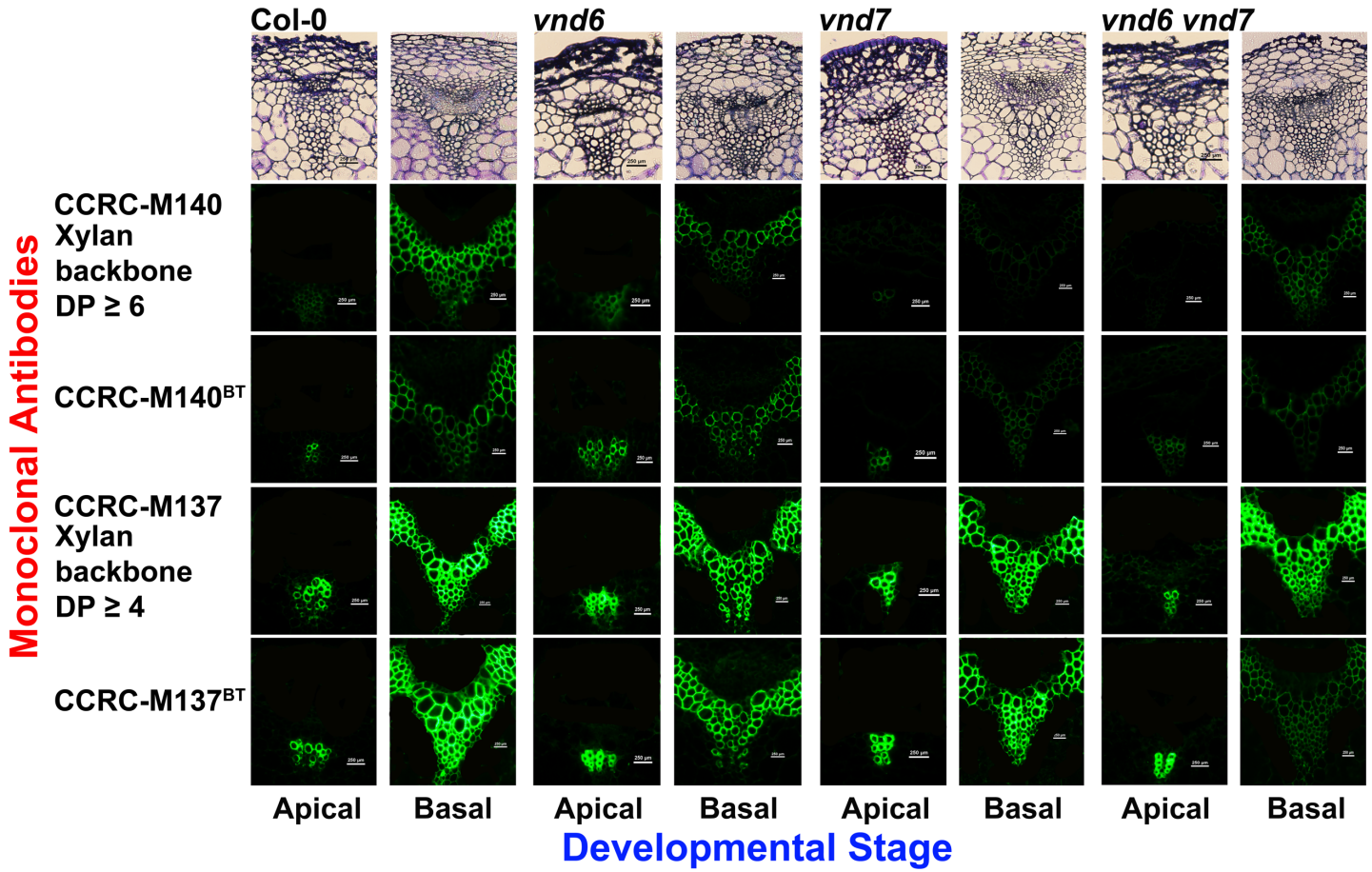

Figure 3.20: Immunofluorescent labelling of cell wall glycan Xylan epitopes in transverse sections of inflorescence stems from Arabidopsis (Col-0, *vnd6*, *vnd7*, *vnd6 vnd7*) taken from apical and basal segments of the stem. Immunolabelling studies were preceded by microscopic inspection of sections using toluidine blue-O staining (top row of images). Bar = 200 µm. BT = base treated.

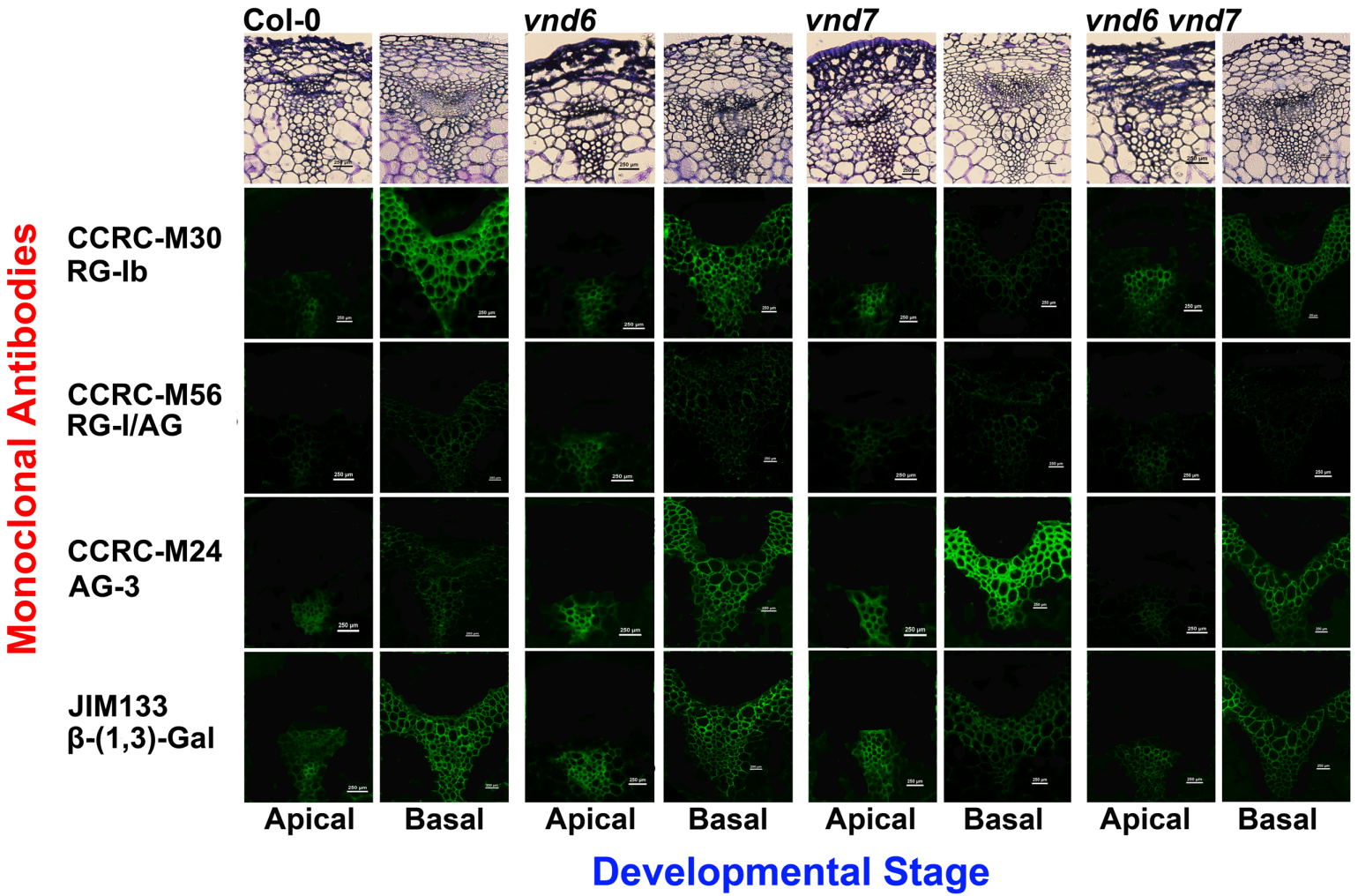

Figure 3.21: Immunofluorescent labelling of cell wall glycan Pectin epitopes in transverse sections of inflorescence stems from Arabidopsis (Col-0, *vnd6*, *vnd7*, *vnd6 vnd7*) taken from apical and basal segments of the stem. Immunolabelling studies were preceded by microscopic inspection of sections using toluidine blue-O staining (top row of images). Bar = 200 µm. BT = base treated.

3.2.8 *in situ* visualisation of *vnd* mutants reveals immunotypic differences in major glycan epitopes *in vivo*.

The labelling patterns obtained using mAbs against a diversity of cell wall glycan epitopes suggest that distinct remodelling of glycan abundance and distributions in the cell-walls of developing xylem tissues are VND-dependent. XG epitope labelling patterns in stem sections demonstrated that, based on the surveyed XG epitopes, there was a reduction in labelling in all the *vnd* mutants in the basal sections compared to wild-type (Col-0) (Figures 11-12). On the other hand, the apical section displayed more intense labelling in the mutants. This labelling pattern confirms that *VND* genes have a temporal pattern of expression and more likely affects processes in secondary cell wall biosynthesis and regulation in basal stem tissues rather than in primary cell wall biosynthesis, which typically occurs in juvenile tissues located in the apical portions. This notion is validated by known separate regulatory mechanisms for primary cell wall synthesis and secondary cell wall synthesis via AP2/ERF and secondary wall NACs (SWN), respectively. Interestingly, it was observed that the *vnd6* mutation affects XG labelling more severely in the vascular stem sections compared to *vnd7* mutants. This was also supported by the labelling patterns in the *vnd6 vnd7* double mutant, where sections from this line showed similar XG labelling patterns compared with the *vnd6* mutant. Another observation from labelling with XG specific epitope mAbs *in situ* was that labelling of interfascicular fibers from *vnd6* and *vnd6 vnd7* was weaker as compared to *vnd7*. This demonstrates the possibility that *vnd6* affects downstream transcription factors and XG-related biosynthesis genes in fibres.

Xylan-directed mAbs demonstrates diverse labelling patterns, suggesting that xylan abundance and structures are clearly affected by *VND* genes and in a cell type manner (Figures 16-21). In the apical sections, labelling of most xylan-directed mAbs were localised to the protoxylem portion of the stem. Additionally, significant differences in metaxylem mAb labelling were detected between Col-0 and *vnd* lines, specifically, metaxylem mutants lack α-(1,2)-Ara, GlcA and MeGlca substitutions in the further indicating that *VND6* and *VND7* glycan epitope composition plays a role in SCW deposition patterns in different cell types. Furthermore, these transcription factors function towards the secondary cell wall biosynthesis process in maturing vascular cells rather than their juvenile counterpart. This is supported by the LCM-GP heat maps where xylan epitopes are present in *vnd* single and double mutants of apical cells from the vascular bundle and interfasicular fibre, but at a decreased intensity when compared to Col-0 apical vascular cells. Specific patterns were also observed in the labelling of *vnd* stem sections. For instance, basal *vnd* sections displayed weak to no signals for CCRC-M108 and CCRC-M110 mAbs that recognise α-1,2-Ara substituted xylans (Figure 3.16). Likewise, similar patterns were observed in sections probed with CCRC-M139 and CCRC-M140 which recognise xylan backbones that have the least tolerance towards side chain addition of Ara*f* (Figures 3.19 and 3.20). Conversely, *vnd* mutants demonstrated similar labelling patterns with Col-0 for the following xylan epitope structures: α-1,3-Ara substituted xylans (CCRC-M154) (Figure 3.17), GlcA (CCRC-M150) (Figure 3.18) and 4-*O*-MeGlcA (CCRC-M145 and CCRC-M146) (Figures 3.15 and 3.16) substituted xylans, and xylan backbones that tolerate arabinsoyl substitutions

(CCRC-M147, and CCRC-M149 (Figures 3.17). Lastly, base treatment of sections with 0.1M KOH to remove the chemical modifications (e.g., acetylated or methylated) of the xylan epitope results in higher labelling intensity during *in situ* visualisation with mAbs. However, for certain mAbs such as CCRC-M154, CCRC-M145, and CCRC-M137, the opposite was observed where base treatment reduced the labelling intensity in basal sections (Figures 3.15, 3.16, and 3.17). The loss of mAb signal post base treatment may be due to the removal of base labile-linked epitopes recognised by the aforementioned mAbs.

Pectic epitope labelling was more scattered amongst the different genotypes in terms of different cell types and developmental stages (Figures 3.20). Col-0 sections, however, had higher pectin labelling supporting that *VND* genes could play an indirect part in pectin biosynthesis by inducing expression of *IRX8/GAUT12* through upregulation of *MYB* genes which are direct targets of *VND7* or even partake in pectin polysaccharide modifications (Yamaguchi et al., 2011); this requires further examination because the LCM-GP heat maps (Figure 3.9) reveals significant changes in homogalacturonan epitope abundance between Col-0 and *vnd6 vnd7* insertional lines. *In situ* visualisation also confirms microarray studies by Yamaguchi et al. (2011) where pectin modification genes were upregulated in *VND7-VP16-GR* plants upon dexamethasone (DEX) treatment. GP and immunolocalisation clearly demonstrate the importance of investigating immunotypic differences between Col-0 and *vnd* mutant genes using both *in vitro* and *in situ* immunological approaches by providing complementary information towards the glycan epitope abundance and distribution.

3.3 Discussion:

Our study, for the first time demonstrates an immunotype from *vnd6* and *vnd7* single and double t-DNA mutants. Whole stem GP of apical and basal stems from Col-0 and wild-type displayed differences in glycan epitope composition between apical and basal portions. Specifically, differences in non-fuc XG, Xylan-3 to 7, acetylated glucomannan, and most pectin epitope clades. However, when comparing cell-type GP, whole glycome profiling is a low-resolution method. LCM-GP reveals subtle differences in the cell types amongst the *vnd* mutants particularly xylan-directed mAbs and XG-directed mAbs that were not detected in whole stem analysis. Further, by presenting a non-cellulosic glycan epitope atlas at a cell type-specific resolution, this offers a tool in deciphering novel molecular descriptions into cell-wall biosynthesis genes and their regulatory dynamics in distinct cell types and during its specialised process such as xylem differentiation. Consequently, the feasibility of LCM-based glycome profiling is a powerful tool for future cell-wall compositional studies. As mentioned earlier, during the time-course of plant growth and differentiation, its cell-wall composition is highly heterogeneous at a tissue and cell type-specific level (Lee et al., 2011, Burton et al., 2010). Moreover, Arabidopsis developmental-dependent GP studies reveals that plant cell-wall glycans are also dynamic throughout different time points of stem maturation (Peralta et al., 2017). Thus, our novel approach facilitates the survey of glycan epitopes from the cell-walls of different cell-types and different differentiation events occurring in Arabidopsis.

3.3.1 Xylan backbone substitution patterns may contribute to metaxylem SCW patterning

Figure 3.7B demonstrates that reduction and losses of mAb signals that recognise Ara, GlcA, and MeGlca substitutions in xylan backbones occur in the *vnd6* single mutant. Since *VND6* regulates the differentiation of fascicular cambial cells to metaxylem (Demura et al., 2002, Endo et al., 2015, Kubo et al., 2005, Yamaguchi et al., 2010a), *vnd6* loss-of-function phenotype is possibly the lack of Ara, GlcA and MeGlcA residues. And these residues may be critical for proper SCW deposition in undifferentiated metaxylem cells to reticulated SCW patterning. Additionally this could provide evidence that *VND6* regulates *GUX1* and *GUX2, GXMT1,* and Arabinosyltransferases (AraT) expression levels either by stepwise or feed-forward mechanism (Hussey et al., 2013, Taylor-Teeples et al., 2015). In addition, the lack of MeGlcA and GlcA substitutions can cause disrupt 2-fold screw conformation required for cellulose interaction via hydrophilic interactions between the two polysaccharides (Busse-Wicher et al., 2014, Busse-Wicher et al., 2016, Kang et al., 2019). Studies in the loss-of-function *gux1*, *gux2*, and *gxmt1* reported that the loss in these substitutions can increase cell-wall extractability (Mortimer et al., 2010, Urbanowicz et al., 2012), and can alter other SCW monomers such increased abundance in the S-lignin monolignol in the *gxmt1* mutant (Urbanowicz et al., 2012). In relation, the absence of development and morphological phenotypes observed in the *vnd* mutants are also reflected in Arabidopsis mutants lacking in GlcA and MeGlcA substitutions (Mortimer et al., 2010, Urbanowicz et al., 2012). To verify whether or not *vnd6* affects GlcA and MeGlcA substitutions directly

or indirectly in xylan backbones, requires examining the expression levels of *GUX1*, *GUX2*, and *GXMT1*.

It is not surprising that *vnd6* affects arabinosylation substitution. Grasses are known to contain highly arabinosylated xylan backbones as compared to dicots (Faik, 2010). Recent studies by Rao and Dixon (2018) demonstrated that the SCW transcriptional regulatory networks in Arabidopsis and grasses is somewhat conserved but contain divergence. Therefore, it is likely that due to the evolutionary conserved regulatory networks in different species, *vnd* mutants, particularly vnd6 play a broader role in regulating plant cell-wall related genes as demonstrated by a loss in α-(1,2)-Ara*f* substitution. However, this needs confirmation by transcriptomic methods at the very least. Taken together, *vnd*s may play an integral role in xylem cell secondary wall deposition patterns, specifically xylans by affecting their substitution patterns; we also provide further evidence that *VND*s are highly conserved amongst different species of plants.

3.3.2 LCM-GP provides further evidence of a secondary cell-wall integrity (SCWI) system in Arabidopsis

The observation of different immunotypes found in *vnd* mutants and Col-0 provides additional evidence to the possibility of an existing secondary cell wall integrity (SCWI) system (Figure 3.20). The Presence of an SCWI system was previously noted by *irx* mutants displaying defects in xylan biosynthesis resulting in perturbation of the SCWI system (Brown et al., 2011, Brown et al., 2009, Persson et al., 2007). A recent transcriptomics analyses by Faria-Blanc et al. (2018) contradicts this, where they showed changes in xylan biosynthetic genes does not activate a secondary cell-wall integrity (SCWI) system. Their observation for a lack of transcriptomic responses in their dataset could be due to limiting their pool to a handful of xylan biosynthetic genes which are endpoints in the SCW biosynthesis network rather than examining multitier regulatory elements involved in the SCW formation further upstream (Taylor-Teeples et al., 2015, Zhang et al., 2018). Furthermore, using transcriptomics does not accurately depict the dynamics of the cell, and therefore cannot rule out the presence of an SCWI.

Cell wall fractionation of separately harvested cells from VB and IFF in different genotypes under harsh conditions (4M KOH) displays immunotypic differences whole stem glycome profiling (Figure 3.9B). There are clearly detectable immunotypic differences of cells types harvested from VB and IFF regions using LCM. *vnd6* and *vnd7* single mutants lack a majority of xyloglucan epitopes in cells collected in the VB and IFF region and at different maturation stages. Interestingly, xyloglucan from *vnd6 vnd7* double mutants have epitope signals that highly correspond to XG epitopes found in

Col-0. For example, CCRC-M58, which recognises the XLLG motif in xyloglucan is present in Col-0 and *vnd6 vnd7* but not *vnd6* or *vnd7*. This would, therefore, provide further support for a secondary cell-wall integrity (SCWI) system as mentioned (Brown et al., 2009, Persson et al., 2007). Bosca et al. (2006) demonstrated that mutations in secondary cell-wall CESAs affects primary cell-wall components. They observed that *cesa7*^{mur10} has altered XG and pectin structures due to perturbed cell-wall integrity signalling. It is possible that the *vnd6 vnd7* double mutant directly or indirectly affect *CESA7*^{mur10} alleles, resulting in an increase of XG epitopes by activating a present but uncharacterised SCWI system.

3.4 Conclusion:

We provide a novel approach that is able to detect changes in glycan immunotypes at a high resolution that is not possible using when organ carbohydrate analyses are used. Our results provide supporting evidence of the notion that cell-wall compositional heterogeneity exists amongst different cell types (Lee et al., 2011, Burton et al., 2010) and the survey of changes in non-cellulosic plant glycans derived from vascular bundle and interfasicular fibre cells from the different *vnd* mutants and at different stem developmental stages could point to the likelihood of an SCWI system in Arabidopsis. This approach detected glycan immunotypic differences in the cell-walls found in the VB and IF from T-DNA insertional mutants displaying no growth or morphological cell-wall phenotype despite their function as master regulators for secondary cell-wall synthesis. In fact, we were able to provide preliminary evidence that changes in glycan epitope abundances affects secondary cell-wall patterning in different

cell types. It is obvious that LCM-GP methods can also be modified to phylogenetically analyse the distinct cell-wall glycans of specific cells across different species especially if integrated with transcriptomic or proteomic methodologies. Implementing LCM-GP allows the monitoring of the changes in glycan structures and their abundance caused by specific mutations either from biosynthetic genes or genes involved the secondary cell-wall regulatory pathways at a cell-type/population level. Lastly, it is likely that this method will enable us to investigate alternative models of wall polysaccharide assembly at the cellular level. Results from these investigations will be potentially transformational in terms of the way we model the cell biology of wall metabolism in plants especially when complemented with proteomic or next-generation sequencing technologies.

3.5 Methods:

3.5.1 Growth and Harvesting

Wild-type and t-DNA insertional mutants *vnd6*, *vnd7*, and *vnd6 vnd7 Arabidopsis thaliana* ecotype Columbia plants were germinated on 0.8% w/v agar plates containing MS nutrients and B5 vitamins for 2 weeks prior to being transferred to compost containing vermiculite and perlite (10:1:1). Plants were subsequently grown at 22°C in controlled-environment cabinets using long-day (16 h light/ 8 h dark) conditions. Arabidopsis inflorescence stems were then grown to a height of 13cm-15cm and the top 1cm from the pedicel and bottom 1cm from the rosette segments were harvested to represent the apical and basal stages of stem development respectively (Figure 3.22).

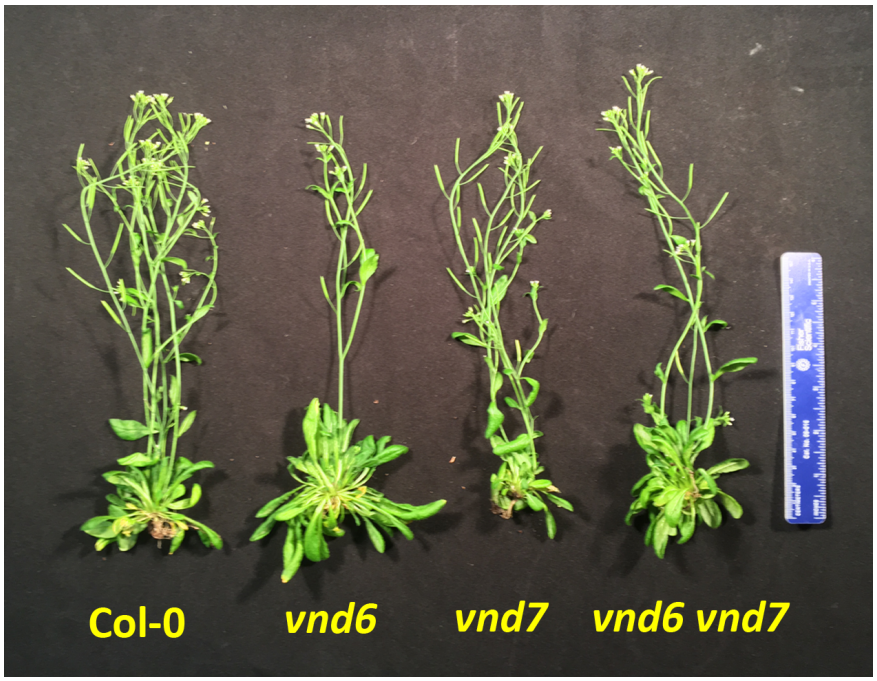

Figure 3.22: Arabidopsis wild-type (Col-0 background), *vnd6*, *vnd7*, and *vnd6 vnd7* grown to 13-15 cm for LCM tissue harvesting.

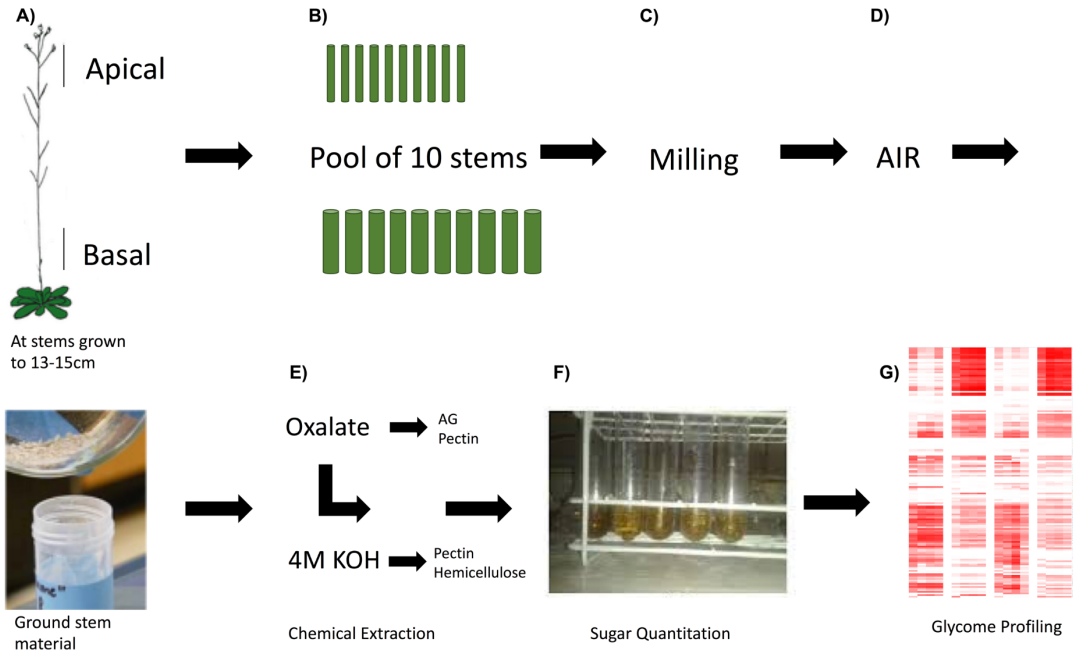

Figure 3.23: Whole stem glycome profiling workflow of *vnd* mutants and Col-0. Apical and basal stem portions were harvested (A) and pooled to 10 stem sections (B). Stem material was milled using TissueLyser II (Qiagen, Maryland) (C), and alcohol insoluble residue (AIR) was performed (D). Sequential extractions occurred using oxalate and 4M KOH (E), the resulting extracts were subjected to sugar quantitation using pheno-sulphuric acid (F) followed by ELISA-based glycome profiling (G).

3.5.2 Histology

Inflorescence stem segments were fixed and embedded according to Gautam et al. (2016). Harvested segments were vacuum infiltrated with 100% ice-cold 100% acetone for 15 minutes. The old fixative was replaced with fresh ice-cold acetone and rotated (20 rpm) overnight at 4°C. The samples were then fixed using 3:1, 1:1, and 1:3 gradients of acetone:histoclear followed by an additional 100% histoclear change for one hour each. This was followed by incubation in 100% histoclear with a couple of paraplast chips, rotated (20 rpm) overnight at room temperature. Tissue samples were then incubated at 57°C for paraplast (wax) infiltration, fresh wax was replaced twice a day for 3 days followed by these stem segments embedded into tissue blocks. Tissue

blocks of appropriate size and orientation were sectioned using a microtome (Lipshaw Manufacturing, Michigan) to obtain strips of 11 μm thick transverse stem sections, which are were flattened on PEN-coated membrane slides (Leica Microsystems) on ddH_2O at 50-55°C and dried at 42°C for 30 minutes. Shortly before capture, slides were deparaffinised in 100% histoclear then 100% ethanol each for 5 minutes. For anatomical observations, sections were stained with 0.025% toluidine blue for 2 minutes and were dehydrated with 70% (v/v) ethanol.

3.5.3 Laser Microdissection

The use of a Leica LMD7000 laser system (Leica Microsystems) to microdissect cells from deparaffinised and dried tissue sections prepared as abovementioned. The laser beam was adjusted to melt the thermoplastic film in a spot of a diameter that visually corresponded to the diameter of the target cell. Captures were performed using 7.5 μm beam diameters. Power settings were 6- mW, and laser pulse durations were 500 μs respectively. Successful harvest was evaluated by comparing the image of cells captured on the cap versus the image of the tissue after removal of harvested cells. In general, individual vascular bundles or interfascicular fibres were captured with a total surface area of ~800,000 μm^2 directly onto an aliquot of ddH2O. The targeted plant cells were precisely removed from the section into a 0.5 ml microcentrifuge tube, with nearly 100% efficiency, and without visible contamination with other cells.

3.6.7 Biological material

Laser microdissected material was transferred into 1.5 ml microcentrifuge for Glycome profiling. Glycome profiling was performed using the method described in Pattathil et al. (2012) with modifications. In brief, laser dissected material was subjected to cell-wall fractionation using 50mM ammonium oxalate, rotated (20 rpm) for 24 hours, centrifuged at 13.5k rpm for 30 min. The supernatant was collected and 4M KOH was directly placed into the microcentrifuge tube without in-between ddH_2O rinses followed by a quick vortex to reconstitute the pellet. 4M KOH extracts were rotated similar to the oxalate fractionation procedure but were subsequently neutralised with glacial acetic acid. The cell-wall extracts were followed by an enzyme-linked immunoabsorbent assay (ELISA) screening of using a comprehensive suite of plant cell wall glycan-directed monoclonal antibodies (mAbs) based on Pattathil et al. (2012). Plant glycan-directed mAbs were from laboratory stocks (CCRC, JIM, and MAC series) at the Complex Carbohydrate Research Center (available through CarboSource Services; http://www.carbosource.net) or were obtained from BioSupplies (Australia) (BG1, LAMP). Additional information about the mAbs employed in glycome profiling can be seen in Appendix A.

3.6.8 Correlation and statistical analyses

Correlation heat maps were performed as previously described in (Pattathil et al., 2010). PCA analyses and ANOVA were performed using R Studio software (v 3.3.1) and visualisation was performed with the ggplot2 package.

3.6.9 Immunolabelling

Stem segments obtained for LCM harvesting were sectioned similarly and placed in charged glass slides. Deparaffinised sections were immunolabelled according to Avci et al. (2012). Sections that were probed with xylan specific antibodies were additionally treated with a solution of 0.1M KOH containing 10mM $NaBH_4$ for 15 minutes and were rinsed with ddH_2O three times. Labelling was visualised using an Eclipse 80i light microscope (Nikon, Melville, NY) equipped with epifluorescence optics and Nikon B-2E/C filter. Images were captured using a Nikon DS-Ri1 camera head (Nikon, Melville, NY) and NISElements Basic Research software. Images were assembled without further processing using Adobe Photoshop (Adobe Systems, San Jose, CA).

3.8 References:

ABE, K. & ICHIKAWA, H. 2016. Gene Overexpression Resources in Cereals for Functional Genomics and Discovery of Useful Genes. *Front Plant Sci,* 7**,** 1359.

ALONSO, J. M., STEPANOVA, A. N., LEISSE, T. J., KIM, C. J., CHEN, H., SHINN, P., STEVENSON, D. K., ZIMMERMAN, J., BARAJAS, P., CHEUK, R., GADRINAB, C., HELLER, C., JESKE, A., KOESEMA, E., MEYERS, C. C., PARKER, H., PREDNIS, L., ANSARI, Y., CHOY, N., DEEN, H., GERALT, M., HAZARI, N., HOM, E., KARNES, M., MULHOLLAND, C., NDUBAKU, R., SCHMIDT, I., GUZMAN, P., AGUILAR-HENONIN, L., SCHMID, M., WEIGEL, D., CARTER, D. E., MARCHAND, T., RISSEEUW, E., BROGDEN, D., ZEKO, A., CROSBY, W. L., BERRY, C. C. & ECKER, J. R. 2003. Genome-wide insertional mutagenesis of Arabidopsis thaliana. *Science,* 301**,** 653-7.

ALTAMURA, M. M., POSSENTI, M., MATTEUCCI, A., BAIMA, S., RUBERTI, I. & MORELLI, G. 2001. Development of the vascular system in the inflorescence stem of Arabidopsis. *New Phytologist,* 151**,** 381-389.

ANGELES, G., BERRIO-SIERRA, J., JOSELEAU, J. P., LORIMIER, P., LEFEBVRE, A. & RUEL, K. 2006. Preparative laser capture microdissection and single-pot cell wall material preparation: a novel method for tissue-specific analysis. *Planta,* 224**,** 228-232.

ASPINALL, G. O., HUNT, K. & MORRISON, I. M. 1966. Polysaccharides of soy-beans. II. Fractionation of hull cell-wall polysaccharides and the ructure of a xylan. *J Chem Soc Perkin 1,* 21**,** 1945-9.

AVCI, U., PATTATHIL, S. & HAHN, M. G. 2012. Immunological approaches to plant cell wall and biomass characterization: immunolocalization of glycan epitopes. *Methods Mol Biol,* 908**,** 73-82.

BARTETZKO, M. P., SCHUHMACHER, F., HAHM, H. S., SEEBERGER, P. H. & PFRENGLE, F. 2015. Automated Glycan Assembly of Oligosaccharides Related to Arabinogalactan Proteins. *Org Lett,* 17**,** 4344-7.

BISWAL, A. K., HAO, Z., PATTATHIL, S., YANG, X., WINKELER, K., COLLINS, C., MOHANTY, S. S., RICHARDSON, E. A., GELINEO-ALBERSHEIM, I., HUNT, K., RYNO, D., SYKES, R. W., TURNER, G. B., ZIEBELL, A., GJERSING, E., LUKOWITZ, W., DAVIS, M. F., DECKER, S. R., HAHN, M. G. & MOHNEN, D. 2015. Downregulation of GAUT12 in Populus deltoides by RNA silencing results in reduced recalcitrance, increased growth and reduced xylan and pectin in a woody biofuel feedstock. *Biotechnol Biofuels,* 8**,** 41.

BISWAL, A. K., TAN, L., ATMODJO, M. A., DEMARTINI, J., GELINEO-ALBERSHEIM, I., HUNT, K., BLACK, I. M., MOHANTY, S. S., RYNO, D., WYMAN, C. E. & MOHNEN, D. 2017. Comparison of four glycosyl residue composition methods for effectiveness in detecting sugars from cell walls of dicot and grass tissues. *Biotechnol Biofuels,* 10**,** 182.

BOGDANOVE, A. J. & VOYTAS, D. F. 2011. TAL effectors: customizable proteins for DNA targeting. *Science,* 333**,** 1843-6.

BOSCA, S., BARTON, C. J., TAYLOR, N. G., RYDEN, P., NEUMETZLER, L., PAULY, M., ROBERTS, K. & SEIFERT, G. J. 2006. Interactions between MUR10/CesA7-

dependent secondary cellulose biosynthesis and primary cell wall structure. *Plant physiology,* 142**,** 1353-1363.

BRADY, S. M., ORLANDO, D. A., LEE, J. Y., WANG, J. Y., KOCH, J., DINNENY, J. R., MACE, D., OHLER, U. & BENFEY, P. N. 2007. A high-resolution root spatiotemporal map reveals dominant expression patterns. *Science,* 318**,** 801-6.

BROMLEY, J. R., BUSSE-WICHER, M., TRYFONA, T., MORTIMER, J. C., ZHANG, Z., BROWN, D. M. & DUPREE, P. 2013. GUX1 and GUX2 glucuronyltransferases decorate distinct domains of glucuronoxylan with different substitution patterns. *Plant J,* 74**,** 423-34.

BROWN, D., WIGHTMAN, R., ZHANG, Z., GOMEZ, L. D., ATANASSOV, I., BUKOWSKI, J. P., TRYFONA, T., MCQUEEN-MASON, S. J., DUPREE, P. & TURNER, S. 2011. Arabidopsis genes IRREGULAR XYLEM (IRX15) and IRX15L encode DUF579-containing proteins that are essential for normal xylan deposition in the secondary cell wall. *Plant J,* 66**,** 401-13.

BROWN, D. M., ZEEF, L. A., ELLIS, J., GOODACRE, R. & TURNER, S. R. 2005. Identification of novel genes in Arabidopsis involved in secondary cell wall formation using expression profiling and reverse genetics. *Plant Cell,* 17**,** 2281-95.

BROWN, D. M., ZHANG, Z., STEPHENS, E., DUPREE, P. & TURNER, S. R. 2009. Characterization of IRX10 and IRX10-like reveals an essential role in glucuronoxylan biosynthesis in Arabidopsis. *Plant J,* 57**,** 732-46.

BURTON, R. A., GIDLEY, M. J. & FINCHER, G. B. 2010. Heterogeneity in the chemistry, structure and function of plant cell walls. *Nat Chem Biol,* 6**,** 724-32.

BUSSE-WICHER, M., GOMES, T. C., TRYFONA, T., NIKOLOVSKI, N., STOTT, K., GRANTHAM, N. J., BOLAM, D. N., SKAF, M. S. & DUPREE, P. 2014. The pattern of xylan acetylation suggests xylan may interact with cellulose microfibrils as a twofold helical screw in the secondary plant cell wall of Arabidopsis thaliana. *Plant J,* 79**,** 492-506.

BUSSE-WICHER, M., GRANTHAM, N. J., LYCZAKOWSKI, J. J., NIKOLOVSKI, N. & DUPREE, P. 2016. Xylan decoration patterns and the plant secondary cell wall molecular architecture. *Biochem Soc Trans,* 44**,** 74-8.

CHAFFEY, N., CHOLEWA, E., REGAN, S. & SUNDBERG, B. 2002. Secondary xylem development in Arabidopsis: a model for wood formation. *Physiol Plant,* 114**,** 594-600.

CHRISTIAN, M., QI, Y., ZHANG, Y. & VOYTAS, D. F. 2013. Targeted mutagenesis of Arabidopsis thaliana using engineered TAL effector nucleases. *G3 (Bethesda),* 3**,** 1697-705.

CROWE, J. D., FERINGA, N., PATTATHIL, S., MERRITT, B., FOSTER, C., DINES, D., ONG, R. G. & HODGE, D. B. 2017. Identification of developmental stage and anatomical fraction contributions to cell wall recalcitrance in switchgrass. *Biotechnol Biofuels,* 10**,** 184.

DALLABERNARDINA, P., RUPRECHT, C., SMITH, P. J., HAHN, M. G., URBANOWICZ, B. R. & PFRENGLE, F. 2017. Automated glycan assembly of galactosylated xyloglucan oligosaccharides and their recognition by plant cell wall glycan-directed antibodies. *Organic & Biomolecular Chemistry,* 15**,** 9996-10000.

DEMARTINI, J. D., PATTATHIL, S., AVCI, U., SZEKALSKI, K., MAZUMDER, K., HAHN, M. G. & WYMAN, C. E. 2011. Application of monoclonal antibodies to investigate plant cell wall deconstruction for biofuels production. *Energy & Environmental Science,* 4**,** 4332-4339.

DEMURA, T. & FUKUDA, H. 2007. Transcriptional regulation in wood formation. *Trends Plant Sci,* 12**,** 64-70.

DEMURA, T., TASHIRO, G., HORIGUCHI, G., KISHIMOTO, N., KUBO, M., MATSUOKA, N., MINAMI, A., NAGATA-HIWATASHI, M., NAKAMURA, K., OKAMURA, Y., SASSA, N., SUZUKI, S., YAZAKI, J., KIKUCHI, S. & FUKUDA, H. 2002. Visualization by comprehensive microarray analysis of gene expression programs during transdifferentiation of mesophyll cells into xylem cells. *Proc Natl Acad Sci U S A,* 99**,** 15794-9.

ELSAYED, M. M. 1982. THE POLYSACCHARIDES OF THE BROWN SEAWEED TURBINARIA-MURRAYANA. *Carbohydrate Research,* 110**,** 277-282.

ENDO, H., YAMAGUCHI, M., TAMURA, T., NAKANO, Y., NISHIKUBO, N., YONEDA, A., KATO, K., KUBO, M., KAJITA, S., KATAYAMA, Y., OHTANI, M. & DEMURA, T. 2015. Multiple classes of transcription factors regulate the expression of VASCULAR-RELATED NAC-DOMAIN7, a master switch of xylem vessel differentiation. *Plant Cell Physiol,* 56**,** 242-54.

ENDO, S., PESQUET, E., YAMAGUCHI, M., TASHIRO, G., SATO, M., TOYOOKA, K., NISHIKUBO, N., UDAGAWA-MOTOSE, M., KUBO, M., FUKUDA, H. & DEMURA, T. 2009. Identifying new components participating in the secondary cell wall formation of vessel elements in zinnia and Arabidopsis. *Plant Cell,* 21**,** 1155-65.

FAIK, A. 2010. Xylan Biosynthesis: News from the Grass. *Plant Physiology,* 153**,** 396-402.

FARIA-BLANC, N., MORTIMER, J. C. & DUPREE, P. 2018. A Transcriptomic Analysis of Xylan Mutants Does Not Support the Existence of a Secondary Cell Wall Integrity System in Arabidopsis. *Front Plant Sci,* 9**,** 384.

GAUTAM, V., SINGH, A., SINGH, S. & SARKAR, A. K. 2016. An Efficient LCM-Based Method for Tissue Specific Expression Analysis of Genes and miRNAs. *Scientific Reports,* 6.

HAGHIGHAT, M., TENG, Q., ZHONG, R. & YE, Z. H. 2016. Evolutionary Conservation of Xylan Biosynthetic Genes in Selaginella moellendorffii and Physcomitrella patens. *Plant Cell Physiol,* 57**,** 1707-19.

HELD, M. A., JIANG, N., BASU, D., SHOWALTER, A. M. & FAIK, A. 2021. Plant Cell Wall Polysaccharides: Structure and Biosynthesis. *In:* RAMAWAT, K. G. & MÉRILLON, J.-M. (eds.) *Polysaccharides: Bioactivity and Biotechnology.* Cham: Springer International Publishing.

HUSSEY, S. G., MIZRACHI, E., CREUX, N. M. & MYBURG, A. A. 2013. Navigating the transcriptional roadmap regulating plant secondary cell wall deposition. *Front Plant Sci,* 4**,** 325.

JOSELEAU, J. P. & RUEL, K. 1997. Study of lignification by noninvasive techniques in growing maize internodes - An investigation by Fourier transform infrared cross-polarization magic angle spinning C-13-nuclear magnetic resonance spectroscopy

and immunocytochemical transmission electron microscopy. *Plant Physiology,* 114**,** 1123-1133.
KAGALE, S. & ROZWADOWSKI, K. 2011. EAR motif-mediated transcriptional repression in plants: an underlying mechanism for epigenetic regulation of gene expression. *Epigenetics,* 6**,** 141-6.
KANG, X., KIRUI, A., DICKWELLA WIDANAGE, M. C., MENTINK-VIGIER, F., COSGROVE, D. J. & WANG, T. 2019. Lignin-polysaccharide interactions in plant secondary cell walls revealed by solid-state NMR. *Nat Commun,* 10**,** 347.
KERK, N. M., CESERANI, T., TAUSTA, S. L., SUSSEX, I. M. & NELSON, T. M. 2003. Laser capture microdissection of cells from plant tissues. *Plant Physiol,* 132**,** 27-35.
KO, J. H., HAN, K. H., PARK, S. & YANG, J. 2004. Plant body weight-induced secondary growth in Arabidopsis and its transcription phenotype revealed by whole-transcriptome profiling. *Plant Physiol,* 135**,** 1069-83.
KRYSAN, P. J., YOUNG, J. C. & SUSSMAN, M. R. 1999. T-DNA as an insertional mutagen in Arabidopsis. *Plant Cell,* 11**,** 2283-90.
KUBO, M., UDAGAWA, M., NISHIKUBO, N., HORIGUCHI, G., YAMAGUCHI, M., ITO, J., MIMURA, T., FUKUDA, H. & DEMURA, T. 2005. Transcription switches for protoxylem and metaxylem vessel formation. *Genes Dev,* 19**,** 1855-60.
LARSON, E. R., TIERNEY, M. L., TINAZ, B. & DOMOZYCH, D. S. 2014. Using monoclonal antibodies to label living root hairs: a novel tool for studying cell wall microarchitecture and dynamics in Arabidopsis. *Plant Methods,* 10**,** 30.
LEE, K. J., MARCUS, S. E. & KNOX, J. P. 2011. Cell wall biology: perspectives from cell wall imaging. *Mol Plant,* 4**,** 212-9.
LEROUX, O., SORENSEN, I., MARCUS, S. E., VIANE, R. L., WILLATS, W. G. & KNOX, J. P. 2015. Antibody-based screening of cell wall matrix glycans in ferns reveals taxon, tissue and cell-type specific distribution patterns. *BMC Plant Biol,* 15**,** 56.
LI, X., JACKSON, P., RUBTSOV, D. V., FARIA-BLANC, N., MORTIMER, J. C., TURNER, S. R., KROGH, K. B., JOHANSEN, K. S. & DUPREE, P. 2013. Development and application of a high throughput carbohydrate profiling technique for analyzing plant cell wall polysaccharides and carbohydrate active enzymes. *Biotechnol Biofuels,* 6**,** 94.
LIEPMAN, A. H., WIGHTMAN, R., GESHI, N., TURNER, S. R. & SCHELLER, H. V. 2010. Arabidopsis - a powerful model system for plant cell wall research. *Plant J,* 61**,** 1107-21.
MACMILLAN, C. P., O'DONNELL, P. J., SMIT, A.-M., EVANS, R., STACHURSKI, Z. H., TORR, K., WEST, M., BALTUNIS, J. & STRABALA, T. J. 2013. A survey of the natural variation in biomechanical and cell wall properties in inflorescence stems reveals new insights into the utility of Arabidopsis as a wood model. *Functional Plant Biology,* 40**,** 662-676.
MALI, P., ESVELT, K. M. & CHURCH, G. M. 2013. Cas9 as a versatile tool for engineering biology. *Nat Methods,* 10**,** 957-63.
MANABE, Y., NAFISI, M., VERHERTBRUGGEN, Y., ORFILA, C., GILLE, S., RAUTENGARTEN, C., CHERK, C., MARCUS, S. E., SOMERVILLE, S., PAULY, M., KNOX, J. P., SAKURAGI, Y. & SCHELLER, H. V. 2011. Loss-of-function mutation of REDUCED WALL

ACETYLATION2 in Arabidopsis leads to reduced cell wall acetylation and increased resistance to Botrytis cinerea. *Plant Physiol,* 155**,** 1068-78.
MANFIELD, I. W., ORFILA, C., MCCARTNEY, L., HARHOLT, J., BERNAL, A. J., SCHELLER, H. V., GILMARTIN, P. M., MIKKELSEN, J. D., PAUL KNOX, J. & WILLATS, W. G. 2004. Novel cell wall architecture of isoxaben-habituated Arabidopsis suspension-cultured cells: global transcript profiling and cellular analysis. *Plant J,* 40**,** 260-75.
MCCANN, M. C. & CARPITA, N. C. 2008. Designing the deconstruction of plant cell walls. *Curr Opin Plant Biol,* 11**,** 314-20.
MITSUDA, N. & OHME-TAKAGI, M. 2009. Functional analysis of transcription factors in Arabidopsis. *Plant Cell Physiol,* 50**,** 1232-48.
MOLLER, I., MARCUS, S. E., HAEGER, A., VERHERTBRUGGEN, Y., VERHOEF, R., SCHOLS, H., ULVSKOV, P., MIKKELSEN, J. D., KNOX, J. P. & WILLATS, W. 2008. High-throughput screening of monoclonal antibodies against plant cell wall glycans by hierarchical clustering of their carbohydrate microarray binding profiles. *Glycoconj J,* 25**,** 37-48.
MORTIMER, J. C., MILES, G. P., BROWN, D. M., ZHANG, Z., SEGURA, M. P., WEIMAR, T., YU, X., SEFFEN, K. A., STEPHENS, E., TURNER, S. R. & DUPREE, P. 2010. Absence of branches from xylan in Arabidopsis gux mutants reveals potential for simplification of lignocellulosic biomass. *Proc Natl Acad Sci U S A,* 107**,** 17409-14.
OBEL, N., ERBEN, V., SCHWARZ, T., KUHNEL, S., FODOR, A. & PAULY, M. 2009. Microanalysis of plant cell wall polysaccharides. *Mol Plant,* 2**,** 922-32.
ODA, Y. & FUKUDA, H. 2013. Rho of plant GTPase signaling regulates the behavior of Arabidopsis kinesin-13A to establish secondary cell wall patterns. *Plant Cell,* 25**,** 4439-50.
OHASHI-ITO, K., ODA, Y. & FUKUDA, H. 2010. Arabidopsis VASCULAR-RELATED NAC-DOMAIN6 directly regulates the genes that govern programmed cell death and secondary wall formation during xylem differentiation. *Plant Cell,* 22**,** 3461-73.
PATTATHIL, S., AVCI, U., BALDWIN, D., SWENNES, A. G., MCGILL, J. A., POPPER, Z., BOOTTEN, T., ALBERT, A., DAVIS, R. H., CHENNAREDDY, C., DONG, R., O'SHEA, B., ROSSI, R., LEOFF, C., FRESHOUR, G., NARRA, R., O'NEIL, M., YORK, W. S. & HAHN, M. G. 2010. A comprehensive toolkit of plant cell wall glycan-directed monoclonal antibodies. *Plant Physiol,* 153**,** 514-25.
PATTATHIL, S., AVCI, U., MILLER, J. S. & HAHN, M. G. 2012. Immunological approaches to plant cell wall and biomass characterization: Glycome Profiling. *Methods Mol Biol,* 908**,** 61-72.
PATTATHIL, S., AVCI, U., ZHANG, T., CARDENAS, C. L. & HAHN, M. G. 2015a. Immunological Approaches to Biomass Characterization and Utilization. *Front Bioeng Biotechnol,* 3**,** 173.
PATTATHIL, S., HAHN, M. G., DALE, B. E. & CHUNDAWAT, S. P. S. 2015b. Insights into plant cell wall structure, architecture, and integrity using glycome profiling of native and AFEX (TM)-pre-treated biomass. *Journal of Experimental Botany,* 66**,** 4279-4294.
PENA, M. J., DARVILL, A. G., EBERHARD, S., YORK, W. S. & O'NEILL, M. A. 2008. Moss and liverwort xyloglucans contain galacturonic acid and are structurally distinct from

the xyloglucans synthesized by hornworts and vascular plants. *Glycobiology,* 18**,** 891-904.

PERALTA, A. G., VENKATACHALAM, S., STONE, S. C. & PATTATHIL, S. 2017. Xylan epitope profiling: an enhanced approach to study organ development-dependent changes in xylan structure, biosynthesis, and deposition in plant cell walls. *Biotechnol Biofuels,* 10**,** 245.

PERSSON, S., CAFFALL, K. H., FRESHOUR, G., HILLEY, M. T., BAUER, S., POINDEXTER, P., HAHN, M. G., MOHNEN, D. & SOMERVILLE, C. 2007. The Arabidopsis irregular xylem8 mutant is deficient in glucuronoxylan and homogalacturonan, which are essential for secondary cell wall integrity. *Plant Cell,* 19**,** 237-55.

PETERSEN, P. D., LAU, J., EBERT, B., YANG, F., VERHERTBRUGGEN, Y., KIM, J. S., VARANASI, P., SUTTANGKAKUL, A., AUER, M., LOQUE, D. & SCHELLER, H. V. 2012. Engineering of plants with improved properties as biofuels feedstocks by vessel-specific complementation of xylan biosynthesis mutants. *Biotechnol Biofuels,* 5**,** 84.

PIDATALA, V. R., MAHBOUBI, A. & MORTIMER, J. C. 2017. Structural Characterization of Mannan Cell Wall Polysaccharides in Plants Using PACE. *J Vis Exp*.

POPPER, Z. A., MICHEL, G., HERVE, C., DOMOZYCH, D. S., WILLATS, W. G., TUOHY, M. G., KLOAREG, B. & STENGEL, D. B. 2011. Evolution and diversity of plant cell walls: from algae to flowering plants. *Annu Rev Plant Biol,* 62**,** 567-90.

RAGNI, L. & GREB, T. 2018. Secondary growth as a determinant of plant shape and form. *Seminars in Cell & Developmental Biology,* 79**,** 58-67.

RANOCHA, P., DENANCE, N., VANHOLME, R., FREYDIER, A., MARTINEZ, Y., HOFFMANN, L., KOHLER, L., POUZET, C., RENOU, J. P., SUNDBERG, B., BOERJAN, W. & GOFFNER, D. 2010. Walls are thin 1 (WAT1), an Arabidopsis homolog of Medicago truncatula NODULIN21, is a tonoplast-localized protein required for secondary wall formation in fibers. *Plant J,* 63**,** 469-83.

RAO, X. & DIXON, R. A. 2018. Current Models for Transcriptional Regulation of Secondary Cell Wall Biosynthesis in Grasses. *Front Plant Sci,* 9**,** 399.

RUPRECHT, C., BARTETZKO, M. P., SENF, D., DALLABERNADINA, P., BOOS, I., ANDERSEN, M. C. F., KOTAKE, T., KNOX, J. P., HAHN, M. G., CLAUSEN, M. H. & PFRENGLE, F. 2017. A Synthetic Glycan Microarray Enables Epitope Mapping of Plant Cell Wall Glycan-Directed Antibodies. *Plant Physiol,* 175**,** 1094-1104.

RYDAHL, M. G., HANSEN, A. R., KRACUN, S. K. & MRAVEC, J. 2018. Report on the Current Inventory of the Toolbox for Plant Cell Wall Analysis: Proteinaceous and Small Molecular Probes. *Frontiers in Plant Science,* 9.

SCHAD, M., MUNGUR, R., FIEHN, O. & KEHR, J. 2005. Metabolic profiling of laser microdissected vascular bundles of Arabidopsis thaliana. *Plant Methods,* 1**,** 2.

SCHMIDT, D., SCHUHMACHER, F., GEISSNER, A., SEEBERGER, P. H. & PFRENGLE, F. 2015. Automated synthesis of arabinoxylan-oligosaccharides enables characterization of antibodies that recognize plant cell wall glycans. *Chemistry,* 21**,** 5709-13.

SHINOHARA, N., KAKEGAWA, K. & FUKUDA, H. 2015. Monoclonal antibody-based analysis of cell wall remodeling during xylogenesis. *J Plant Res,* 128**,** 975-86.

SHINOZAKI, Y., NICOLAS, P., FERNANDEZ-POZO, N., MA, Q., EVANICH, D. J., SHI, Y., XU, Y., ZHENG, Y., SNYDER, S. I., MARTIN, L. B. B., RUIZ-MAY, E., THANNHAUSER, T. W., CHEN, K., DOMOZYCH, D. S., CATALA, C., FEI, Z., MUELLER, L. A., GIOVANNONI, J. J. & ROSE, J. K. C. 2018. High-resolution spatiotemporal transcriptome mapping of tomato fruit development and ripening. *Nat Commun,* 9**,** 364.

SIMS, I. M. & NEWMAN, R. H. 2006. Structural studies of acidic xylans exuded from leaves of the monocotyledonous plants Phormium tenax and Phormium cookianum. *Carbohydrate Polymers,* 63**,** 379-384.

STRABALA, T. J. & MACMILLAN, C. P. 2013. The Arabidopsis wood model-the case for the inflorescence stem. *Plant Sci,* 210**,** 193-205.

TAMURA, K., KAWABAYASHI, T., SHIKANAI, T. & HARA-NISHIMURA, I. 2016. Decreased Expression of a Gene Caused by a T-DNA Insertion in an Adjacent Gene in Arabidopsis. *PLoS One,* 11**,** e0147911.

TAYLOR-TEEPLES, M., LIN, L., DE LUCAS, M., TURCO, G., TOAL, T. W., GAUDINIER, A., YOUNG, N. F., TRABUCCO, G. M., VELING, M. T., LAMOTHE, R., HANDAKUMBURA, P. P., XIONG, G., WANG, C., CORWIN, J., TSOUKALAS, A., ZHANG, L., WARE, D., PAULY, M., KLIEBENSTEIN, D. J., DEHESH, K., TAGKOPOULOS, I., BRETON, G., PRUNEDA-PAZ, J. L., AHNERT, S. E., KAY, S. A., HAZEN, S. P. & BRADY, S. M. 2015. An Arabidopsis gene regulatory network for secondary cell wall synthesis. *Nature,* 517**,** 571-5.

THE ARABIDOPSIS GENOME, I. 2000. Analysis of the genome sequence of the flowering plant Arabidopsis thaliana. *Nature,* 408**,** 796-815.

URBANOWICZ, B. R., PENA, M. J., RATNAPARKHE, S., AVCI, U., BACKE, J., STEET, H. F., FOSTON, M., LI, H. J., O'NEILL, M. A., RAGAUSKAS, A. J., DARVILL, A. G., WYMAN, C., GILBERT, H. J. & YORK, W. S. 2012. 4-O-methylation of glucuronic acid in Arabidopsis glucuronoxylan is catalyzed by a domain of unknown function family 579 protein. *Proceedings of the National Academy of Sciences of the United States of America,* 109**,** 14253-14258.

VERHERTBRUGGEN, Y., WALKER, J. L., GUILLON, F. & SCHELLER, H. V. 2017. A Comparative Study of Sample Preparation for Staining and Immunodetection of Plant Cell Walls by Light Microscopy. *Front Plant Sci,* 8**,** 1505.

WANG, H., AVCI, U., NAKASHIMA, J., HAHN, M. G., CHEN, F. & DIXON, R. A. 2010. Mutation of WRKY transcription factors initiates pith secondary wall formation and increases stem biomass in dicotyledonous plants. *Proc Natl Acad Sci U S A,* 107**,** 22338-43.

WANG, J., ANDERSSON-GUNNERAS, S., GABOREANU, I., HERTZBERG, M., TUCKER, M. R., ZHENG, B., LESNIEWSKA, J., MELLEROWICZ, E. J., LAUX, T., SANDBERG, G. & JONES, B. 2011. Reduced expression of the SHORT-ROOT gene increases the rates of growth and development in hybrid poplar and Arabidopsis. *PLoS One,* 6**,** e28878.

WANG, T. & HONG, M. 2016. Solid-state NMR investigations of cellulose structure and interactions with matrix polysaccharides in plant primary cell walls. *J Exp Bot,* 67**,** 503-14.

WILSON, M. H., HOLMAN, T. J., SORENSEN, I., CANCHO-SANCHEZ, E., WELLS, D. M., SWARUP, R., KNOX, J. P., WILLATS, W. G., UBEDA-TOMAS, S., HOLDSWORTH, M., BENNETT, M. J., VISSENBERG, K. & HODGMAN, T. C. 2015. Multi-omics analysis identifies genes mediating the extension of cell walls in the Arabidopsis thaliana root elongation zone. *Front Cell Dev Biol,* 3**,** 10.

XIAO, C., SOMERVILLE, C. & ANDERSON, C. T. 2014. POLYGALACTURONASE INVOLVED IN EXPANSION1 functions in cell elongation and flower development in Arabidopsis. *Plant Cell,* 26**,** 1018-35.

XUE, J., BOSCH, M. & KNOX, J. P. 2013. Heterogeneity and glycan masking of cell wall microstructures in the stems of Miscanthus x giganteus, and its parents M. sinensis and M. sacchariflorus. *PLoS One,* 8**,** e82114.

YAMAGUCHI, M., GOUE, N., IGARASHI, H., OHTANI, M., NAKANO, Y., MORTIMER, J. C., NISHIKUBO, N., KUBO, M., KATAYAMA, Y., KAKEGAWA, K., DUPREE, P. & DEMURA, T. 2010a. VASCULAR-RELATED NAC-DOMAIN6 and VASCULAR-RELATED NAC-DOMAIN7 Effectively Induce Transdifferentiation into Xylem Vessel Elements under Control of an Induction System. *Plant Physiology,* 153**,** 906-914.

YAMAGUCHI, M., KUBO, M., FUKUDA, H. & DEMURA, T. 2008. Vascular-related NAC-DOMAIN7 is involved in the differentiation of all types of xylem vessels in Arabidopsis roots and shoots. *Plant J,* 55**,** 652-64.

YAMAGUCHI, M., MITSUDA, N., OHTANI, M., OHME-TAKAGI, M., KATO, K. & DEMURA, T. 2011. VASCULAR-RELATED NAC-DOMAIN7 directly regulates the expression of a broad range of genes for xylem vessel formation. *Plant J,* 66**,** 579-90.

YAMAGUCHI, M., OHTANI, M., MITSUDA, N., KUBO, M., OHME-TAKAGI, M., FUKUDA, H. & DEMURA, T. 2010b. VND-INTERACTING2, a NAC domain transcription factor, negatively regulates xylem vessel formation in Arabidopsis. *Plant Cell,* 22**,** 1249-63.

ZHANG, J., XIE, M., TUSKAN, G. A., MUCHERO, W. & CHEN, J. G. 2018. Recent Advances in the Transcriptional Regulation of Secondary Cell Wall Biosynthesis in the Woody Plants. *Front Plant Sci,* 9**,** 1535.

ZHONG, R., BURK, D. H., MORRISON, W. H., 3RD & YE, Z. H. 2002. A kinesin-like protein is essential for oriented deposition of cellulose microfibrils and cell wall strength. *Plant Cell,* 14**,** 3101-17.

ZHONG, R., LEE, C., ZHOU, J., MCCARTHY, R. L. & YE, Z. H. 2008. A battery of transcription factors involved in the regulation of secondary cell wall biosynthesis in Arabidopsis. *Plant Cell,* 20**,** 2763-82.

ZHOU, J., ZHONG, R. & YE, Z. H. 2014. Arabidopsis NAC domain proteins, VND1 to VND5, are transcriptional regulators of secondary wall biosynthesis in vessels. *PLoS One,* 9**,** e105726.

3.9 Appendices:

Appendix A: Detailed list of cell wall glycan-directed monoclonal antibodies (mAbs) used in glycome profiling analyses. The groupings of antibodies are based on the hierarchical clustering of ELISA data generated from screening all mAbs against a comprehensive panel of plant polysaccharide preparations (Pattathil et al., 2010; Pattathil et al., 2012) which clusters mAbs according to their predominant polysaccharides recognition patterns. The majority of the listings link to the Wall*Mab*DB plant cell wall monoclonal antibody database (http://www.wallmabdb.net) which provides the detailed descriptions for each mAb, including immunogen, antibody isotype, epitope structure (to the extent known), supplier information, and related literature citations.

Glycan Group Recognised	mAb Names
Non-Fucosylated Xyloglucan-1	CCRC-M95 CCRC-M101
Non-Fucosylated Xyloglucan-2	CCRC-M104 CCRC-M89 CCRC-M93 CCRC-M87 CCRC-M88
Non-Fucosylated Xyloglucan-3	CCRC-M100 CCRC-M103
Non-Fucosylated Xyloglucan-4	CCRC-M58 CCRC-M86 CCRC-M55 CCRC-M52 CCRC-M99

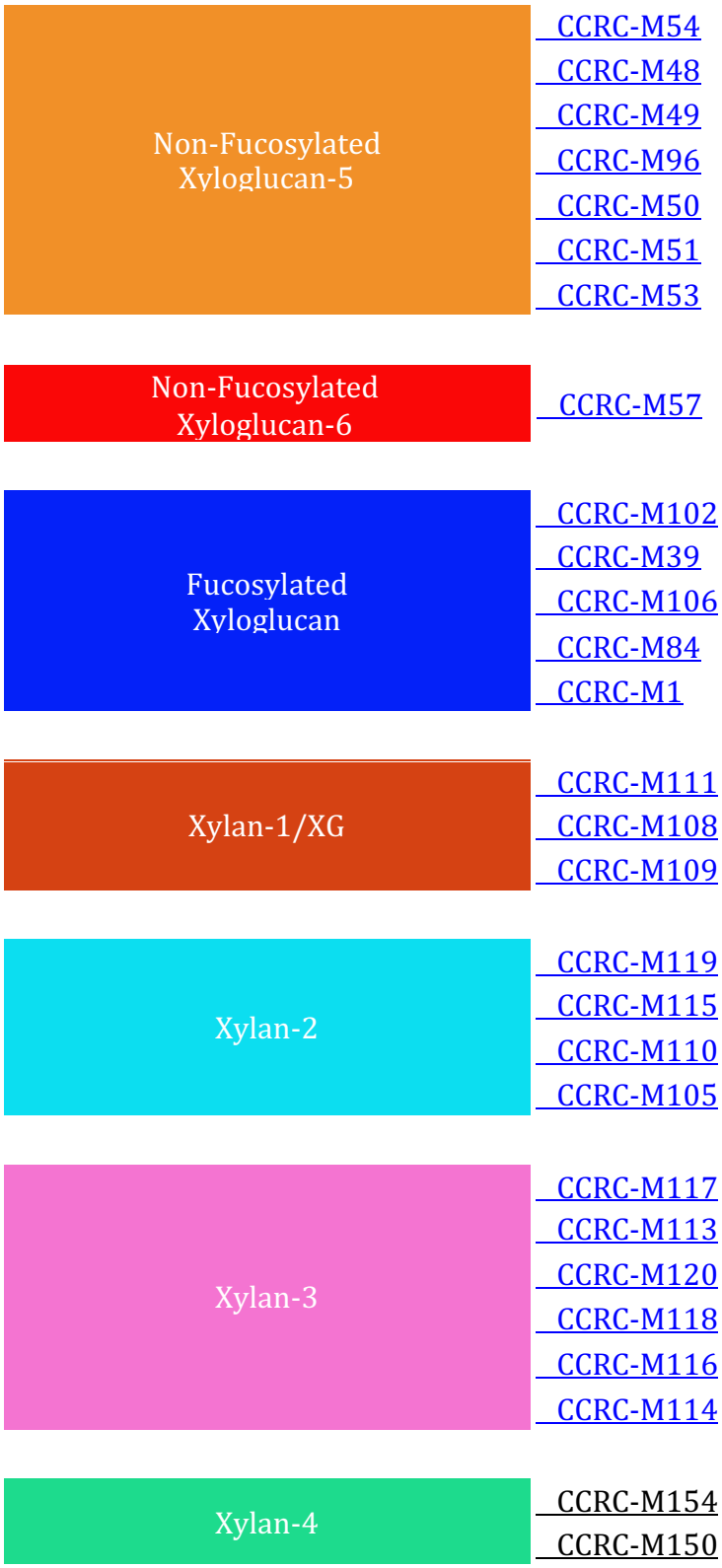
Non-Fucosylated Xyloglucan-5
CCRC-M54
CCRC-M48
CCRC-M49
CCRC-M96
CCRC-M50
CCRC-M51
CCRC-M53
Non-Fucosylated Xyloglucan-6
CCRC-M57
Fucosylated Xyloglucan
CCRC-M102
CCRC-M39
CCRC-M106
CCRC-M84
CCRC-M1
Xylan-1/XG
CCRC-M111
CCRC-M108
CCRC-M109
Xylan-2
CCRC-M119
CCRC-M115
CCRC-M110
CCRC-M105
Xylan-3
CCRC-M117
CCRC-M113
CCRC-M120
CCRC-M118
CCRC-M116
CCRC-M114
Xylan-4
CCRC-M154
CCRC-M150

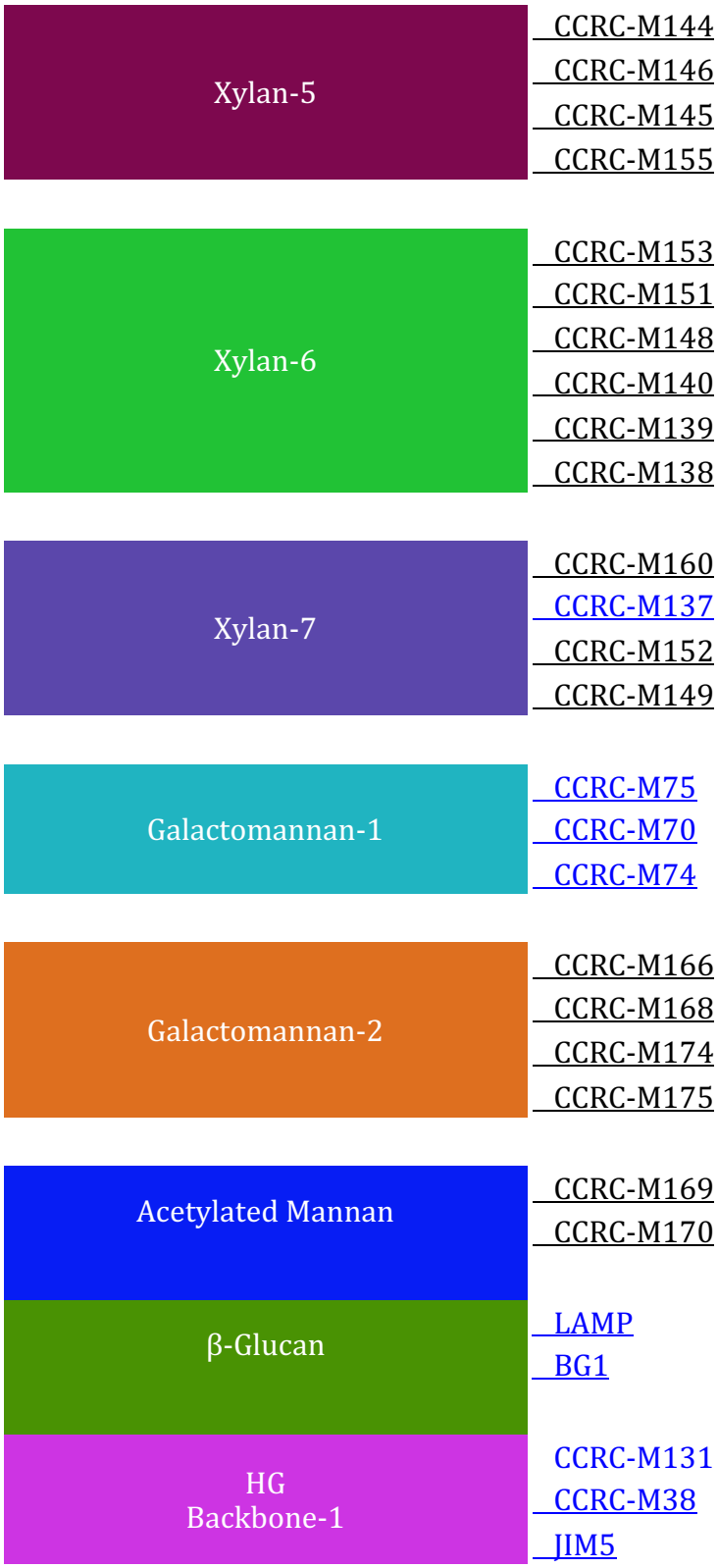
Xylan-5
CCRC-M144
CCRC-M146
CCRC-M145
CCRC-M155
Xylan-6
CCRC-M153
CCRC-M151
CCRC-M148
CCRC-M140
CCRC-M139
CCRC-M138
Xylan-7
CCRC-M160
CCRC-M137
CCRC-M152
CCRC-M149
Galactomannan-1
CCRC-M75
CCRC-M70
CCRC-M74
Galactomannan-2
CCRC-M166
CCRC-M168
CCRC-M174
CCRC-M175
Acetylated Mannan
CCRC-M169
CCRC-M170
β-Glucan
LAMP
BG1
HG
Backbone-1
CCRC-M131
CCRC-M38
JIM5

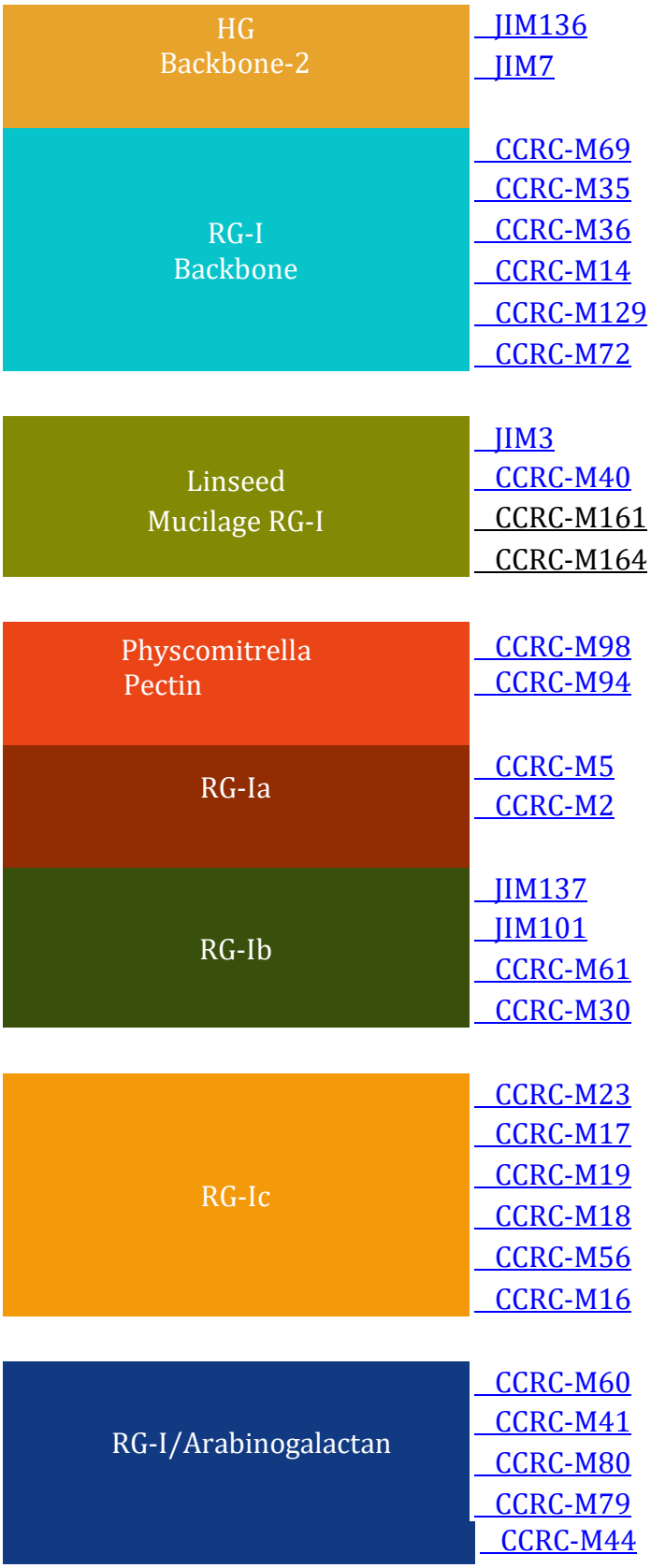
HG
Backbone-2
JIM136
JIM7
RG-I
Backbone
CCRC-M69
CCRC-M35
CCRC-M36
CCRC-M14
CCRC-M129
CCRC-M72
Linseed
Mucilage RG-I
JIM3
CCRC-M40
CCRC-M161
CCRC-M164
Physcomitrella
Pectin
CCRC-M98
CCRC-M94
RG-Ia
CCRC-M5
CCRC-M2
RG-Ib
JIM137
JIM101
CCRC-M61
CCRC-M30
RG-Ic
CCRC-M23
CCRC-M17
CCRC-M19
CCRC-M18
CCRC-M56
CCRC-M16
RG-I/Arabinogalactan
CCRC-M60
CCRC-M41
CCRC-M80
CCRC-M79
CCRC-M44

CCRC-M33
CCRC-M32
CCRC-M13
CCRC-M42
CCRC-M24
CCRC-M12
CCRC-M7
CCRC-M77
CCRC-M25
CCRC-M9
CCRC-M128
CCRC-M126
CCRC-M134
CCRC-M125
CCRC-M123
CCRC-M122
CCRC-M121
CCRC-M112
CCRC-M21
JIM131
CCRC-M22
JIM132
JIM1
CCRC-M15
CCRC-M8
JIM16

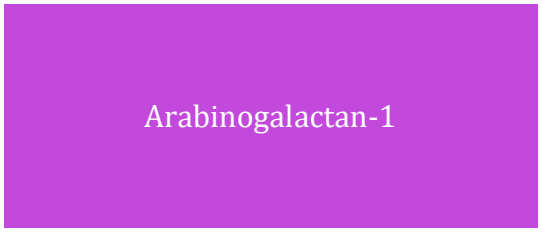

JIM93
JIM94
JIM11
MAC204
JIM20

JIM14
JIM19
JIM12
CCRC-M133
CCRC-M107

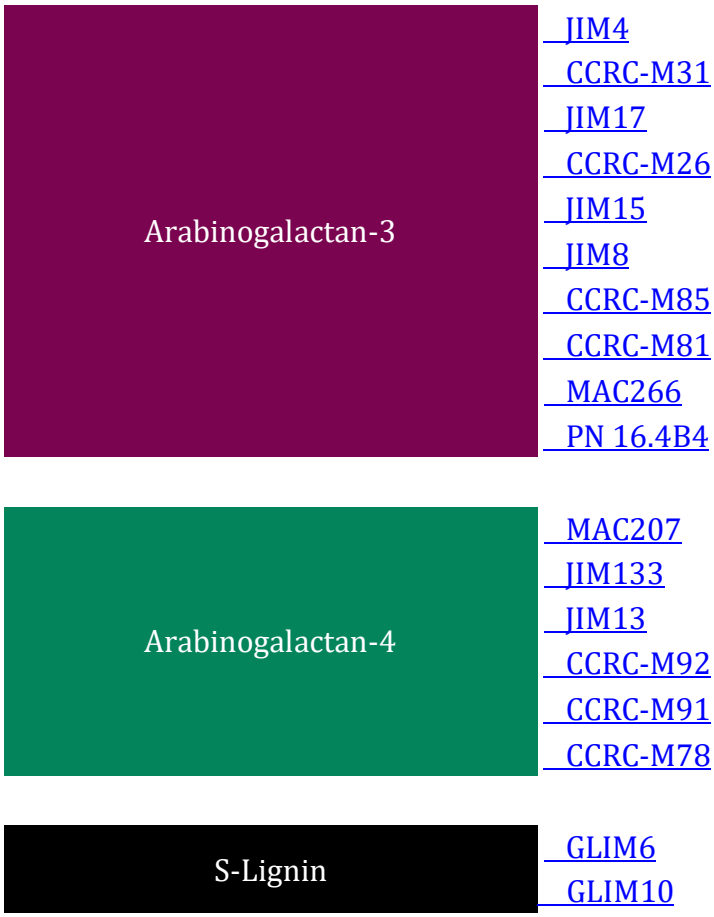
Arabinogalactan-3
JIM4
CCRC-M31
JIM17
CCRC-M26
JIM15
JIM8
CCRC-M85
CCRC-M81
MAC266
PN 16.4B4
Arabinogalactan-4
MAC207
JIM133
JIM13
CCRC-M92
CCRC-M91
CCRC-M78
S-Lignin
GLIM6
GLIM10

Appendix B: Raw unaltered immunolabelling images used in Figures 14 – 22. Images are ordered: Xyloglucan, Xylan, and Pectin. Bar = 200 µm.

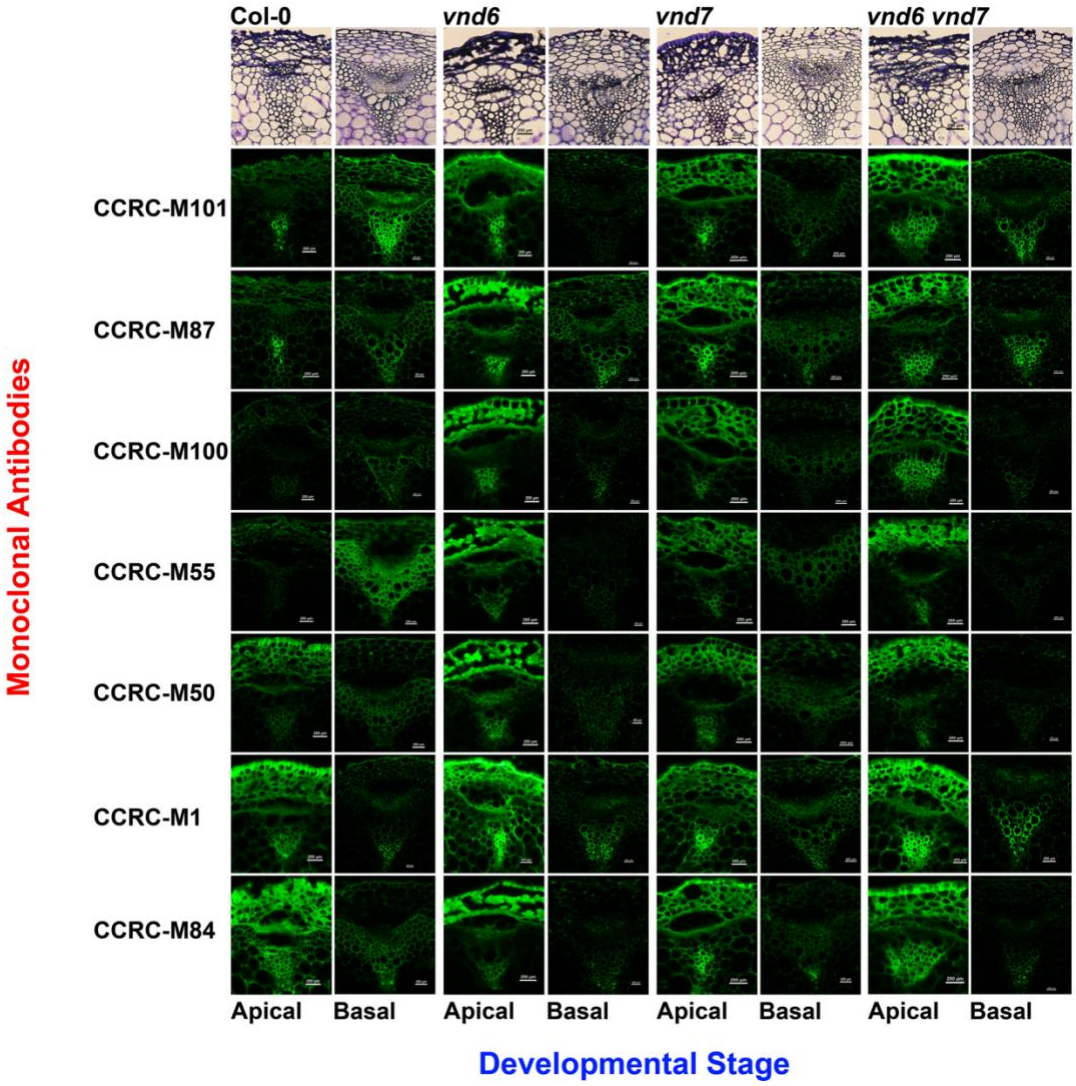

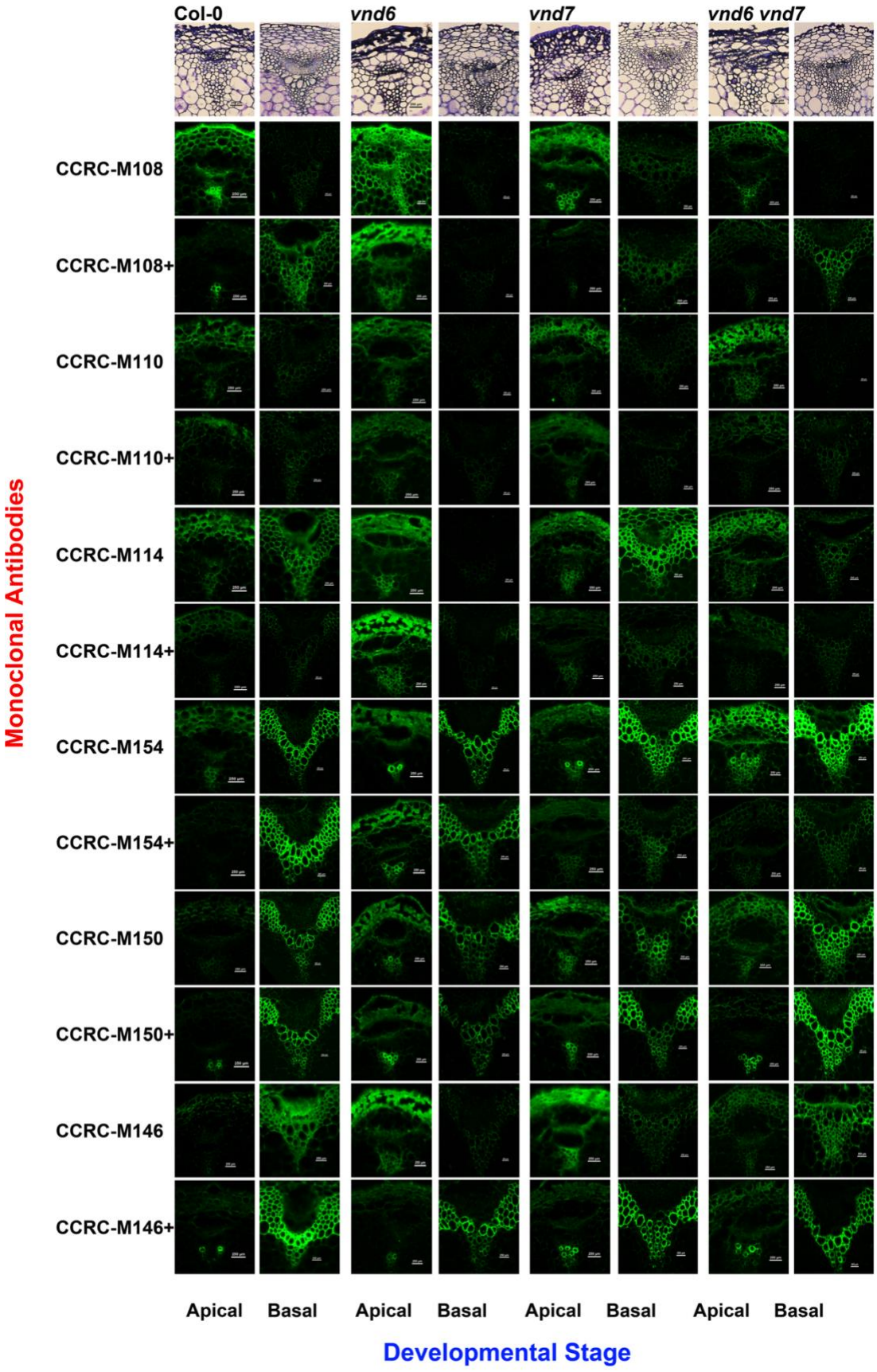
Col-0
vnd6
vnd7
vnd6 vnd7
CCRC-M108
CCRC-M108+
CCRC-M110
CCRC-M110+
CCRC-M114
CCRC-M114+
CCRC-M154
CCRC-M154+
CCRC-M150
CCRC-M150+
CCRC-M146
CCRC-M146+
Monoclonal Antibodies
Apical
Basal
Apical
Basal
Apical
Basal
Apical
Basal
Developmental Stage

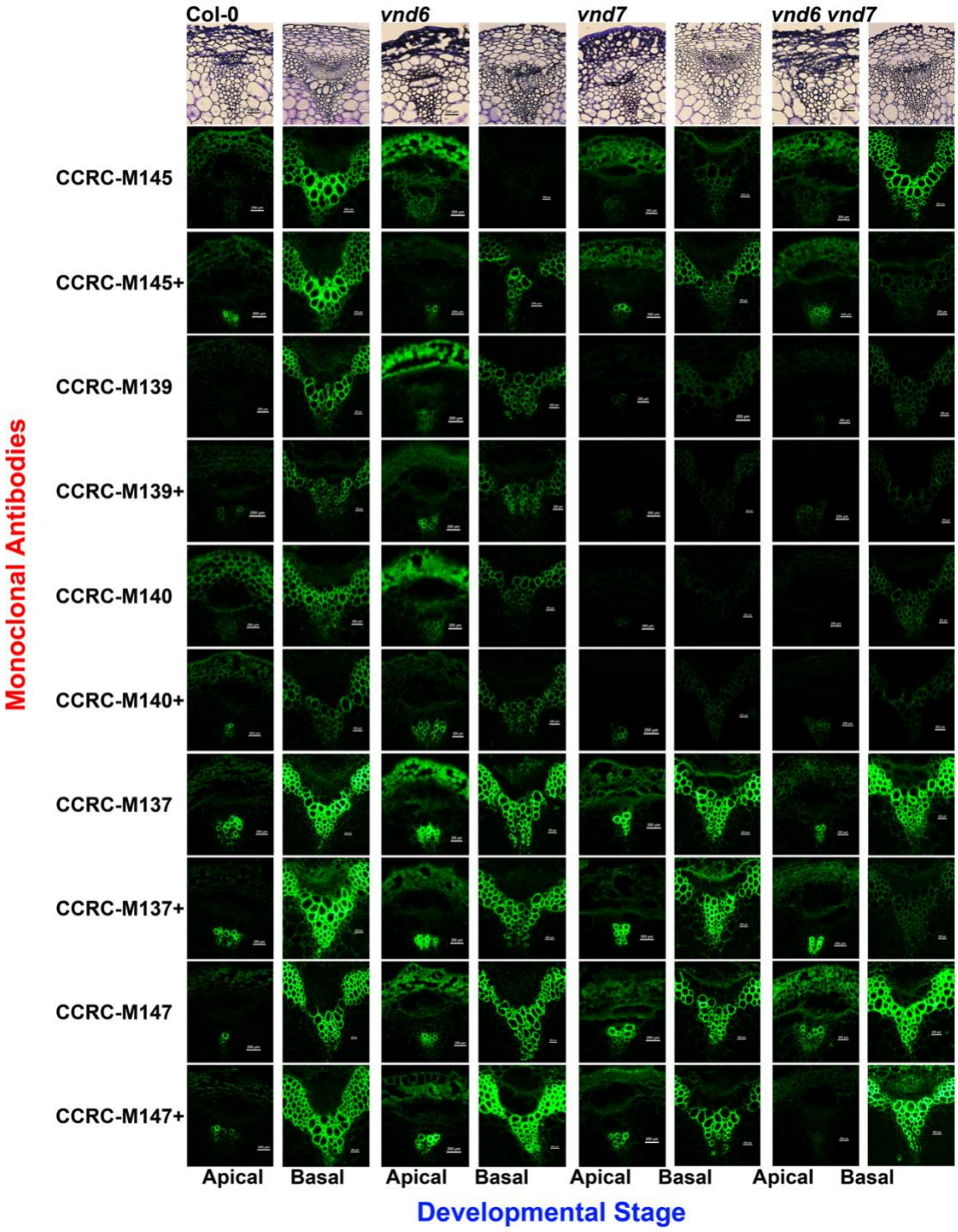
Col-0
vnd6
vnd7
vnd6 vnd7
CCRC-M145
CCRC-M145+
CCRC-M139
CCRC-M139+
CCRC-M140
CCRC-M140+
CCRC-M137
CCRC-M137+
CCRC-M147
CCRC-M147+
Monoclonal Antibodies
Apical
Basal
Apical
Basal
Apical
Basal
Apical
Basal
Developmental Stage

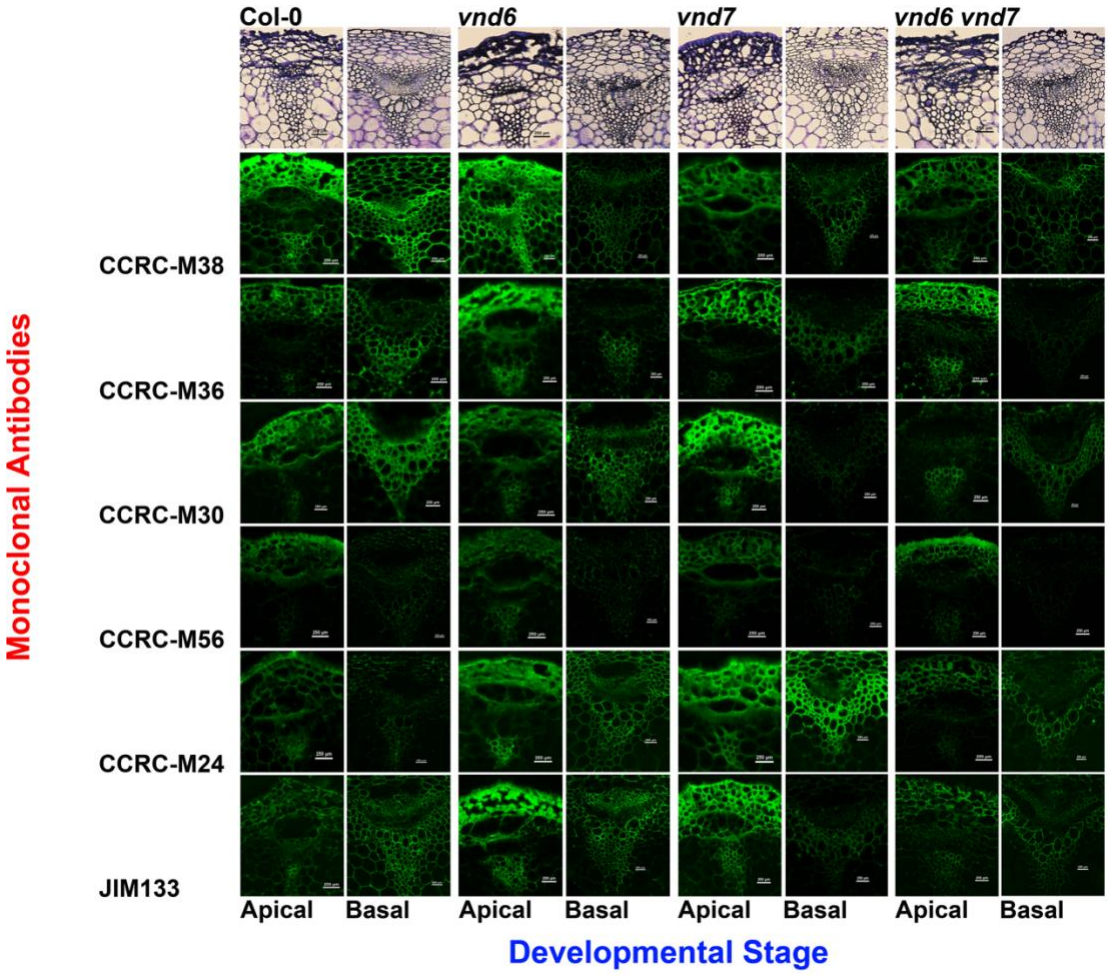
Col-0
vnd6
vnd7
vnd6 vnd7
Monoclonal Antibodies
CCRC-M38
CCRC-M36
CCRC-M30
CCRC-M56
CCRC-M24
JIM133
Apical
Basal
Apical
Basal
Apical
Basal
Apical
Basal
Developmental Stage

CHAPTER 4: CONCLUSIONS

The work described in this dissertation focussed on the development of methods for monitoring changes in glycan structural epitopes and their abundances using immunological approaches such as glycome profiling and immunolabelling.

In Chapter 2, I described the application of integrating glycome profiling and immunolabelling to provide comprehensive details towards the presence, relative abundances, and the dynamics of diverse xylan epitope structures that are integrated into the cell-walls throughout different stages of Arabidopsis stem development. This provides a robust tool for characterising altered xylan integration patterns in the cell-walls during the stem maturation process. Our findings suggested that different sub-classes of xylans exist within the cell-walls of the Arabidopsis inflorescence stem and there is an overall increase in xylan epitopes as the stem matures. Therefore, this approach could rapidly and reliably survey xylan deposition patterns in the cell walls of plants belonging to different phylogenies and provide new information into the roles of xylans in overall plant growth and development.

Chapter 3 described the development of glycome profiling, an enzyme-linked immunosorbent assay (ELISA)-based glycan epitope characterisation at a cell type/population resolution. My results reveal that through laser capture microdissection (LCM), glycome profiling is a reproducible and robust method to

determine the glycome profiles of the cell-walls in different cell types from wild-type Arabidopsis and from plants carrying mutation in genes that regulate secondary cell-wall deposition in vessels. We are able to demonstrate that cell-wall extracts from these cell types displayed different glycan epitope contents, specifically in terms of xyloglucan and xylan epitope compositions, depending on the genetic background of the plants being studied. Our results demonstrate that it is possible to immunotype cell-walls from specific cells in selected plant tissues, thereby opening up the opportunity to examine the structure and composition of the cell-walls of different plant cell-types along developmental gradients.

As a whole, my work contributes to a novel approach in analysing plant cell-wall composition at a higher-resolution via mid-to-high-throughput methods.